Ressortforschungsberichte zur kerntechnischen Sicherheit und zum Strahlenschutz

Retrospektive Dosimetrie in Notfallsituationen für die Bevölkerung – Vorhaben 3607S04560

Auftragnehmer:
Helmholtz Zentrum München - Deutsches Forschungszentrum für Gesundheit und Umwelt
Institut für Strahlenschutz

C. Woda

I. Fiedler

L. Urso

J. C. Kaiser

Das Vorhaben wurde mit Mitteln des Bundesministeriums für Umwelt, Naturschutz und Reaktorsicherheit (BMU) und im Auftrag des Bundesamtes für Strahlenschutz (BfS) durchgeführt.

Bundesamt für Strahlenschutz

BfS-RESFOR-44/12

Bitte beziehen Sie sich beim Zitieren dieses Dokumentes immer auf folgende URN:
urn:nbn:de:0221- 201201307218

Salzgitter, Januar 2012

Forschungsvorhaben 3607S04560

Final Report

Retrospective Dosimetry for the population in emergency situations

Retrospektive Dosimetrie in Notfallsituationen für die Bevölkerung

Clemens Woda, Irene Fiedler, Laura Urso, Jan Christian Kaiser

Helmholtz Zentrum München - Deutsches Forschungszentrum für Gesundheit und Umwelt, Institut für Strahlenschutz, Arbeitsgruppe Radioökologische Modellierung und Retrospektive Dosimetrie*

*Seit 01.01.2011. Vorher Arbeitsgruppe Risikoanalyse

Zusammenfassung

In dem Vorhaben wurden bestimmte Vergussmassen von Chipkarten, die als EC-,Kredit, Krankenkassen- und SIM-Karten vorkommen, sowie elektronische Komponenten in tragbaren elektronischen Geräten als Materialien ermittelt, die für die Rekonstruktion von individuellen Strahlenexpositionen in radiologischen Notfällen geeignet sind. Mit den entwickelten Messverfahren können individuelle Dosiswerte innerhalb eines Tages ermittelt werden, mit Nachweisgrenzen von 10 -20 mGy bis zu 10 Tage nach Exposition. Allen Materialien gemein ist ein lineares Dosiswachstum bis ca. 10 Gy, sowie eine Langzeitinstabilität des Lumineszenzsignals bei Lagerung bei Raumtemperatur. Dies bedeutet, dass der Zeitpunkt der Exposition bekannt sein muss, um mit den in dem Vorhaben bestimmten Fadingkurven eine Signalkorrektur durchführen zu können. Es wurde weiterhin ein wartungsfreier Lumineszenz-Detektor auf BeO–Basis entwickelt, mit hoher Empfindlichkeit und geringer Photonenenergieabhängigkeit. Es wurden zwei Berechnungsmethoden entwickelt, um für zwei verschiedene Fälle aus den lokalen Dosismessungen eine Karte der Kontamination bzw. der effektiven Dosis zu erhalten.

Abstract

In this project, certain encapsulations of chip card modules, that find use in debit, credit, health insurance and SIM-cards and electronic components in portable electronic devices were identified as materials that are useful for reconstruction of individual radiation exposures in radiological emergencies. The developed measurement protocols allow the determination of individual doses within one day, with minimum detectable doses of 10-20 mGy for up to 10 days after exposure. All materials have the common feature of showing a linear dose response up to approx. 10 Gy but also a long-term signal instability for storage at room temperature. This implies that the time of exposure has to be known, in order to correct the signal using the fading curves determined in the project. Further, a maintenance-free BeO based luminescence detector was developed, showing high sensitivity and an essential flat photon energy response. Two computational procedures for two different cases were developed, in order to produce maps of contamination or effective dose from the localized dose measurements.

Contents

1. Introduction

There is a growing public concern about accidental radiation exposures due to the aging of nuclear power plants, illegal dumping of radioactive waste or terrorist attacks with Radiological Dispersion Devices (RDD), so called "dirty bombs" (dispersion of radionuclides through the blast of conventional explosives). According to the judgment of national and international security authorities, it is a question of when, not if, terrorist groups will have the know-how to use dirty bombs to attack the public. It can be expected that the malevolent attacks will occur without any advance warning and will target as many people as possible in order to cause the maximum damage. In such a large-scale emergency situations means of rapidly assessing the absorbed dose of exposed individuals are highly desirable.

Intensive research efforts are undertaken to identify and characterize materials that are carried close to the human body, are ubiquitously available and posses appropriate radiation sensitivity for use as emergency dosimeters. It was the main task of the first workpackage of this project to identify (at least) three of such personal items, that are in principle suitable for reconstruction of individual radiation exposures. Appropriate methods were then to be developed, which allow the assessment of individual doses with detection limits of 10 mGy within one day.

Previous studies have shown that certain types of chip cards, that find use as health insurance, ID, cash and credit cards, have high potential to be used as such individual dosemeters in the case of radiological accidents (Mathur et al. 2007, Göksu 2003 and Göksu et al. 2003). The radiation sensitive component of the chip card module was traced to silica in the epoxy encapsulant, the latter protecting the chip and wiring from the environment and physical damage (Barkyoumb and Mathur 2008 and Göksu et al. 2007). Using IRSL the minimum detectable dose was above 100 mGy, while specific US ID chip card modules showed an estimated minimum detectable dose of only $\sim$ 20 mGy for OSL (Mathur et al., 2007). In a previous project (Göksu et al., 2007) it was investigated, in how far the dosimetric properties of the chip card could be improved by adding phosphorescent substances (powder) such as Al_2O_3:C, BeO and LiF:Mg,Cu,P to the epoxy before hardening. This lead to detection limits below 10 mGy for freshly thermally annealed encapsulants. However, due to the readout method employed (TL) and an observed signal recovery after thermal treatment, the practical minimum detectable dose was about 60 mGy.

Portable electronic devices (PEDs), such as mobile phones, music players, USB flash drives and digital cameras are nowadays almost ubiquitously distributed among the general population and usually carried close to the body, therefore their usability as emergency dosimeters would be highly advantageous. Aided by a study published soon after this project started (Inrig et al., 2008), reporting on the suitability of certain

electronic components (resistor substrates) for dosimetry, it was first investigated, if the results can be confirmed for PEDs available in Germany, which properties needed further investigation and which other components or modes of stimulation are also applicable.

Generally, a fortuitous dosimeter should meet several requirements to be useful in accident and retrospective dosimetry: it should show a unique and reproducible signal response to doses up to several Gy, no signal in the unexposed state, a lower detection limit of tens of mGy and allow dose assessment with reasonable accuracy up to several days after the exposure. It will be shown that the personal objects investigated in this project (specific chip card modules and PEDs), although showing partly complex luminescence properties, fulfill all these requirements.

In the second workpackage of the project a maintenance-free, passive luminescence detector was to be developed, which could be fixed at places of high importance (public squares, subway stations) and which allows the determination of absorbed doses with a detection limit of 10 mGy within one day. At least five prototypes were to be developed, three of which were to be submitted to the BfS and the end of the project. To relate the dose in the dosimeter to doses of population groups, a procedure is developed to produce maps of reference gamma dose rate, air kerma, surface contamination and effective dose in urban areas from localized dose measurements. This procedure distinguishes two approaches depending on the number of measurements and/or the scenario.

For very few measurements, as can be expected after an RDD event, a Gaussian plume model is used, which can make estimates of the effective doses from radiation from the ground ("ground shine") and from the passing cloud ("cloud shine"). For a sufficient number of measurements (meaning more than 10 in our case), which would be available after a large-scale incident such as a major accident in a nuclear power plant, an existing monitoring module (IAMM, Kaiser and Pröhl, 2007) is adapted to handle dose data in order to produce maps of surface contamination using either geo-statistical interpolation or data assimilation. Doses to population groups can then readily be calculated from these maps by applying well-known dose conversion coefficients.

In this report the fundamentals of luminescence dosimetry and the instrumentation used are briefly described (chapter 2). The dosimetric properties of chip cards and portable electronic devices are then investigated in chapters 3 and 4. The development of the passive luminescent detector is outlined in chapter 5 and the procedure for map production in chapter 6. The report concludes with a summary and recommendation for future studies.

2. Material and Methods

2.1. Fundamentals of luminescence dosimetry

Luminescence is the stimulated emission of light from an insulator or semiconductor following the previous absorption of energy from radiation (McKeever, 1985). If the stimulation is provided by heat, the emission is termed Thermoluminescence (TL), if it is provided by light it is termed optically stimulated luminescence (OSL) and if it is provided by infrared light it is termed infrared stimulated luminescence (IRSL). Luminescence may also be produced by other types of excitation than radiation (e.g. electrical, mechanical, chemical energy) but within the context of dosimetry, the excitation is always to be understood as nuclear radiation (i.e. alpha, beta, gamma radiation, X-rays etc.).

The driving agents in producing TL or OSL in a material are defects in the material structure. In crystalline materials, the defects form metastable states in the forbidden zone between valence and conduction band and function as traps for free charge carriers (electrons/holes), produced within the crystal by the ionizing radiation. If the energetic difference between defect ground state and conduction or valence band is sufficiently high, the trapped charge carriers will not be able to escape at room temperature and thus charges will accumulate within the defects as long as the radiation continues. Thus the amount of trapped charge carriers in a defect is directly proportional to the amount of absorbed dose of the material.

In the laboratory the trapped charges are set free by supplying sufficient amount of energy either in the form of heat (TL) or light (OSL) and recombination with charge carriers of opposite signs can take place (electron-hole recombination). The recombination process can be accompanied by the emission of light which constitutes the luminescence signal. Non-radiative recombinations, which will go undetected, are however also possible. In the simplest case of only one trap and one recombination center, the luminescence signal is proportional to the amount of trapped charges and thus directly proportional to the dose the material has received.

Since the charge carriers (electrons and holes) are trapped in metastable states, there is a finite probability that they are thermally released from their trapping states to the conduction/valence band even at room temperature, leading to a loss in luminescence signal. Since this effect is strongly dependent on temperature, it is termed thermal fading. In order to avoid a systematic underestimation of the absorbed dose, the mean lifetime of the luminescence signal should be large compared to the time interval between exposure and measurement, in the case of a single event or the duration of irradiation, in the case of a continuous exposure. For some materials, however, a lumi-

nescence signal decay has been observed which is much faster than expected from pure thermal effects. This phenomenon is called anomalous fading and it is due to tunneling of charge carriers from the trap to the recombination centre. The main characteristic of the anomalous fading is a rapid initial decay and then a gradual decrease of the decay rate for longer storage times.

The readout process is very similar for both TL and OSL measurements, except for the stimulation mechanism. During a TL measurement, the sample is placed in a stream of heated gas or on a thin metal heater, its temperature is linearly raised with time and the luminescence signal is detected by means of a photomultiplier (PM) tube, operating in photon counting mode. The light yield is then recorded as a function of the sample temperature in a glow curve. The quantity related to the total number of the emitted photons, and thus to the radiation exposure, is the area under the glow curve. For an OSL measurement, the sample is stimulated with a strong light source such as a laser or a high power light emitting diode and the signal is again detected with a PM tube. Generally, the stimulation is carried out with a continuous excitation source, like a continuous wave laser, illuminating the sample and recording the light yield simultaneously over a time period of many seconds. Other stimulation modes, such as linearly increasing the light intensity or pulsing the light source, are also in use. In order to discriminate the luminescence signal from the simulating light and to protect the PM tube, appropriate optical filters need to be inserted between sample and detection unit.

2.1.1. Relative Energy Response

The energy response of a dosimetric material is the variation of the detected luminescence output, for a fixed dose, as a function of the energy of the absorbed radiation (McKeever et al., 1995). It is a result of the different dependence of the material's absorption coefficient on radiation energy as compared to that of a reference material (usually air). For photon irradiation, the photon energy response $S_E(E)$ is defined as the ratio of the mass energy absorption coefficient of the material, $(\mu_{en}/\rho)_m$, and of the reference material $(\mu_{en}/\rho)_{ref}$:

$$S(E) = \frac{(\mu_{en}/\rho)_m}{(\mu_{en}/\rho)_{ref}} \,. \tag{2.1}$$

$S_E(E)$ is usually normalized to the response at the energy of ^{60}Co (1250 keV) or ^{137}Cs (660 keV). This defines the *R*elative *E*nergy *R*esponse, $(RER)_E$ of a dosimetric material:

$$(RER)_E = \frac{S(E)}{S(1,25\,\mathrm{MeV}\,^{60}\mathrm{Co})} \,. \tag{2.2}$$

The photon energy response is an important characteristic for relating the dose in the material to dose in air and ultimately to organ doses or the effective dose of the exposed individual. An ideal dosimeter would show a flat $(RER)_E$, which is the case for

materials with low Z_{eff}. For compounds, the energy dependence is calculated from the sum of the mass energy absorption coefficients of the respective elements, multiplied with their fraction by weights w_i, according to:

$$S(E) = \frac{\sum w_i(\mu_{en}/\rho)_{m,i}}{(\mu_{en}/\rho)_{ref}} \,. \tag{2.3}$$

2.2. Methods

OSL measurements were performed on a Risø TL/OSL-DA-15 automated reader, equipped with blue LEDs (470±30 nm) for stimulation, delivering approximately 40 mW cm^2 at the sample position and a Thorn-EMI 9235 bialkali photomultiplier combined with a 7.5 mm U-340 Hoya filter (290–370 nm) for detection. The built-in ^{90}Sr/^{90}Y source is calibrated against a ^{60}Co source of the Secondary Standard Dosimetry Laboratory (SSDL) of the Helmholtz Zentrum München for quartz in the grain size fraction of 140-200 µm and has a dose rate of approx. 45.5 mGy s^{-1}. For some components of personal objects to be discussed below and individual calibration was performed (see chapter 4). TL measurements were either conducted on this reader using the same filter or a combination of a Corning 7-59 and heat-absorbing filter HA-3 (detection window of 300-500 nm). Comparative TL measurements were also done on a Risø TL-DA-12 automated reader, equipped with the same photomultiplier tube but using a HA-3 together with a blue (300–530 nm) transmitting Schott BG12 glass filter. Unless stated otherwise, all TL measurements were made with a heating rate of 2°C s^{-1} and background correction.

Trial irradiations were performed at the Secondary Standard Dosimetry Laboratory (SSDL) of the Helmholtz Zentrum München using a ^{137}Cs source. For measurements of the photone energy response ^{137}Cs, ^{60}Co and two X-ray sources of the SSDL were used. To produce X-rays with ISO narrow spectrum qualities (ISO, 1996), the following Filter combinations were used (Table 2.1).

Mean Energy (keV)	tube voltage (kV)]	Filter (mm)	max. current (mA)	max. dose rate at 80 cm distance (µGy/s)
24	30	4.0 Al	45	90.52
33	40	0.21 Cu + 4.0 Al	45	78.87
48	60	0.6 Cu + 4.0 Al	45	137.65
65	80	2.0 Cu + 4.0 Al	37.50	56.53
83	100	5.0 Cu + 4.0 Al	30	21.92
100	120	1.0 Sn + 5.0 Cu + 4.0 Al	25	20.43
118	150	2.5 Sn + 4.0 Al	20	121.96
164	200	1.0 Pb + 3.0 Sn + 2.0 Cu + 4.0 Al	15	52.26
208	250	3.0 Pb + 2.0 Sn + 4.0 Al	15	54.37
250	300	5.0 Pb + 3.0 Sn + 4.0 Al	14	50.35

Tabelle 2.1.: Filter combination at given tube potential for narrow spectrum quality X-rays (ISO, 1996) and maximum settable current. The last column lists the maximum dose rate, measured with an ionization chamber, at the distance used for irradiations in this work.

3. Chip cards as emergency dosimeters

In this chapter the potential of OSL of chip cards for retrospective and accident dosimetry is investigated on representative and world-wide spread wire-bond chip card modules. They were manufactured by Infineon Technologies using either a widely spread UV-cured epoxy product for encapsulation or molding technology for contact-based and contactless modules.

3.1. Wire-bond chip card modules with UV-cured encapsulations

The chip card modules were produced at Infineon Technologies AG in 2006. For data security reasons, they consist of a blank silicon chip without wiring but otherwise are identical to actual wire-bond chip card modules that are produced for costumers. They are encapsulated with a one component UV-cured epoxy compound for the 'dam&fill' technology (Fig. 3.1). The epoxy contains approx. 43 weight % filler material (silica, amorphous SiO_2), with grain sizes smaller than approx. 32 µm, which is added to control the thixotropic properties of the epoxy. After UVA illumination (320–400 nm) for about 30 s, the epoxy hardens over a time range of approx. 24 h at room temperature, becoming a light gray translucent layer of approx. 500 µm thickness. Samples of 8 mm diameter were punched out to fit into a stainless steel cup of a luminescence reader.

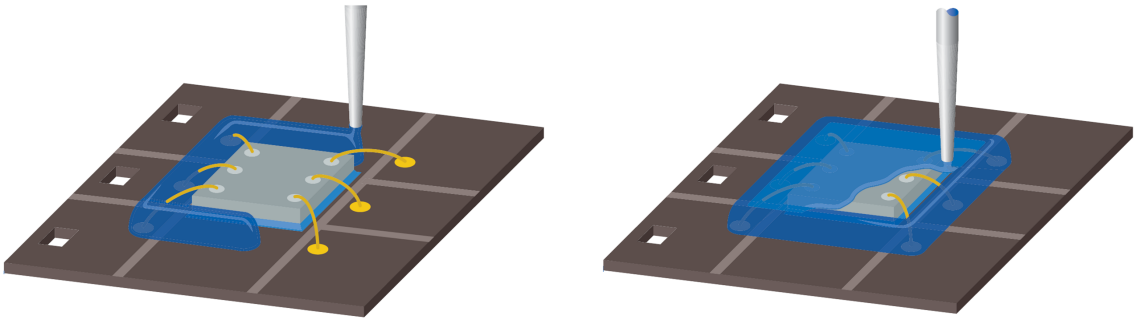

Figure 3.1.: Dam&Fill Technology in chip card production. In the first step, a dam is dispensed around the chip by using a highly thixotropic, 1-component encapsulation compound (left). In the second step, the dam is filled with a low-viscous filler resulting in a rectangular casting geometry with minimum height (right). Reproduced from Smart Card/Smart Label brochure with kind permission of DELO Industrial Adhesives.

Considering the average density of the epoxy of approx. 1.4 g cm^{-3}, the beta absorption characteristics are expected to roughly correspond to 250 µm quartz grains. As dose rate has found to vary little for quartz grain sizes from 100 to 250 µm (Goedicke, 2007), the present calibration value for quartz of the OSL and TL readers seems to be applicable to chip card modules as well. Unless stated otherwise, OSL decay curves were integrated for the first 20 s and for 40–60 s for determination of signal and background, respectively. Part of the TL measurements were conducted on the OSL reader using the same filter, but for comparison also on the Risø TL-DA-12 automated reader in the blue wavelength range.

3.1.1. Indications for OSL from TL

As already observed in previous studies there is a strong zero dose signal of unexposed chip card modules in TL, peaking around 170°C (Fig. 3.2). The signal is similar in shape in the UV and blue wavelength range, but roughly an order of magnitude more intense in the latter, indicating that the emission band peaks at wavelengths greater than 370 nm. The zero dose signal varies in intensity of a factor of two between different modules and is more than an order of magnitude more intense than a subsequent 1 Gy regenerated TL signal (Fig. 3.2, a). The latter peaks around 100°C and shows a broad structure until 280°C (higher temperatures are not applicable, as the epoxy then decomposes).

If the chip card modules are irradiated with high doses before the first TL measurement, the low temperature peak at 100°C becomes visible on top of the zero dose signal (Fig. 3.2, b). Optical stimulation with blue LEDs after irradiation reduces the TL signal over the entire temperature range, with the tendency of a possible slower reduction rate for the 100°C peak compared to the 170°C peak. The zero dose signal in an unirradiated chip card module can also be strongly reduced by 300 s of optical stimulation alone and phototransfer into the 100°C TL trap is visible (Fig. 3.2, a).

The TL investigations demonstrate that both the non-radiation induced zero dose signal and radiation induced signals are light sensitive, thus the photo-active defects and mechanisms involved can contribute to an observed OSL signal. The TL results also indicate that part of an OSL signal after irradiation might originate from defects which are thermally unstable at room temperature.

3.1.2. Origin of the zero dose signal

As a result of the TL measurements, OSL was first investigated after preheating the chip card module at 100°C for 60 s, in order to empty the 100°C TL trap. OSL was then measured at 110°C to keep the 100°C TL trap empty during optical stimulation, similar to the OSL measurement approach of quartz. With this approach a zero dose signal is also observed for unexposed chip card modules in OSL, albeit at a smaller level than in TL (Fig. 3.3).

Depending on the choice of integration interval and background, this signal corresponds to doses between -500 and 1000 mGy. The signal shape of the zero dose signal

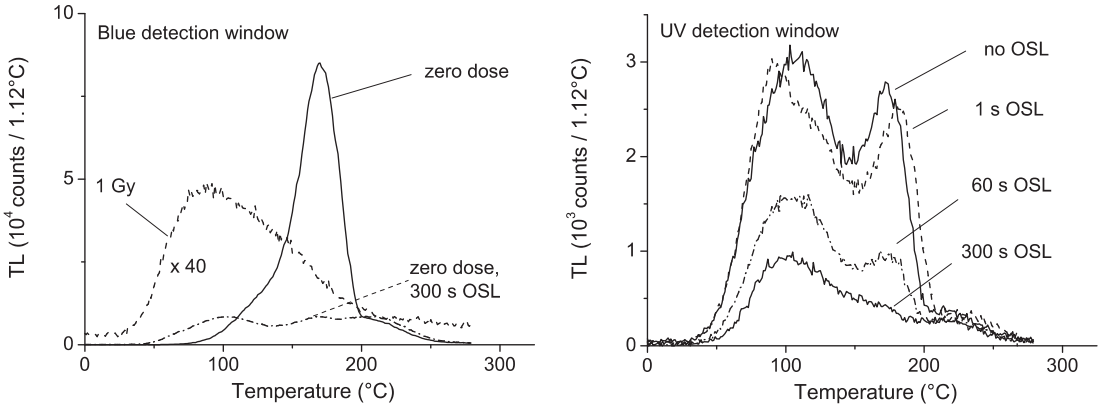

Figure 3.2.: TL signals of chip card modules with different pretreatments. The upper panel displays measurements in the 300-530 nm (blue) wavelength range (BG12). The 1 Gy irradiated sample is a regenerated TL signal after erasing the zero dose signal by the first TL run and has been multiplied by a factor of 40 for better comparison. The lower panel displays measurements in the 290-370 nm (UV) wavelength range (U-340). All chip card modules in this panel were given a dose of 9.13 Gy and stimulated with blue LEDs for different times before TL measurement. For the sake of clarity, the zero dose signal of an unexposed module is not shown in this detection window but it is similar in intensity to the 'no OSL' glow curve. A different chip card module was used for every measurement displayed.

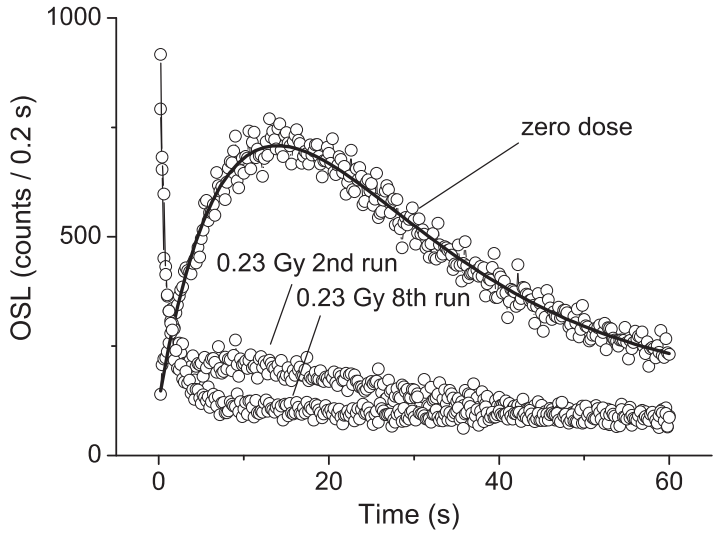

Figure 3.3.: Zero dose signal for OSL measurements at 110°C after preheating at 100°C for 60 s. The solid black line is a fit of function (3.1) to the data. Also shown is the OSL response to a subsequent dose of 0.23 Gy (2nd run) and the same OSL response to a dose after several cycling of dosing and OSL measurements (8th run).

can be described by the empirical function:

$$I_{OSL} = \underbrace{a - b\,\exp\left(-\lambda_1 t\right)}_{build-up} + \underbrace{c\,\exp\left(-\lambda_2 t\right)}_{decay} \tag{3.1}$$

where I_{OSL} (s^{-1}) is the OSL intensity, t (s) the stimulation time, $\lambda_{1,2}$ (s^{-1}) decay constants and a, b, c (s^{-1}) empirical constants. This functional behaviour can be qualitatively explained by the combined effect of thermo-optical release of electrons from the epoxy and transfer into the OSL trap(s) of the silica (buildup term) and simultaneous detrapping of electrons from the OSL defect(s) (decay term). The presumed effect of the epoxy can still be seen at a reduced level in the subsequent measurement of the OSL response to a 0.23 Gy dose: the otherwise typical OSL decay behaviour is distorted in the stimulation time interval, where the zero dose signal peaks. After several cycles of dosing, preheating and OSL measurements finally, no more effect of the epoxy is seen. This demonstrates that the thermo-optical release of electrons from the epoxy is an irreversible one-time effect.

A similar shape of a zero dose signal in OSL is also obtained by OSL measurement at room temperature without preheat, i.e. by pure optical stimulation (Fig 3.4 a). However, the information is spread over a much larger time range (1800 s in comparison to 60 s), which is possibly caused by the reduced efficiency of pure optical (blue) electron release from the epoxy. As a result, an only gradually increasing baseline is observed for the first 100 s. If integration intervals are chosen appropriately an essential zero OSL signal at zero dose can be obtained (see below).

If samples are preheated but OSL measured at room temperature, an increase in the zero dose signal is observed for preheat temperatures below 180°C and a reduction for higher temperatures (Fig. 3.4 b). This is in accordance with the development of the zero dose signal in TL, which peaks around 170-190°C and then sharply falls off for higher temperatures. This similarity also implies that most, if not all, of the zero dose signal in TL and OSL is due to the epoxy and not to the silica grains. A more quantitative analysis of the zero dose signal and of its origin will be given in section 3.1.7.

3.1.3. Thermal stability

The OSL signal of an irradiated chip card module is reduced if the sample is heated to temperatures above 60°C, but cannot be fully erased even after heating to 280°C (Fig. 3.5). No plateau is seen, implying that the OSL signal originates from a range of defects of comparatively low (i.e. the 100°C TL peak) to high thermal stability.

The long-term OSL signal stability at room temperature was investigated by storing irradiated chip card modules for durations of minutes to up to 100 days before measurement. This was done for modules irradiated with doses ranging from 91.3 mGy to 9.13 Gy, i.e. covering two orders of magnitude and measured without preheat. For comparison, the signal stability was also checked for modules irradiated with 0.91 Gy and preheated for 10 s at 100°C, 140°C and 180°C before OSL measurement (Fig. 3.6

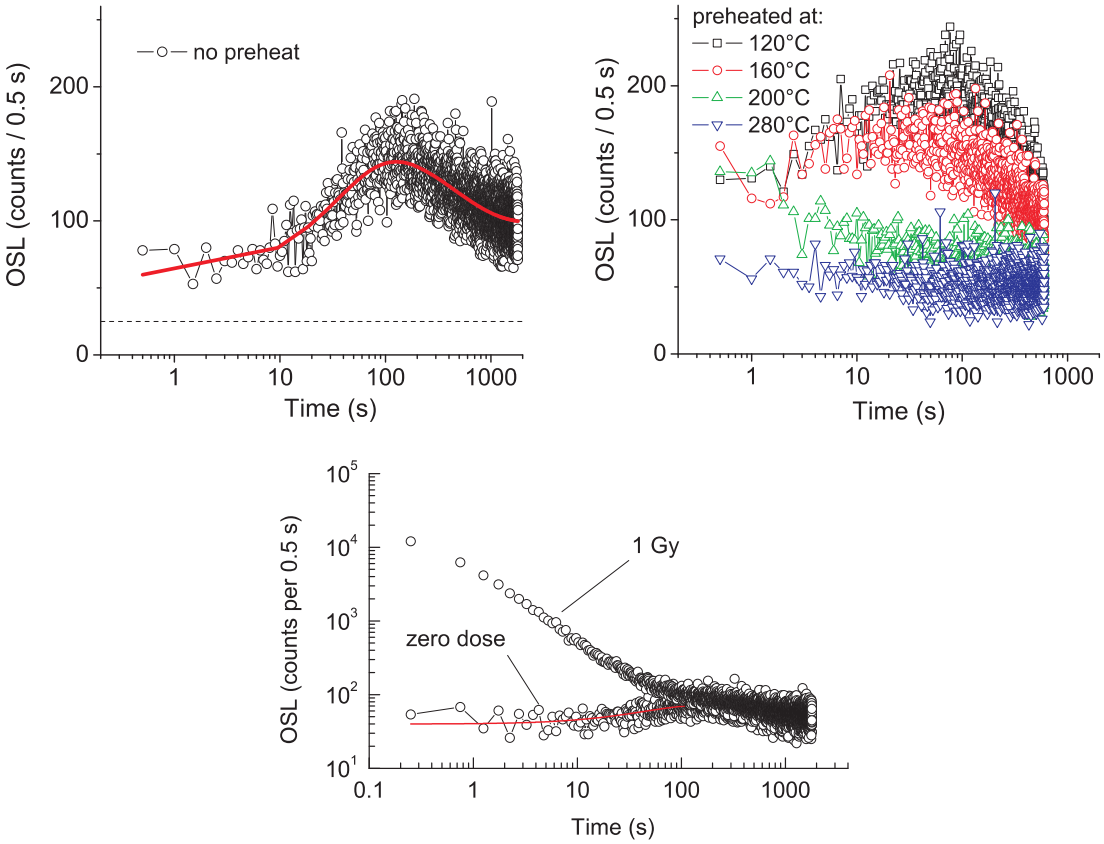

Figure 3.4.: Zero dose OSL signals measured at room temperature without preheat (panel a) and after preheating at various temperatures (panel b). The solid line in panel a is a fit of function (1) to the data. The instrumental background is indicated by the dashed line in panel a.

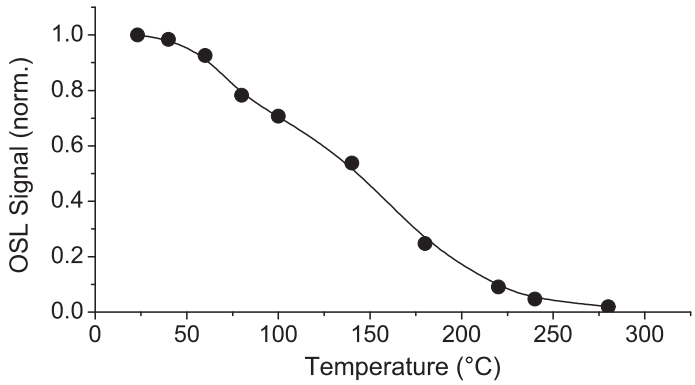

Figure 3.5.: Thermal stability of the OSL signal after irradiation with 0.94 Gy. A fresh chip card module was used for each datum point. Data points are interpolated for the purpose of illustration using a B-spline.

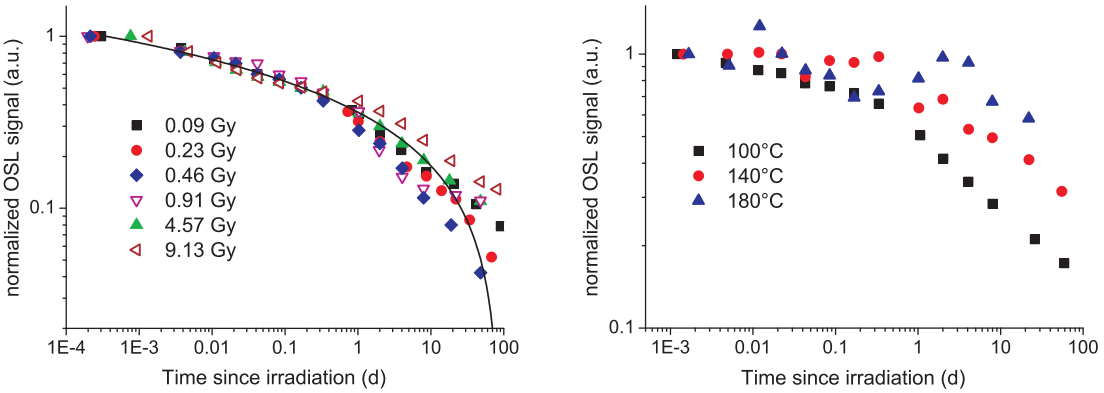

Figure 3.6.: Fading of the OSL signal for different storage times at room temperature for unheated samples (panel a) and for samples preheated before OSL measurement for 10 s at the given temperatures (panel b). The solid line in panel a was obtained by fitting the function $y = a + b \times \ln(t)$ to all data points. Estimated parameters are: $a = 0.362 \pm 0.005$ and $b = 0.081 \pm 0.001$.

a, b).

The OSL signal measured without preheat shows a high degree of fading at room temperature, with a relative signal loss of over 60% in the first day after irradiation and over 80% 10 days after irradiation. While the short-term signal loss can be ascribed to thermal fading, the long-term signal decay is unexpected, considering that heating to temperatures above 180°C are necessary to remove 80% of the OSL signal immediately after irradiation (Fig. 3.5). A possible explanation would be athermal (anomalous) fading of part of the OSL signal, a phenomena often observed in feldspars (Huntley and Lamothe 2001) and also suspected in alumina substrates (see 4). It is corroborated by the observation that also for the samples preheated at 100°C and 140°C long-term signal decay is higher than expected from pure thermal effects. It is interesting to note, that for the sample preheated at 140°C the OSL signal remains approximately constant over the first 8 hours of storage. This is in accordance with the expected removal of most of the low temperature TL peak by such a heat treatment (Fig. 3.2). For the preheat temperature of 180°C no definite conclusions can be drawn, as large scatter in the data points masks a possible athermal decay. The increase in scatter can already be observed to a lesser extent in the 140°C data and is presumably caused by the thermal electron release from the epoxy during preheating.

For the samples measured without preheating, the relative signal decay in the first day is remarkably independent of dose but variability increases for longer durations. A similar trend in signal decay is however still observed. A function of the form $y = a + b \times \ln(t)$ is fitted to all data points, which often is an observed functional relationship of anomalous fading in feldspars (Huntley and Lamothe 2001). Here it is seen more as a useful empirical interpolating function for signal correction, as the total data set reflects with certainty thermal and athermal effects. A different possible explanation for the observed long-term signal instability at room temperature is given

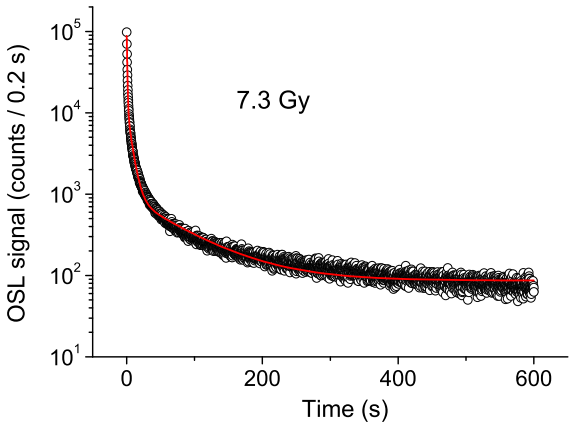

Figure 3.7.: OSL of an irradiated chip card module (7.3 Gy) measured at RT without preheating, immediately after irradiation. The data has been fitted with equation 3.2 (red line). The instrumental background is around 10 counts per 0.2 s (bottom value).

in 3.1.7.

3.1.4. Dose response and detection limit

A typical OSL decay curve, measured for 600 s at room temperature after irradiation with 7.3 Gy is depicted in Fig. 3.7. Similar to quartz, the OSL signal shows a complex shape with stimulation time and needs at least three components plus a constant for an approximately reasonable fit:

$$I_{OSL} = a_1 \exp(-\lambda_1 t) + a_2 \exp(-\lambda_2 t) + a_3 \exp(-\lambda_3 t) + c \tag{3.2}$$

The intensity ratio of the three components is approx. 10:1.1:0.9, the respective decay times 0.76 s, 6.61 s and 76.8 s. The dominating fastest component thus has a decay time similar to the decay time of the so called 'fast component' in quartz. Within the framework of this model, stimulation times of 60 s should be sufficient to completely read out the fast and medium component.

The dose response of a chip card module was thus first investigated with this read out parameter, using a simple regeneration protocol, without sensitivity correction and preheat, in the dose range from 0.23 Gy to 9.13 Gy, with a zero-dose and lowest dose recycling point added at the end of the sequence. This resulted in a slightly supralinear dose behaviour, a recuperation signal corresponding to a dose of 300 - 400 mGy and a recycling ratio of approx. 2. It was observed that the fast component could be regenerated up to a small extent after high dose irradiation and optical readout, even during the short time it takes the luminescence reader to move from one OSL measurement step to the next. The amount of regenerated signal can be increased

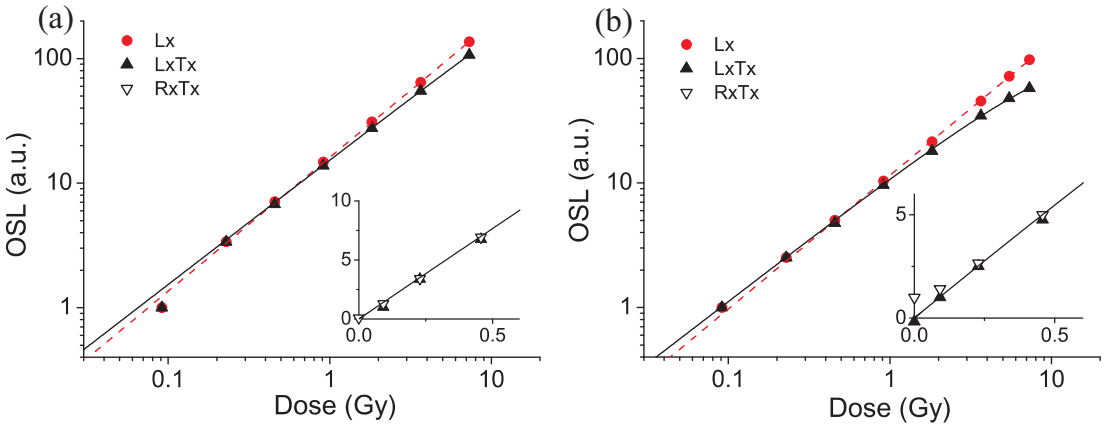

Figure 3.8.: Dose response of the uncorrected (L_X) and sensitivity corrected (L_X/T_X) OSL of a chip card module without preheating (panel a) and with a 10 s@100°C preheat (panel b). The dashed line in both panels is a function of the form $y = a\,D^b$, fitted to the L_X data points, the solid line is a function of the form $y = a\,(1 - \exp(-D/D_0))$, fitted to the L_X/T_X data points. The respective insets show the low-dose data points, including recycling points (L_X/T_X) and zero dose signals, on a linear scale.

by increasing the delay time between the two subsequent OSL measurements. It is speculated that the effect is caused by the slower overall reduction rate of the 100°C TL peak on optical stimulation, which can be either caused by a comparatively low photo-ionization cross section or a high retrapping probability. As a result, part of the remnant electron population in the 100°C TL trap can be thermally released after optical readout and subsequently retrapped into the defects responsible for the fast OSL component, leading to the observed signal recuperation. Consequently, the high level of recuperation could be eliminated by increasing the readout time to 300 s. It is believed that due to the prolonged stimulation time, depletion of the lower temperature OSL traps is sufficient to prevent significant thermal transfer into the fast component traps from one measurement cycle to the next.

The dose response of two chip card modules from 0.09 to 7.3 Gy measured without and with a 10s@100°C preheat is shown in Fig. 7 a+b. A single-aliquot regeneration (SAR) protocol with test dose normalization (0.13 Gy) was used. In both cases, the uncorrected growth curve shows slightly supralinear behaviour ($L_X \sim D^{1.07}$, dashed lines in Fig. 3.8). The sensitivity corrected growth curve (L_X/T_X) can be described by a saturating exponential function (solid lines in Fig. 3.8), with saturation doses D_0 of (9.6 ± 0.7) Gy and (77 ± 13) Gy for modules measured with and without preheat, respectively. Sensitivity changes amount to an increase of 27% and 65% for the highest dose irradiation and for the measurement sequence without and with preheat, respectively. Recycling ratios are generally excellent (< 1.05), except for the 91 mGy dose point, where ratios of 1.3 and 1.4 were observed. This could not be improved by reducing the size of the test dose.

The zero dose OSL measurement following the highest dose measurement shows no recuperation signal for the chip card module measured without preheat, as described above (see inset in Fig. 3.8, a). However, a significant level of signal recuperation is observed for the 10s@100°C preheated sample (inset in Fig. 3.8, b). This is most likely due to the fact that the 100°C TL peak is not completely annealed after a 300 s OSL measurement (Fig. 3.2), so that a subsequent 100°C preheat will provide an effective mean of thermal transfer.

Using the weaker beta source of the TL-DA-12 reader, a dose of 8 mGy could be clearly detected by OSL 3 min after irradiation, if no preheating is applied. From signal analysis a sensitivity of 43 counts mGy^{-1} and three standard deviation of the background as $3\sigma = 137$ counts was determined. This results in an estimated minimum detectable dose of 3.2 mGy immediately after irradiation. If the interpolating function of Fig. 3.6 is used to account for signal fading, the minimum detectable dose is estimated to increase to ~10 mGy and ~20 mGy for readouts 1 day and 10 days after exposure, respectively.

3.1.5. Recommended protocol and dose recovery

The present investigations indicate that the highest radiation sensitivity, lowest zero dose signal and consequently lowest minimum detectable dose and negligible signal recuperation should be obtained by refraining from any preheat treatment and measuring the OSL at room temperature. A comparatively long stimulation time of 300 s is necessary to prevent significant signal recuperation and the SAR protocol with test dose normalization has to be applied, in order to correct for sensitivity changes.

If no preheating is applied, the OSL signal will have an appreciable contribution of shallow traps (Fig. 3.2). The anticipated thermal decay of these traps during storage at room temperature might pose a problem for dose assessment, if, as is usually the case in a real accident, there is a time delay between hours to days between exposure and measurement. Fig. 3.6 demonstrates that the relative signal decay during storage is approx. independent of dose, thus a universal correction curve for signal fading should be applicable. Preheating at 100°C for 10 s will reduce the contribution of shallow traps but will not remove the need for fading correction as the thermally stable traps have been shown to be prone to anomalous fading.

Nevertheless, the high degree of fading of the OSL signal and thus the necessity of using large signal correction factors in an a posteriori dose assessment makes the obtainable accuracy of a dose measurement an issue. To address this, a dose recovery test was performed: six sets of chip card modules were each given doses of 0.18, 0.68, 1.36 and 2.72 Gy. Two sets were then measured immediately after irradiation, two about one day and two about 6 days after irradiation, using either no or a 10s@100°C preheat. The same five regeneration doses between 0.23 Gy and 4.5 Gy, a zero dose, lowest dose recycling point and a test dose of 0.23 Gy was used for all measurements, irrespective of the expected dose. This was done to additionally check how well a standardized protocol could recover a range of doses. The first four seconds and the interval from 12 to 14 s of the OSL signal were integrated for determination of signal

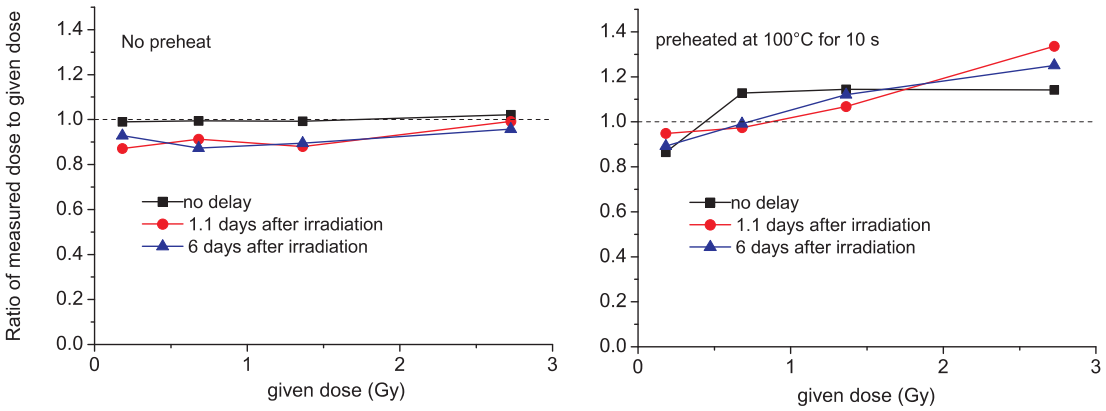

Figure 3.9.: Dose recovery test for six different sets of chip card modules, stored for different durations at room temperature and measured with and without preheat.

and background, respectively. Results are shown in Fig. 3.9.

For the samples measured immediately after irradiation, where no signal correction is necessary, the measurement approach without preheat yields significantly better results than the preheated samples. This clearly demonstrates that the OSL properties are best defined if the chip card modules are not subjected to any kind of thermal treatment. For the samples measured one and 6 days after irradiation both approaches perform on an equally acceptable level. Obviously, the systematic uncertainty of the fading correction dominates over systematic uncertainties introduced by the measurement protocol. Except for the 2.72 Gy irradiated sample measured with 10s@100°C preheat, all measured doses lie within ±14% of the given dose.

3.1.6. Optimization of the protocol

The requirements for this project were to develop methods of retrospective dosimetry, which allow individual dose assessment using personal objects within one day. The measurement of one chip card using the protocol described in the previous section takes a little more than one hour and thus certainly meets this requirement. In terms of optimized capacity in a real accident scenario, where a large number of samples have to processed in the shortest amount of time possible, the present protocol is on the other hand far from optimal. In the ideal case, one would like to do a rapid screening of the samples at first with lower precision, to sort out the probably majority of cards exposed with no dose or a dose below the detection limit and thus not showing any signal and then to do a more precise and time consuming dose assessment only on those samples with a significant dose. As a luminescence measurement generally leads to the loss of the stored information and a re-investigation at some later time is not possible, the rapid assessment of the exposure signal must still allow a precise later dose measurement using that same signal.

In section 3.1.5 it was observed that the fast and medium component of the OSL curve

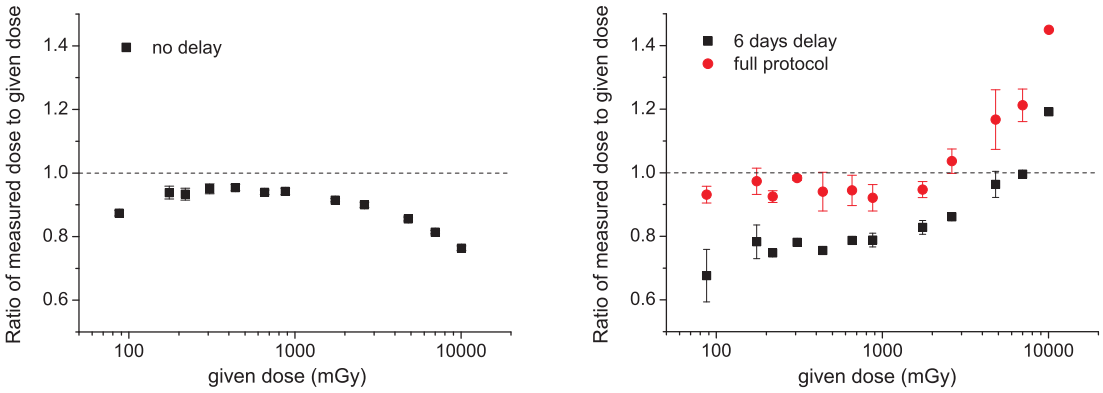

Figure 3.10.: Test of a time optimized protocol for rapid dose assessment with chip cards. The left panel shows the results of dose measurements immediately after irradiation, using an OSL readout time of 30 s and a single, 1 Gy calibration point. Six modules were measured per dose point and the average and standard deviation plotted (total number of 60 modules). The right panel displays the results for dose measurement six days after irradiation, with fading correction. Three modules were measured per dose point (total number of 36 modules). The red, circle symbols denote the later measurement of the same modules using a full, extended protocol, similar to the one described in section 3.1.5 (approx. 1 hour measurement time per module).

decay within 30 s and that the long readout times of 300 s are mainly necessary to allow the construction of a precise, high resolution calibration curve. Similarly, sensitivity correction is only needed in the course of several cycles of dosing and measurements, within the first two cycles sensitivity changes are generally small and can be neglected. Thus for a first, crude estimation of the absorbed dose it should be possible to reduce the readout time to 30 s, omit the test dose normalization and use only one calibration point. Such an approach would allow the measurement of up to 30 chip cards per hour, in comparison to only one per hour. This was examined using the chip card modules provided by Infineon Technologies, applying simulated accident doses between 90 mGy and 10 Gy and always using a single calibration dose point of 1 Gy without any test dose normalization. Two set of modules were used, one measured immediately after irradiation and the second one 6 days after irradiation. The first ten seconds and the interval from 10 to 20 s of the OSL signal were integrated for determination of signal and background, respectively. For the second set of modules the samples were then re-measured some time later, using an extended protocol with 300 s readout time, test dose normalization, four regeneration doses, a zero dose and lowest dose recycling point, similar to the protocol described in 3.1.5. A second dose was then calculated using the initial 30 s OSL measurement and the extended calibration curve (Fig. 3.10).

As expected, for measurements promptly after irradiation, the accuracy obtained with the rapid protocol is not as good as when applying an extended protocol, such as in Fig. 3.9. However, the results are still acceptable: for doses up to approx. 1 Gy, the measured dose is within 10% of the applied dose. For higher doses there is a systematic

decrease in the measured dose, but even for 10 Gy the underestimation is still only 25%. This would be fully acceptable as a first screening result. The underestimation is probably due to the previously described thermal transfer at room temperature from the 100°C TL trap into the trap(s) responsible for the fast OSL components, as a result of the short OSL stimulation time, leading to a too high calibration dose signal and thus to a somewhat too low inferred dose. This effect will be more pronounced for higher accident-calibration dose ratios, as observed.

For the measurement six days after irradiation, the performance of the rapid protocol is somewhat poorer, but still acceptable. For 90 mGy the measured dose is 75% of the given dose, for 200 mGy to 1 Gy around 80% and for higher doses the ratio systematically increases from 80% up to 120% (10 Gy). The subsequent application of the extended protocol leads to a significant improvement in accuracy for doses up to approx. 3 Gy but also to an increase in the overestimation for higher doses (40% for 10 Gy). Obviously, similar to Fig. 3.9, a systematic effect/error of the fading correction reverses the otherwise expected decrease of the measured dose with the rapid protocol for higher doses. This systematic effect might be that the fading correction curve, discussed in section 3.1.3, is no longer even approximately dose independent for doses higher than 3-4 Gy and that as a consequence, the applied fading correction factor in Fig. 3.10 is somewhat too high. The possibility of such an effect is indicated in Fig. 3.6, where it can be seen that the OSL signal of the 9.13 Gy irradiated module shows a continuous smaller degree of fading than the signals of all the other modules. This possibility needs to be further investigated in detailed studies but for the present project a pragmatic conclusion is that for doses higher than 3 Gy, the application of the extended protocol following the rapid dose assessment does not lead to an improvement in accuracy and is thus not recommended.

3.1.7. Luminescence mechanisms and trapping parameters

So far the investigations on chip cards were driven by the aim of understanding the dosimetric properties to such a degree as to be able to develop a suitable measurement protocol for emergency dosimetry. (Having established this goal...) The luminescence properties turned out to be relatively complex and interpretation of the results were done considering the physical properties but still on a qualitative level. This section will give results on trying to understand the luminescence mechanism also on some, albeit simplified, quantitative level, with particular focus on the origin of the zero dose signal and trapping parameters.

For recapitulation, fig. 3.11 gives the glow curves of an unexposed, irradiated and regenerated chip card module. Comparison of the former two glow curves reveals the existence of at least three peaks (I, II, III), with peak temperatures of approx. 100°C, 170°C and 200°C (2°C s^{-1} heating rate). Also shown is the difference in OSL signal of an unexposed module when stimulating at room temperature or at 100°C and a pure phosphorescence signal at the same temperature.

Obviously the combined effect of optical and isothermal stimulation leads to a much stronger effect than both of the stimulation modes alone and also leads to an apparent

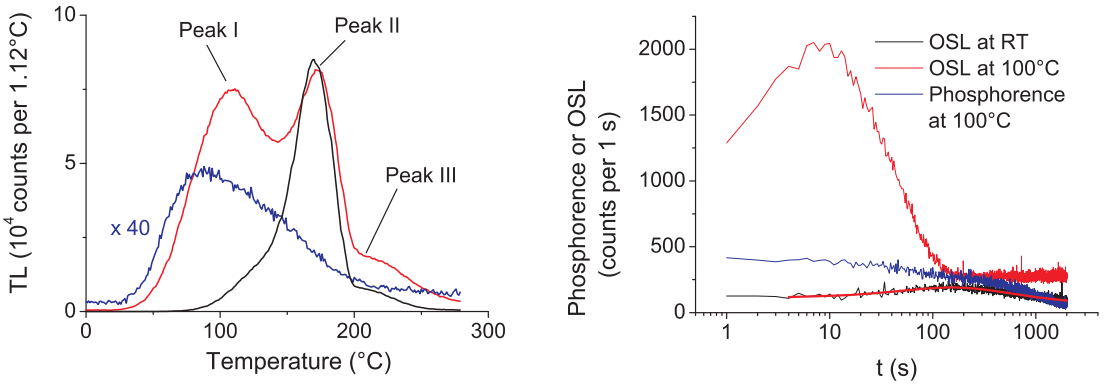

Figure 3.11.: Left panel: TL glow curve of an unexposed chip card module (black line), a module irradiated with 9.3 Gy (red line) and a 1 Gy regenerated glow curve, all measured in the blue wavelength range (compare Fig. 3.2). The clearly identifiable peaks in the glow curve of the irradiated module are indicated and numbered. Right panel: Comparison of the OSL signal of an unexposed chip card module at room temperature and at 100°C with the phosphorescence signal at 100°C of a similar unexposed module.

steady-state signal for long stimulation times. To simplify the situation for quantitative analysis only thermal effects are studied in the following. Under the assumption that the same defects are active in both TL and OSL (see section 3.1.1), the results from thermal studies will have a relevance for the OSL traps as well. In the first set of experiments, the phosphorescence of unexposed chip card modules was measured at temperatures between 50°C and 220°C (Fig. 3.12).

Similar to OSL the phosphorescence shows the overlapping of build-up and decay components at temperatures between 50°C and 100°C and only decay components for temperatures between 160°C and 220°C. The data in Fig. 3.12 could be well fitted using the following expression (compare eq. 3.1).

$$I_{Ph} = \pm a_1\, e^{-\lambda_1 t} + a_2\, e^{-\lambda_2 t} + a_3\, e^{-\lambda_3 t} + c\,, \tag{3.3}$$

with I_{Ph} (s^{-1}) being the intensity of the Phosphorescence signal, t (s) the measurement time,$\lambda_{1,2,3}$ (s^{-1}) respective decay (or build-up) constants of the three components, $a_{1,2,3}$ (s^{-1}) the (relative) intensity of the three components and c (s^{-1}) a constant. For the fitting c was fixed to the instrumental background (45 counts s^{-1}). For the datasets up to temperatures of 120°C a_1 was negative, reflecting the build-up term of equation 3.1, for higher temperatures a_1 was positive (pure decay). This observation strengthens the hypothesis that the origin of the zero dose signal in OSL and in phosphorescence is charge carrier production in the epoxy, presumably by thermo-optical bond breaking and subsequent diffusion into the silica grains, where luminescence is produced. It is interesting to note, that the remaining TL signal, recorded after completion of the respective phosphorescence measurement (bottom right panel in Fig. 3.12) shows a strong reduction or almost complete removal of the previously predominating 170°C

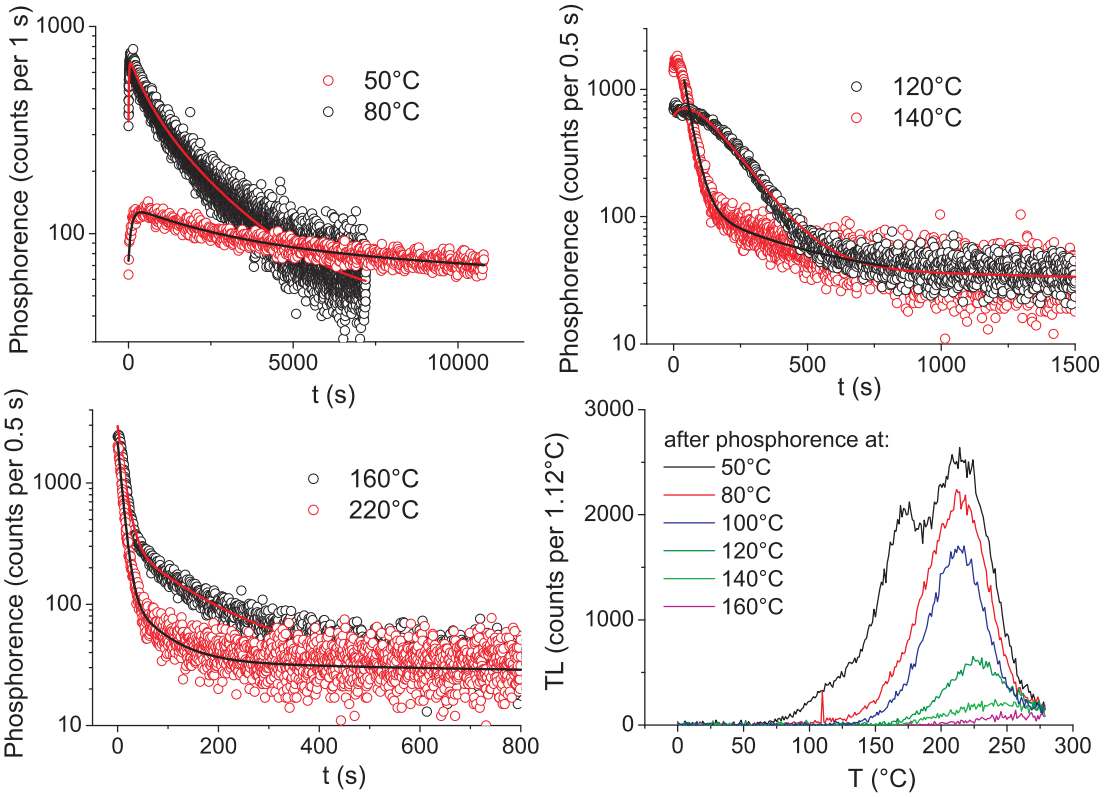

Figure 3.12.: Selected plots of the phosphorescence of unexposed chip card modules measured at various elevated temperatures. For 120°C - 220°C, phosphorescence was measured for longer times than displayed here. The bottom right plot shows the TL glow curves recorded after completion of the respective phosphorescence measurements. All measurements were done in the blue wavelength range (Filters used: 7-59 and HA3).

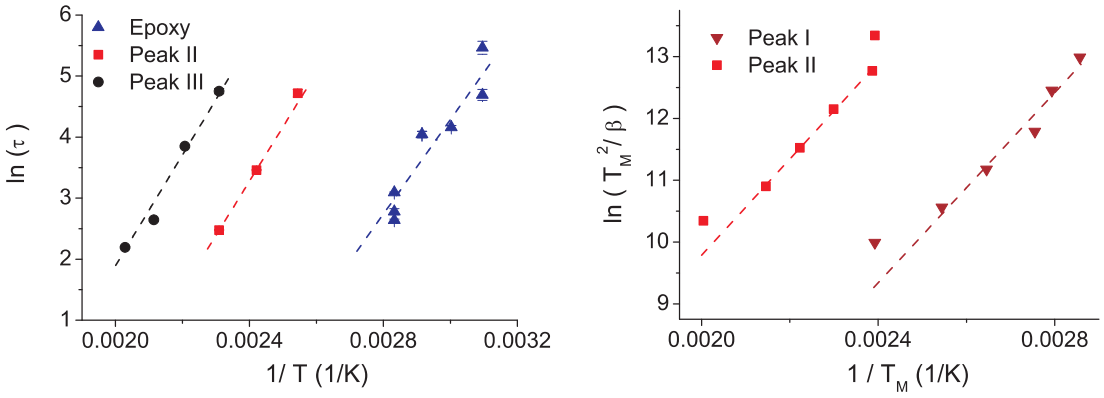

Figure 3.13.: Analysis of trapping parameters resulting from the analysis of the phosphorescence curves (left plot) and of the method of various heating rates (right plot) for the different peaks indicated in figure 3.11 and the presumed epoxy signal. At the highest heating rate (8°C s-1) the peaks become very broad and the peak temperature is no longer clearly identifiable leading to a possible bias in the estimated value in addition to the possible effect of thermal lag. Therefore these data points were excluded from analysis.

Peak (see for comparison Fig. 3.11), even after comparatively low temperature treatment (50°C and 80°C). Such an effect is unexpected from normal "crystalline" kinetics and e.g. is not observed for similar peak temperatures in crystalline quartz. It is a first indication that kinetics might be different for this amorphous material.

For the development of a simplified quantitative model, the trapping parameters (activation Energy E and frequency factor s) of the tree TL peaks were determined by using the fitting results of the phosphorescence decay curves and by applying the method of various heating rates (Chen and McKeever, 1997) to unexposed, 10 Gy irradiated before measurement and 10 Gy regenerated chip card modules. The regeneration approach was done on the same module while a fresh module was used for each heating rate for the unexposed and 10 Gy before measurement approach. If the build-up term of equation 3.3 ($-a_1\, e^{-\lambda_1 t}$) is interpreted as the thermal release of charge carriers from the epoxy, then the parameters for this process can be determined as well. Results are given in Fig. 3.13 and table3.1.

As this analysis is only meant to give an order of magnitude estimate, an error calculation was not attempted. For the same reasons the exact numerical values should not be over-interpreted. However, it is striking that regardless of peak temperature and employed method of analysis the obtained activation energies and frequency factors are unusually low, in the range of 0.6-0.8 eV for E and $10^6 - 10^8 \mathrm{s}^{-1}$for s. This is in sharp contrast to the crystalline modification of SiO_2, quartz, for which the corresponding parameters for similar peaks (at 110°C, 160°C and 210°C) lie in the range of 1.0-1.5 eV for E and $10^{12} - 10^{14}$ $\mathrm{s}^{-1}$for s (Woda et al., 2011; Veronese et al., 2004 and Spooner and Questiaux, 2000). As a consequence, although peaks II and III appear at higher temperatures, they are thermally unstable at room temperature (last column in Table

Peak	Method	E (eV)	s (s^{-1})	$T_{1/2}$(d)
Epoxy	ID	0.67	1.6×10^8	0.02
I	VHR	0.66	6.9×10^7	0.03
		0.68	1.7×10^8	0.03
II	VHR	0.66	2.5×10^6	1.1
	ID	0.77	7.0×10^7	1.7
III	ID	0.78	1.1×10^7	19.6

Table 3.1.: Trapping parameters and half lifes at 20°C of the defects involved. The upper parameters for peak I were measured with chip card modules irradiated with 10 Gy before measurement, the lower value with thermally annealed, 10 Gy regenerated and 60°C preheated (at 2°C s^{-1}) modules. The abbreviations for the methods employed are: *ID*: isothermal decay, *VHR*: various heating rates.

3.1). This would also, at least qualitatively, explain the unusual glow curve results obtained after the phosphorescence measurements at lower temperatures mentioned above (Fig. 3.12). At 50°C half lives of peaks I, II and III are calculated as 0.06 h, 2.24 h and 27 h, respectively. At 80°C these values lie at 0.008 h, 0.29 h and 2.5 h, respectively. The TL glow curve after heating at 50°C for 3 hours should thus show a roughly 50% reduced Peak II and almost no reduction of Peak III. After heating at 80°C for 2 hours, Peak II should be completely annealed and Peak III significantly reduced. This is what is observed, although not quite to the same numerical extent as predicted. It should be kept in mind that the methods of analysis employed (fitting of a triple exponential decay and method of various heating rates) have some simplifying assumptions, which are not necessarily met in glassy materials and thus it is not expected that the results are highly accurate.

Having determined the set of trapping parameters for the system, it was next attempted to reproduce, at least on a qualitative level, the main features of the phosphorescence signal of unexposed chip card modules using a simple energy level model, frequently used in thermoluminescence analysis of crystalline and sometimes also amorphous materials (Chen and McKeever, 1997), with some modifications to consider, in a simplified approach, the interaction of the epoxy resin and the silica grains. The model consists of three trapping states (corresponding to Peaks I to III), one recombination center and a thermally activated injection of a finite reservoir of electron-hole pairs from the epoxy into the conduction and valence band. Simultaneous thermal eviction and retrapping is considered for the traps, while simultaneous trapping of holes and recombination with electrons from the conduction band is considered for the recombination center. The governing rate equations for this process then are:

$$\begin{aligned}
\frac{dn_i}{dt} &= A_{ni}\,(N_i - n_i)\,n_c - s_i \exp\left(-\frac{E_i}{k\,T}\right) n_i \\
\frac{dm}{dt} &= B_m\,(M - m)\,n_v - A_m m\,n_c \\
\frac{dn_v}{dt} &= R\,(t) - \frac{dm}{dt} - A_m m\,n_c \\
\frac{dn_c}{dt} &= \frac{dm}{dt} + \frac{dn_v}{dt} - \sum_{i=1}^{3} \frac{dn_i}{dt}
\end{aligned} \tag{3.4}$$

with i=1,2,3. N_i (cm^{-3}) is the concentration of the electron traps, n_i (cm^{-3}) the concentration of trapped electrons, M (cm^{-3}) the concentration of hole traps, m (cm^{-3}) the concentration of trapped holes, n_c (cm^{-3}) the concentration of electrons in the conduction band, n_v (cm^{-3}) the concentration of holes in the valence band, A_{ni} ($\mathrm{cm}^{-3}\ \mathrm{s}^{-1}$) the transition coefficient for electrons from the conduction band to the electron trap, B_m ($\mathrm{cm}^{-3}\ \mathrm{s}^{-1}$) the transition coefficient for holes from the valence band to the hole trap, A_m ($\mathrm{cm}^{-3}\ \mathrm{s}^{-1}$) the recombination transition coefficient for electrons in the conduction band with holes in centres, s_i (s^{-1}) and E_i (eV) the frequency factor and activation energy of the electron traps, respectively, k (eV) the Boltzmann constant and finally $R(t)$ ($\mathrm{cm}^{-3}\ \mathrm{s}^{-1}$) the time-dependent injection rate of electron-hole pairs (by diffusion) from the surrounding epoxy resin into the silica grains. This latter quantity is assumed to be thermally activated and can be described as:

$$R(t) = R_0 \exp\left[-s_R \exp\left(-\frac{E_R}{k\,T}\right) t\right], \tag{3.5}$$

with R_0 ($\mathrm{cm}^{-3}\ \mathrm{s}^{-1}$) being the initial diffusion (or production) rate and s_R (s^{-1}) and E_R (eV) the frequency factor and activation energy of the thermally driven charge carrier production in the epoxy. Charge conservation is implicitly contained in the last line of equation 3.4. Phosphorescence is defined in its usual form as:

$$I_{Ph}(t) = -\eta\,\frac{dm}{dt}, \tag{3.6}$$

with η being a (possibly temperature dependent) luminescence efficiency factor. For the simulations η was assumed as 1. An energy level scheme of the model is depicted in figure 3.14.

For a numerical solution of the rate equations (using the software Mathematica ®) the transition coefficients and trap concentrations have to be guessed. This was aided by using reported values for quartz in the literature as starting values an optimizing them so as to arrive at a qualitatively similar simulated signal as the experimental one. The best level of agreement for the phosphorescence signal at 80°C is shown along with chosen parameters in Fig. 3.15.

As can be seen, the model is able to reproduce the principal exponential build-up

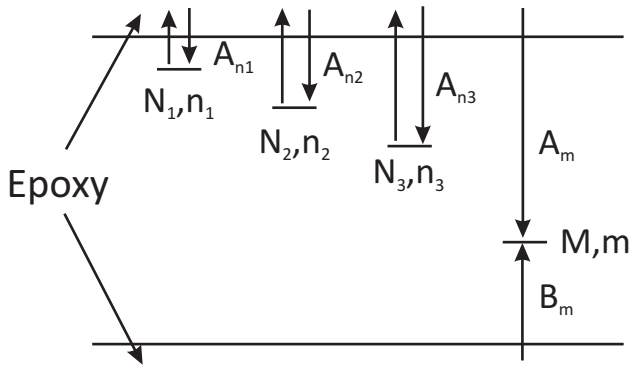

Figure 3.14.: Energy level scheme used in the model of phosphorescence of unexposed chip cards. For explanation of symbols see text.

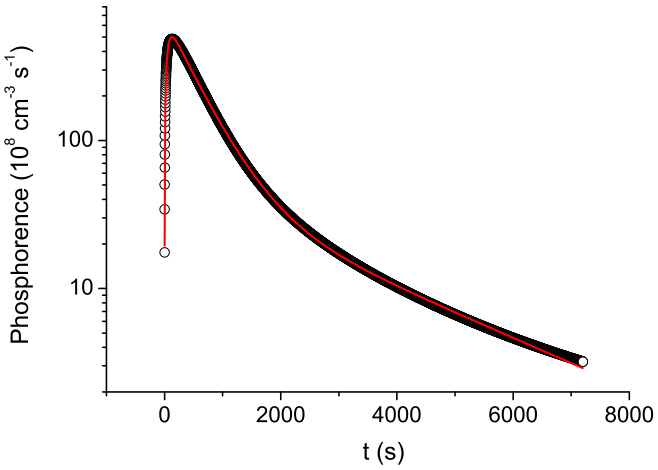

Figure 3.15.: Simulated phosphorescence at 80°C for unexposed chip card modules. The following parameters were used: $R_0 = 10^{11}\,\mathrm{cm^{-3}\,s^{-1}}$, $E_R = 0.76$ eV, $s_R = 1.6 \times 10^8\ \mathrm{s^{-1}}$, $N_1 = 10^{13}\,\mathrm{cm^{-3}}$, $N_2 = 4 \times 10^{13}\,\mathrm{cm^{-3}}$, $N_3 = 7 \times 10^{12}\,\mathrm{cm^{-3}}$, $M = 10^{14}\,\mathrm{cm^{-3}}$, $A_{n1} = A_{n2} = 10^{-9}\,\mathrm{cm^{-3}\,s^{-1}}$, $A_{n3} = 8 \times 10^{-10}\,\mathrm{cm^{-3}\,s^{-1}}$and $A_m = B_m = 10^{-8}\,\mathrm{cm^{-3}\,s^{-1}}$. For s_1, s_2, s_3 and E_1, E_2, E_3 the values from table 3.1 were used. The red line is a fit of function 3.3 to the dataset, with c set to 0.

and decay characteristics of the experimentally observed phosphorescence signal, with similar decay constants but different relative intensities $a_{1,2,3}$ of the three components of equ. 3.3. However, it was found necessary to increase the activation energy ER of the epoxy somewhat, from 0.67 to 0.76 eV. This is because the I don't know really what. As a consequence, direct determination of the activation parameters of the epoxy from analysis of the phosphorescence possibly delivers slightly underestimated results.

In summary, from analysis of the OSL signal at room and elevated temperature and after different preheatings, from analysis of the phosphorescence at different temperature and from the model results, it seems that the origin of the zero dose signal lies in the epoxy and interaction with the silica and not in remnant charge populations in deep traps in the silica grains. Although all experiments and analyses thus give a consistent picture, it should not be overlooked that a main problem lies in the low activation parameters and corresponding half live at room temperature of the epoxy (Table 3.1). Thus the complete emptying of the reservoir of electron-hole pairs should be accomplished within hours after production and the subsequent filling and complete emptying of the relevant traps well within a few months. As the chip card modules were produced in 2006 and measured between 2008 and 2009, no more zero-dose signal should have been observable. A possible explanation for this apparent contradiction is that the thermal release of electron-hole pairs from the epoxy is not continuously dependent on temperature as eq. 3.5 suggests but that there is a threshold temperature between room temperature and 50°C, below which no thermal eviction takes place. An alternative, and perhaps more realistic explanation is that eq. 3.5 is a too course description of a much more complex process and that in particular the extrapolation to room temperature is not adequate and delivers underestimated results. This would leave the principal property that the zero dose signal decreases with time elapsed since production untouched, it would just correct the perhaps unrealistic small timescale inferred from the decay analysis at elevated temperatures. An indication that this might be true comes from the results of measuring additional chip card modules from the same production batch in early 2011. The intensity of the zero dose signal of these modules has clearly decreased in comparison to the modules measured in 2008, with a stronger decrease for the 170°C peak than for the 210°C peak.

It should also be noted, that the same parameters and model which could in principle describe the phosphorescence of unexposed chip card modules failed at reproducing the corresponding TL glow curves of Fig. 3.2. In addition, it has been observed in previous studies (Barkyoumb and Mathur, 2008; Göksu et al., 2003, Göksu et al., 2007) and also in this project, that the zero dose signal in TL recovers up to certain degree after readout and storage in dark at room temperature for several days, a feature which the present models also clearly is unable to predict. Obviously, the physical reality is much more complex than the simplistic approach can describe. Nevertheless, models as the one developed here are very useful in demonstrating that some observed effects are at all possible and that the interpretation of the experimental results could potentially be correct.

A final comment is made on the unusual low values for E and s in Table 3.1. Normally

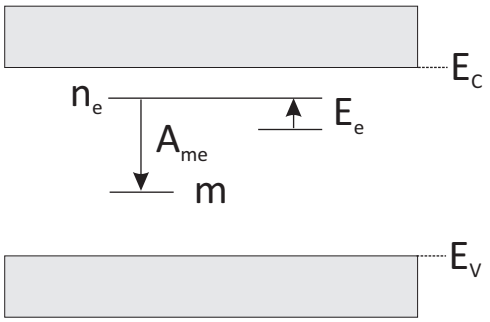

Figure 3.16.: Model of direct recombinations. E_e is the energy difference from the ground state to the excitet state of the electron in the trap, ne the concentration of trapped electrons in the excited state and Ame the transition coefficient for direct recombinations. Adapted from Chen and McKeever (1997).

one would expect the frequency factor to be in the same order of the lattice vibrations, in the range of 10^{12} to 10^{14} s^{-1} (McKeever, 1985). Order of magnitude lower values for s can be explained within the model of direct recombinations (Chen and McKeever, 1997 and Fig. 3.16).

In this concept, electrons have the possibility of directly recombining from the trap to a neighbouring recombination center via an excited state with excitation energy E_e, without going via the conduction band. Detailed kinetic analysis shows that this process follows an apparent first order kinetics law with the glow curve having the same shape as if the recombination pathway would be via the conduction band, but that the energy measured is not the trap depth but the excitation energy E_e and that the apparent frequency factor s is not the true frequency factor but the transition probability for direct recombinations. For this latter quantity much lower values than for s are possible, down to 10^{-5} s^{-1}(Chen and McKeever, 1997). The three peaks I, II, III observed in the TL of chip card modules could then all be from the same type of trap with the same excitation energy E_e but different (increasing) spatial separation between trap and recombination center leading to decreasing transition probabilities for direct recombinations, and thus for the apparent value of s. Whether this model is true for silica grains and leads to a better agreement between simulated and observed phosphorescence and TL glow curves remains to be investigated.

Irrespective of the true nature of the recombination pathways, the experimental fact of the low values for the trapping parameters opens a different possible view on the the long-term OSL signal stability at room temperature, investigated in section 3.1.3. Fig. 3.17 shows the decay of the OSL signal of chip card modules irradiated with 0.94 Gy with storage time. For comparison, the data were fitted with the lin-log relationship typical of anomalous fading and with the triple exponential decay function (eq. 3.3) with λ_i calculated from the trapping parameters listed in Tab. 3.1 and kept fixed during iterations.

Both models describe the data equally well in some parts and show some discrepancies in other parts. Thus the data can be also interpreted as being caused by pure thermal

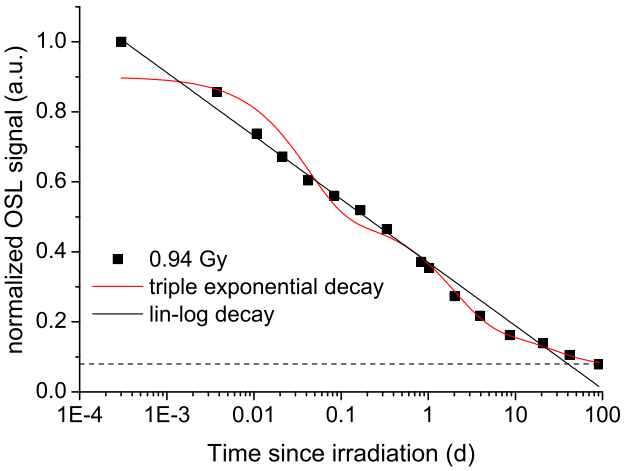

Figure 3.17.: Comparative description of the fading of the OSL signal of the chip card modules irradiated with 0.94 Gy (Fig. 3.6) using either a linear-log decay function of the form given in Fig. 3.6 (black line) or a triple exponential decay function plus constant (red line). For the latter, the decay constants were calculated from Table 3.1 and kept fixed during the fitting. The dashed line indicates the constant.

fading and not anomalous fading, as suggested in section 3.1.3. This would open the possibility of isolating thermally more stable components by appropriate preheating. For this, the thermal analysis should be confirmed directly for the OSL signal and not indirectly from the phosphorescence and TL signals. In addition, thermal pretreatment has been shown not be advantageous for an accurate dose measurement. This could possibly be circumvented by extended preheating at lower temperatures. It will be up to future studies to find out, which mechanism is definitely responsible for the signal fading and to find the optimum compromise between accuracy in calibration, speed of response and isolation of thermally sufficiently stable signals.

3.1.8. Conclusions

Although the response of the investigated wire-bond chip card modules to irradiation, thermal and optical stimulation is relatively complex and many mechanisms are not yet fully understood, the potential of OSL for retrospective and accident dosimetry has clearly been demonstrated. The minimum detectable dose is estimated at ~3 mGy, ~10 mGy and ~20 mGy for readouts immediately, 1 day and 10 days after exposure, respectively. Considering the appreciable contribution of thermally unstable traps to the overall OSL signal when measuring without preheat, the results of the dose recovery test using a dose independent fading correction are remarkable and very encouraging. Nevertheless, the fading rate at high doses requires additional attention in the future.

On the other hand, the usefulness of a low preheat approach deserves further investigation, as kinetic analysis have shown that this could potentially lead to the isolation of thermally more stable signals and in addition would reduce uncertainties introduced by variable ambient temperatures between radiation exposure and dose assessment.

3.2. Wire-bond chip card modules with molding

All chip cards studies so far have a translucent encapsulation, which however is less frequently encountered when security relevant chips are used. In this case molding technology is often applied, where a thermosetting plastic composition is injected around the chip with pressure and high temperature, resulting in a black, nontransparent encapsulation. This at first seems to preclude the application of any luminescence dosimetry method but the high amount of silica powder used as filler (up to approx. 80%) indicates that there still could be some potential of these kind of chip card modules for emergency dosimetry.

3.2.1. Materials

Investigations were carried out on sample tapes of molded encapsulations without or with mechanically broken chips (for security reasons). Contact-based and contactless modules were studied, the latter finding potential use in electronic documents (e.g. electronic passports, electronic identity cards). Measurements were conducted on intact, on mechanically crushed (in an agate mortar) as well as on chemically dissolved modules using fuming HNO_3. Contactless modules could be dissolved at room temperature within a few minutes, whereas for contact-based modules heating of the $HNO_3$to 70-80°C is necessary. In first experiments this was achieved using a heating plate while taking care to prevent superheating and boiling over. Complete dissolving of the module was then achieved within 6-10 minutes. For greater control of the actual temperature at the sample, subsequent experiments were carried out using a heatable ultrasonic bath and setting the temperature to 80°C. After several cycles of dilution and careful decanting, the samples were washed in acetone and directly pipetted onto the measuring cup. For dose-recovery tests, intact modules were irradiated with ^{137}Cs at the Secondary Standard Dosimetry Laboratory (SSDL) of the Helmholtz Zentrum München, in a Perspex holder with 6 mm wall thickness. Accounting for the attenuation in the holder, the air kerma was 475 mGy and this was treated as the unknown accident dose. Modules were then prepared under subdued red light conditions (also for testing for zero dose signals). Examples of the different kind of chip card modules are given in Fig. 3.18.

The value for the dose rate of the built-in ^{90}Sr/^{90}Y source of the OSL reader should be readily adoptable for the extracted silica but might be somewhat too high for the intact module due to stronger attenuation in the 500 µm thick and 80% silica filled epoxy and the silicon chip. Unless stated otherwise, OSL decay curves were integrated for the first 6 s and for 6–12 s for determination of signal and background, respectively.

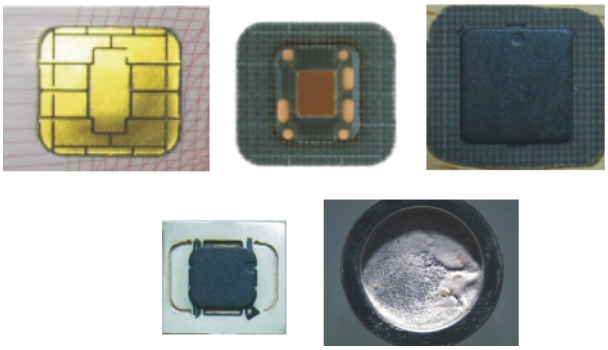

Figure 3.18.: Examples of chip card technologies. From top left to bottom right: Typical front side of a contact-based chip card module found on debit cards. Back side of the same module revealing a UV-cured translucent encapsulation. Back side of the same type of module but with molded encapsulation. Contactless module with molding, potentially found in electronic documents. Measuring cup with chemically extracted filler material (silica) of a contact-based molded encapsulation.

TL measurements were made on the same reader using a heating rate of 2°C s^{-1}.

3.2.2. Zero dose signal and correlation between TL and OSL

Similar to UV-cured translucent encapsulations, a zero-dose signal is observed in TL, peaking around 175°C but roughly corresponding to a dose of only 1 Gy at the higher temperature side, as compared to more than 40 Gy for UV-cured encapsulations (Fig. 3.19 and Woda and Spöttl, 2009). This difference might be attributable to the exposure of the epoxy to higher temperature during hardening for the molding technology as compared to the hardening at room temperature for the UV-cured encapsulations. A subsequent irradiation with 1 Gy produces a broad signal structure with peaks around 80°C and 140°C. A zero dose signal is not observed in OSL for the intact and chemically dissolved module (Fig. 3.19), but a short lived signal is observed for the mechanically crushed sample (not shown), roughly corresponding to 200 mGy. For this reason, the latter technique was not further pursued. Extracting the silica increases the sensitivity by a factor of 40-100, as compared to the intact module. It also results in an increase of the fast component of the OSL decay curve, presumably due to a reduced attenuation of stimulating and emitted light as compared to the intact module (Fig. 3.19).

Fig. 3.20 a demonstrates that the defects responsible for the TL emissions are also photo-active in the temperature region up to approx. 250°C, with a possible faster depletion on the lower temperature side, leading to an overall shift in peak temperature with optical stimulation time towards higher temperatures. Similar results were observed for the 190°C TL peak in alumina rich electronic components from portable electronic devices (Woda et al., 2010). Defects responsible for the higher temperature emission above 250°C seem to be comparatively insensitive to blue photon stimulation. On the other hand the defects responsible for the OSL emissions are thermally sensitive

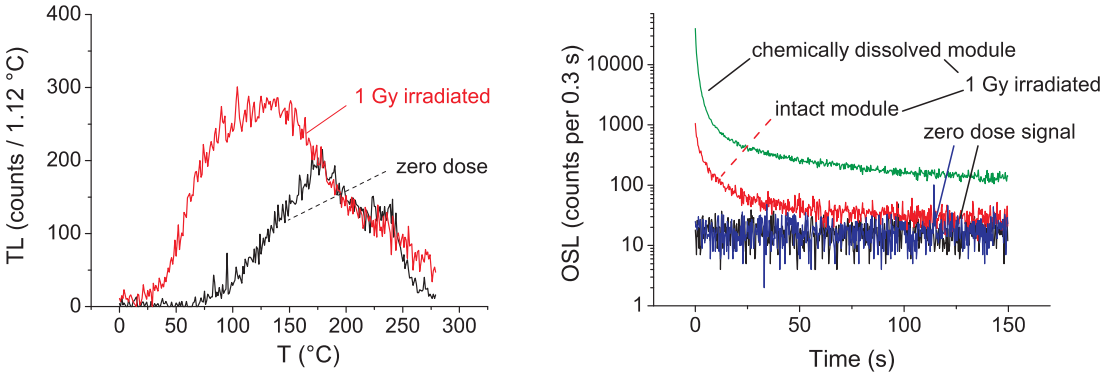

Figure 3.19.: Zero dose and radiation induced signals of a contact-based module in TL (upper panel) and OSL (lower panel). For OSL, the zero dose signal of the intact and chemically dissolve module are identical. OSL measurements were done at room temperature with no preheat applied.

in a very similar region (50-250°C) in which the optically active TL signals occur (Fig 3.20, upper right, the same heating rate was used for the OSL pulse anneal curve as for recording the TL glow curve). Thus it might be that the same defects are involved in TL up to approx. 250°C and OSL. As a consequence the OSL signal has an appreciable contribution from thermally relatively unstable traps, similar to silica in UV cured encapsulations (Woda and Spöttl, 2009).

A somewhat more detailed view of the correlation between OSL and TL is given in the lower two panels of Fig. 3.20. The OSL pulse anneal curve can be well interpolated using a fourth order polynomial regression. There is almost no difference in the fit if higher polynomial orders are used (Fig. 3.20, upper right). By differentiating the polynomial expression(s), a numerical derivative of the OSL pulse anneal curve is obtained. As the area under the OSL decay curve is proportional to the number of trapped electrons n, the derivative will be proportional to $^{dn}/_{dt}$ and thus this will give a TL-like representation of the thermal stability of the OSL traps. Comparison with the actual glow curve in Fig. 3.20, lower left panel, shows that, as expected, the OSL "glow curve" lies in the same region as the main TL signal but that is peaks at a higher temperature, around 200°C, as compared to the TL glow curve, which shows two peaks around 80°C and 150°C (compare also Fig. 3.2). This implies that the OSL signal, if integrated within the limits given in 3.2.1, will have less contribution from the more shallow, thermally less stable traps in the temperature region between 50-100°C and a higher contribution from deeper, thermally more stable traps around 200°C than the TL glow curve indicates. Finally, the lower right panel in Fig. 3.20 demonstrates that there is a clear positive correlation between the loss in TL signal due to optical stimulation and the intensity of the observed OSL signal for different stimulation times and two modules and that in addition for one module this correlation is strictly a direct proportionality.

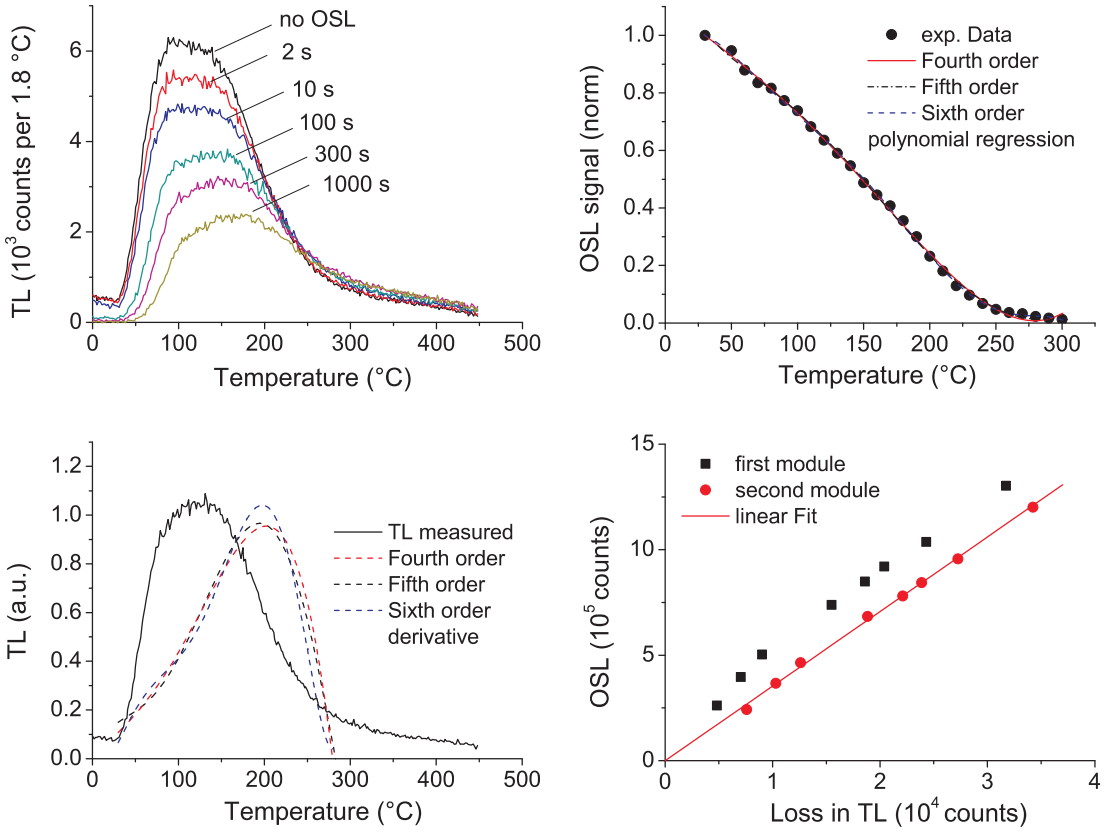

Figure 3.20.: Effect of optical stimulation using the blue LEDs on the TL glow curve of a contact-based module (upper left panel). Measurements were done on a single aliquot of extracted silica, after several cycles of dosing and TL readout to ensure constant sensitivity. Pulse anneal curve of the OSL signal on the same aliquot (upper right panel). The aliquot was immediately cooled after reaching the respective temperature and OSL subsequently measured at room temperature. A fourth, fifth and sixth order polynomial was fitted to the data points. Applied dose before each OSL/TL measurement was 2.5 Gy. Comparison of the TL glow curve with the derivatives of the polynomial expressions (lower left panel). Comparison of the OSL signal and loss in TL signal for two modules and different optical simulation times (lower right panel). A line through origin is fitted to the second module data points (red circles).

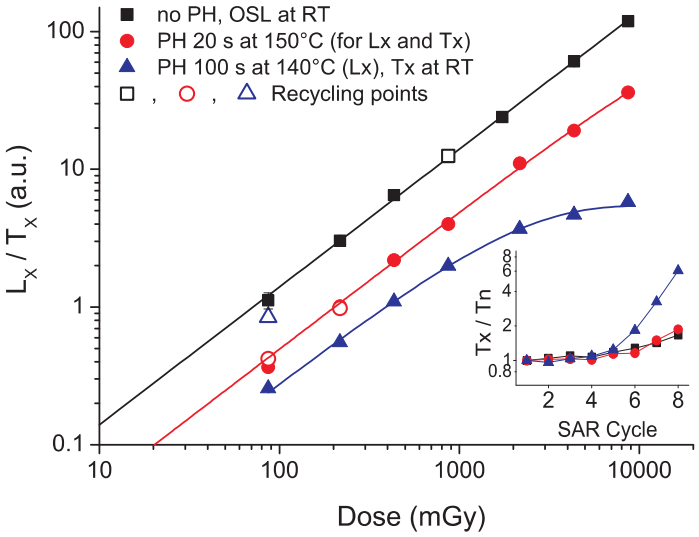

Figure 3.21.: Dose response of an intact contact-based module (close squares) measured at room temperature without preheating and of the extracted filler material, with either preheating at 150°C for 20 s (closed circles, Test dose measurement at same condition) or at 140°C for 100 s (closed triangles, OSL measurement at room temperature, Test dose measurement at room temperature without preheating). Recycling points are plotted in the respective open symbols. A straight line was fitted to the intact module data, while exponentially saturating functions were fitted to the extracted filler data. Saturation dose for the 150°C data is 63 Gy. The inset shows the respective sensitivity changes.

3.2.3. Dose response

For intact modules the dose response is linear up to 10 Gy, when measuring OSL at room temperature and applying no preheat treatment. For chemically dissolved modules a preheat is necessary to account for the heating during the dissolving process. Preliminary results from isothermal decay experiments indicate that a short heating for 100 s at 140°C or for 20 s at 150°C has the same effect as a prolonged heating at 100°C for 15 min. The latter was used as an upper (conservative) estimate of the actual time-temperature path experienced by the silica grains during sample preparation. Different combinations of preheat and measurement temperature were tried out, satisfactory results could be obtained by preheating at 150°C for 20 s and measuring OSL at 140°C, both for the regeneration and the test dose measurements. Thermal transfer is then largely suppressed, which otherwise can be quite significant and lead to apparent strong sensitivity changes and unacceptable recycling ratios (Fig. 3.21, 140°C data points). For both the unheated intact and preheated (150°C) dissolved module, sensitivity changes could be successfully corrected and given doses excellently recovered using a single aliquot regeneration protocol with test dose normalization.

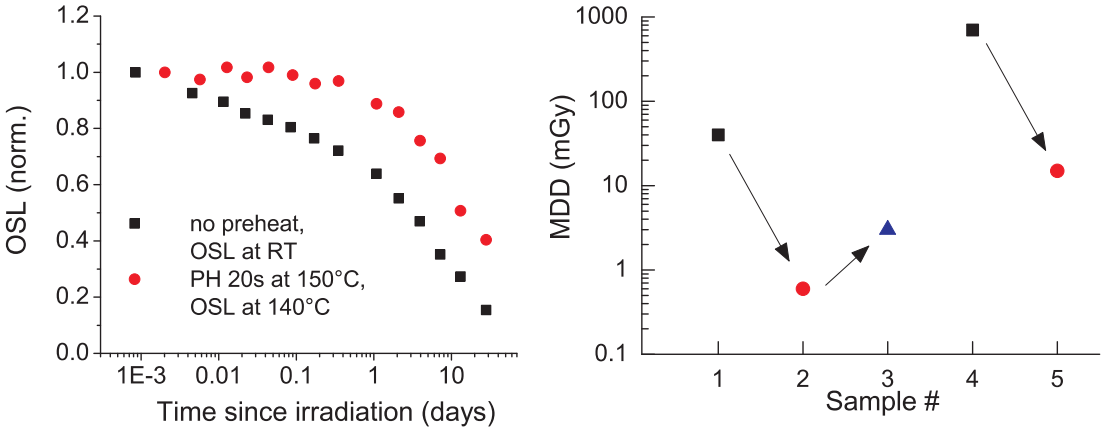

Figure 3.22.: Left: Fading of the OSL signal for different storage times at room temperature for unheated samples (square symbols, OSL measured at room temperature) and for samples preheated before OSL measurement for 20 s at 150°C (OSL at 140°C, circle symbols). All measurements were done on extracted silica of contact-based modules. Applied dose before storage was 2.5 Gy. Right: Minimum detectable dose for contact-based and contactless modules with different pre-treatment immediately after irradiation. Square symbols mark intact modules, circle and triangle symbols chemically extracted filler material, measured without and with preheating, respectively.

3.2.4. Long- term signal stability

Both the unheated and preheated modules show long-term instability of the OSL signal at room temperature, following irradiation (Fig. 3.22). However, preheating does reduce the overall fading rate and leads to negligible fading (10%) within the first day.

3.2.5. Detection limit

For contact-based intact modules, the minimum detectable dose (MDD) is around 40 mGy (Sample #1 in Fig. 3.22), immediately after irradiation. Chemically extracting the filler material reduces the MDD to 0.6 mGy (#2). The necessary preheating increases the value to around 3 mGy (#3). After 10 days of storage these values increase to 130 mGy and to 5 mGy for intact and chemically prepared modules, respectively. For contactless modules, the MDD immediately after irradiation is around 700 mGy (#4) and 15 mGy (#5) for intact and dissolved modules, respectively.

3.2.6. Dose recovery tests.

Preliminary dose recovery tests were carried out on contact-based modules to investigate how adequately the suggested protocol corrects for both heating during sample preparation and fading (Fig. 3.23). For comparison, intact modules were also investigated. For measurements promptly after irradiation, measured doses for both intact and prepared modules are in general agreement with the given dose. For longer time

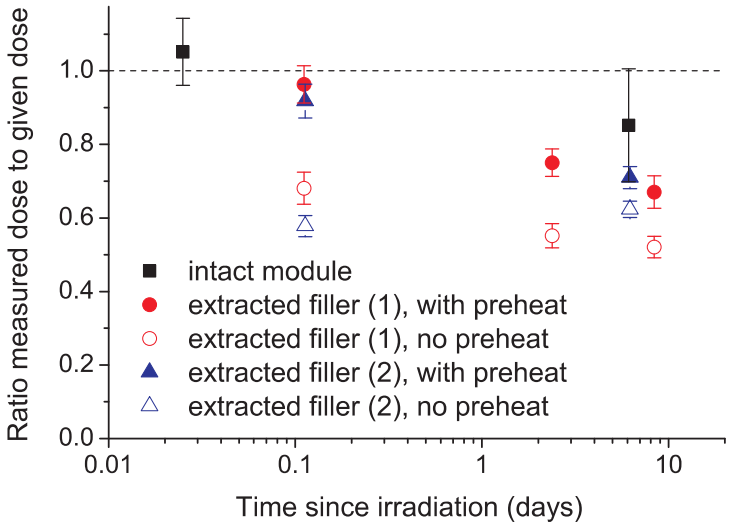

Figure 3.23.: Result of dose recovery tests using contact-based modules, irradiated with ^{137}Cs (475 mGy) and different pretreatments. The intact module and the "extracted filler, no preheat" module were both measured at room temperature without preheat, the third sample was preheated at 150°C for 20 s and measured at 140°C. (1) refers to sample preparation using a heating plate, (2) to sample preparation in a heatable ultrasonic bath. All dose values were corrected using the respective fading curves of Fig. 3.22.

delays however, the prepared modules, measured with preheat, systematically underestimate the given dose by around 30%. For the intact module, no similar definite conclusion can be drawn as the large uncertainty of the dose assessment, due to very low signal intensity, makes an agreement with the given dose as well as a similar degree of underestimation possible. For the prepared modules, there is no systematic dependency of the degree of underestimation on the sample preparation technique (heating on a heating plate, with uncontrolled (potentially much higher) temperature and heating in a highly temperature controlled heatable ultrasonic bath) but a possible dependency is indicated on the time elapsed since irradiation. This would imply that the degree of fading is different for a module which is first prepared and then irradiated and for a module which is first irradiated and then prepared (the latter corresponding to the situation encountered in an actual accident or radiological emergency). Whether this is true and what the physical mechanisms are behind this observation or whether a different explanation exists needs to be investigated in further studies. For all prepared modules and delay times, the doses measured without preheat were consistently lower then the ones measured with preheat, even when using the two different fading curves of Fig. 3.22 for signal correction, as expected.

3.2.7. Conclusions

Although the developed methodology was not yet successful in recovering applied doses for contact-based modules days after the exposure, the luminescence properties investigated nevertheless clearly demonstrate the high potential of chip card modules with molded encapsulations for retrospective dosimetry: absence of zero dose signal, linear dose response up to 10 Gy, high sensitivity (low detection limit) and potentially reduced fading when measuring extracted filler material with preheat. For population triage contact-based modules can be measured as they are, which allows high throughput. Dose assessment below 100-200 mGy with reasonable precision however requires sample preparation at the expense of somewhat longer processing times (approx. 1-2 hours per 6 modules). The greatest impact of the filler extraction procedure is expected for contactless modules, which otherwise would be limited for use in situations involving high exposures (>1 Gy). Thus one can envisage that also electronic documents (ID cards, passports) can be used as fortuitous dosimeters in the future. For this, the luminescence properties of contactless modules must be investigated in detail. With a successful development of a suitable measurement protocol for contact-based and contactless molded encapsulations, the range of chip cards with usable dosimetric properties could be greatly enhanced thus bringing chip cards closer to the definition of a truly ubiquitous emergency dosimeter.

3.3. Investigations on arbitrary chip cards

So far the investigations and protocols developed were solely based on chip card modules produced and provided by Infineon Technologies. Although Infineon is the global market leader in chip card ICs, their market share amounts to currently 27% (Infineon Press release July 2011), meaning that more than 70% will be from other producers which could use a different encapsulation technology with different luminescence properties. In her pioneering paper, Göksu (2003) remarked that some of the chip cards investigated (mostly telephone cards at the time of her investigation) had a black cover which was unsuitable for luminescence measurements. Similarly, Bassinet et al. 2010 investigated a number of chip cards in France and concluded that only a small number had usable luminescence properties. To get a first rough estimate of the percentage of usable chip cards in Germany and the degree of similarity of their dosimetric properties, 67 chip cards, that were no more in use, were collected from employees of the Helmholtz Zentrum München, predominantly debit cards and health insurance cards. Almost all cards showed a front, contact side of the chip of one of the ten examples shown in Fig. 3.24.

67% of the cards showed a transparent UV cured encapsulation, 40 % of these were from Infineon. One card (a SIM card) displayed a chip with molded encapsulation. The remaining chip cards had a blackish, semi-opaque encapsulation. The chip cards with a transparent encapsulation displayed minimum detectable doses from 2 mGy to 14 mGy, immediately after irradiation, the chip card with the molded encapsulation

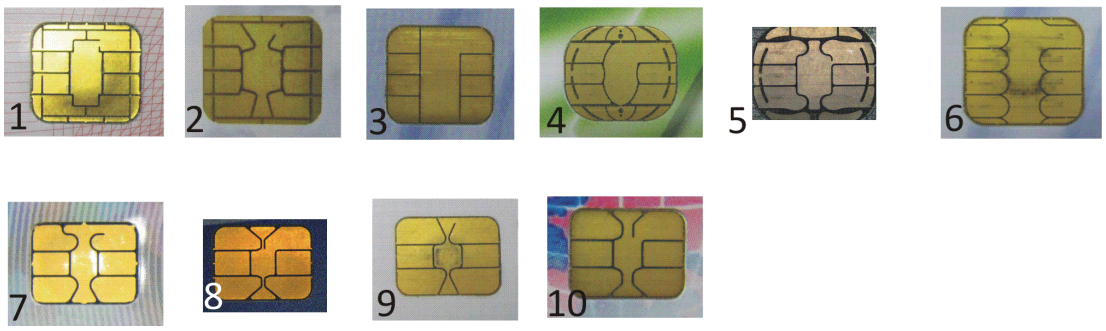

Figure 3.24.: Overview of the front side of various chip cards collected (donated) from employees of the Helmholtz Zentrum München. No. 1-6 are debit and SIM cards (for contact based controller and memory IC), no. 7-10 health insurance cards (contact based memory IC). No. 1, 2 and 7 are produced by Infineon Technologies AG. Health insurance cards from the "Techniker Krankenkasse" are almost exclusively equipped with either modules 9 or 10.

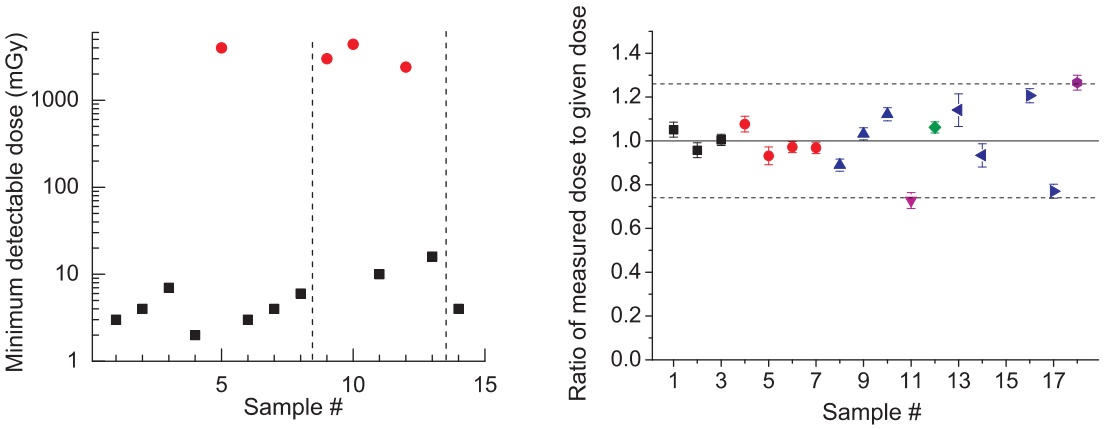

Figure 3.25.: Left panel: Minimum detectable dose immediately after irradiation of various chip cards. Sample no.s 1-8 are debit cards, 9-13 health insurance cards and 14 a Munich Cinema card. Red circle symbols denote chip cards with a blackish, semi-opaque encapsulation. This was found for card type 6, 9 and 10 in figure 3.24. Right panel: Dose recovery test for various chip cards. All modules were given a dose of 1 Gy and stored in dark at room temperature for 7 days before measurement. The different symbols and colours refer to the different chip categories of figure 3.24. Sample No.1-3: cat. 1, 4-7: cat. 2, 8-10: cat. 3, 11: cat. 4, 12: cat. 6, 13-14: cat. 7, 15-16: cat. 8.

40 mGy (see 3.2.5), the cards with blackish encapsulation 2 to 4 Gy, making them unsuitable for emergency dosimetry (Fig. 3.25, left). Generally, debit cards had on average a larger chip and thus a larger encapsulation area, leading to a somewhat lower detection limit as compared to health insurance cards. However, all chip cards with a translucent encapsulation meet the requirement of a MDD in the order of 10 mGy.

To investigate in how far the developed methodology for UV-cured transparent chip card modules is applicable to an arbitrary chip card (with a transparent encapsulation), several chip cards from each category displayed in Fig. 3.24 were given a dose of 1 Gy, stored in dark for 7 days and subsequently read out using the protocol given in section 3.1.5 and fading correction given in Fig. 3.6. The result is shown in Fig. 3.25, right. All measured doses lie within 26% of the given dose, the mean of all values is 1.00 ± 0.03. Thus within an enlarged uncertainty of 13% (at the $1-\sigma$ level), corresponding to degree of observed variability, the developed procedure delivers the correct dose independent of the chip card producer.

4. Portable electronic devices as emergency dosimeters

Portable electronic devices (PEDs), such as mobile phones, portable computers, music and video players, USB flash drives, digital cameras and watches, are becoming increasingly popular and are already carried today by a large part of the general population. Thus they would make a very efficient emergency dosimeter and would ideally complement the chip cards, if their usability as a fortuitous dosimeter can be proven. In the initial stage of this project a study was published, reporting on the suitability of thin film chip resistors found in mobile phones for retrospective dosimetry (Inrig et al., 2008). The radiation sensitive component was identified as the ceramic substrate, made predominantly out of Al_2O_3, on which the metallic resistive film is deposited. The substrate displayed a radiation induced TL and OSL signal, with high sensitivity and linear dose characteristics. Both the dosimetric TL peak and the OSL signal showed a high degree of anomalous fading at room temperature. This necessitates the application of a fading correction factor, when measuring an accident dose days after the exposure. Only OSL was favoured for dose assessment.

In the initial phase of this project, it was thus first investigated, if the results of Inrig et al. (2008) can be confirmed for PEDs available in Germany. It soon turned out that some properties, such as OSL decay curve shape, choice of integration intervals, choice of preheat temperature, detection limit and variability of fading rates needed further investigation. Also it was discovered within the course of the project that multilayer chip inductors have a similar high potential for retrospective dosimetry, therefore they were included in the analysis. Finally the possible advantages and disadvantages of using TL, especially for inductors, were subject of a further in-depth investigation.

4.1. Materials and Methods

A large variety of PEDs was analyzed within this project. The main emphasis was on mobile phones but also a number of USB flash drives, music players and digital cameras were included in the analysis. Production years ranged from 2001 to 2010. Complementary investigations were carried out using resistors and inductors from sample kits from three producers (Taiyo Yuden, North America; TDK Corporation, Japan).

A schematic view of the composition of a typical surface mount thin film chip resistor and multilayer inductor is displayed in Fig. 4.1. The TL/OSL sensitive component is the ceramic substrate/alumina layer.A picture showing how these components can be identified on the circuit board is given in Fig. 4.2.

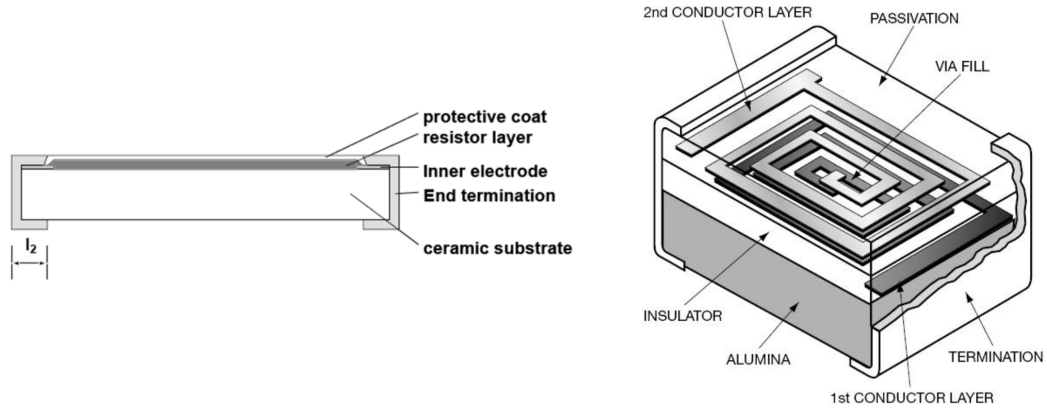

Figure 4.1.: Left: Side view of a chip resistor. Right: Body of a multilayer SMD inductor chip developed for high frequency applications in radio communication systems such as cellular phones, GPS etc. (Breen et al.)

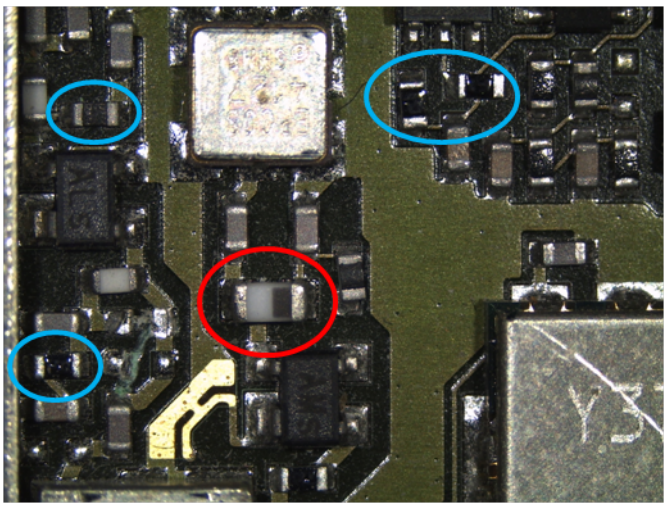

Figure 4.2.: Enlarged view of part of a circuit board of a mobile phone. The inductor is marked with a red, the resistors (with the black coating up) with a blue oval line.

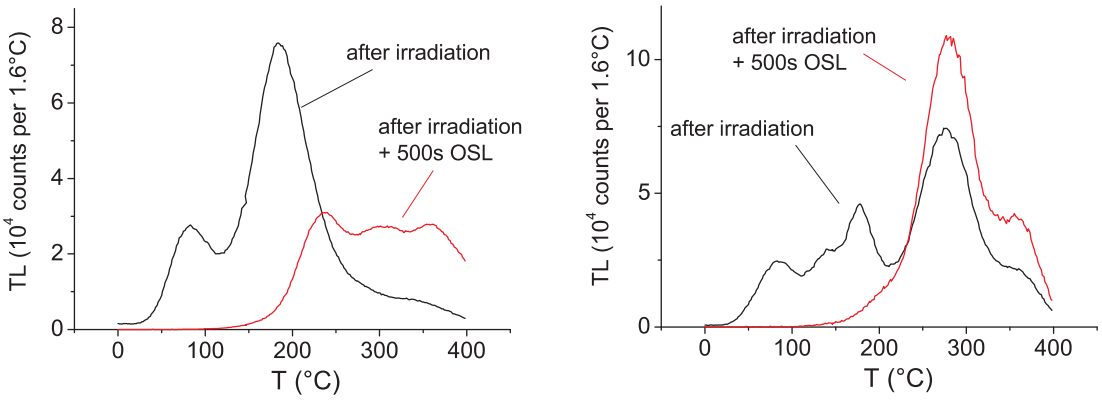

Figure 4.3.: TL glow curves of a ceramic resonator and of a set of four chip inductors, with and without 500 s of optical stimulation. The resonator and the inductors were irradiated with 1.9 Gy and 8.8 Gy of beta irradiation, respectively.

The extracted resistors and inductors from the PEDs were cleaned with acetone in an ultrasonic bath for 15 min to remove adhesive residues which could potentially perturb the TL/OSL measurement due to darkening during (pre)heating. All OSL measurements were performed on the Risø TL/OSL-DA-15, all TL measurements on the Risø TL-DA-12 automated reader. The beta sources of both readers were calibrated for the electronic components by irradiating samples from the kits with the ^{137}Cs source of the Secondary Standard Dosimetry Laboratory in a perspex holder and subsequently measuring them in the luminescence readers using the developed protocols.

4.2. Dose assessment using OSL

4.2.1. Correlation between OSL and TL

Fig. 4.3 shows for comparison the TL glow curves of a ceramic resonator and chip inductors, irradiated with different doses before and after optical stimulation for 500 s.

The glow curve of the resonator is very similar to that of chip resistors. Similar to Al_2O_3:C and to what is reported in Inrig et al. (2008), TL peaks at approximately 80°C and 190°C are observed in the glow curve of the resonator, with both peaks being photosensitive and almost completely bleachable by 500 s stimulation with blue LEDs. For inductors, three additional peaks at approx. 140°C, 270°C and 320°C are visible and the third peak is somewhat narrower and located more at 170°C than 190°C. Similar to the resonator and resistors, all peaks up to 200°C are readily reduced by optical stimulation, whereas the higher temperature peaks actually appear to increase somewhat on exposure to blue LEDs. The same is true for resistors and the resonator, although intensity of the glow curve in the higher temperature range is insufficient to resolve individual peaks.

The TL investigations demonstrate that the radiation induced signals up to 200°C are light sensitive, thus the photo-active defects and mechanisms involved can con-

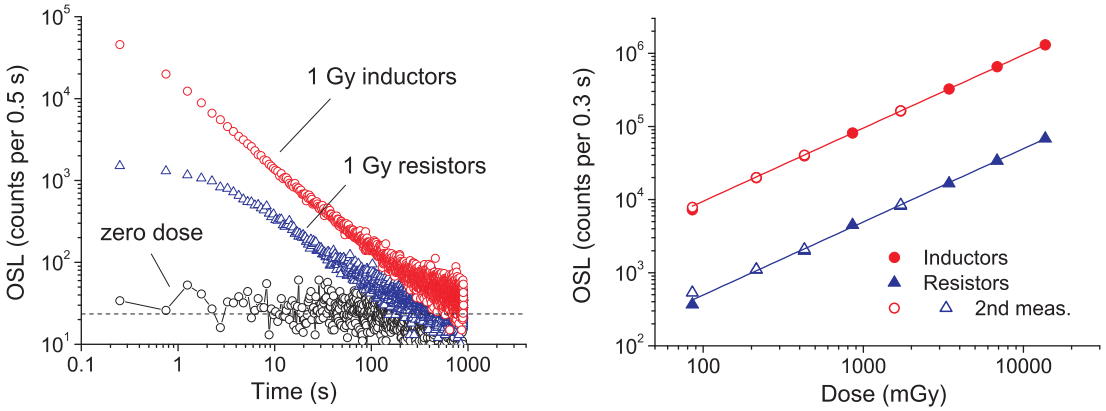

Figure 4.4.: Left: Zero dose and 1 Gy irradiated OSL signals of a set of 10 resistors and inductors, from two different producers, respectively. The dashed line indicates the instrumental background. Right: Dose response curve of the same set of resistors and inductors from 90 mGy up to 16 Gy. Open symbols denote the second measurement (= recycling points). The solid lines are linear fits to the respective datasets.

tribute to an observed OSL signal. As the 80°C peak is thermally unstable at room temperature, a preheat of 10 s at 120°C (2°C s^{-1} heating rate) is recommended prior to OSL measurement.

4.2.2. OSL decay curves and dose response

From measurements of the OSL signal at different temperatures it was observed, that the OSL efficiency is maximized by stimulating at 100°C. At higher temperatures, the signal starts decreasing due to thermal detrapping of the electrons in the traps responsible for the OSL signal. Therefore, all OSL measurements were performed at 100°C after preheating. Typical OSL decay curves of a set of resistors and inductors after irradiation with 1 Gy are shown in the left hand side of Fig. 4.4.

As can be seen, there is no zero dose signal in OSL of both resistors and inductors (fresh electronic components from mobile phones, extracted under subdued red light conditions, were used for this analysis). Both OSL decay curves after irradiation show markedly 'fast' and 'slow' components (one to two orders of signal loss in the first 10 and the subsequent 1000 s). For higher doses, the instrumental background isn't reached even after stimulation times of 1000 s. For a full optical readout, quite long measurement times would thus be necessary, making the dose assessment on a single sample unacceptably large. Shorter readout times will result in a remnant residual charge of the 'slow' component, which will be carried on into the next irradiation and measurement sequence. Therefore, a careful choice of stimulation time and integration windows has to be made, in order to avoid unwanted artifacts. This will be investigated and discussed further below.

In general, the OSL signal of inductors shows a faster initial decrease than the signal

of resistors. The exact reason for this difference is not clear but it may lie in the narrower curve shape of the 170°C TL peak of inductors as compared to resistors and in the additional presence of the 140°C TL peak (although the trap of this latter peak is significantly emptied by the applied preheat treatment). The OSL decay curves of both components immediately after beta irradiation can be approximately described by a generalized hyperbolic decay function plus a constant of the form:

$$I_{OSL} = a\,(1 + b\,t)^{-1} + d\,, \tag{4.1}$$

with a (s^{-1}), b (s^{-1}), c and d (s^{-1}) being empirical constants. For the curve fitting, d was fixed to the instrumental background of the reader. It is not possible to arrive at an equally good fit when assuming the sum of three exponential decay functions plus a constant (at least for higher doses).

The right hand side of Fig. 4.4 demonstrates that the dose response curve of the OSL signal of both electronic components is linear up to at least 16 Gy, for resistors linearity was confirmed by own measurements and by Inrig et al. (2008) up to 90 Gy. For these specific components, taken from two sample kits from two producers, the inductors are more than an order of magnitude more sensitive than resistors, with the same number (10) of components of the same size. From the dose response curves, a minimum detectable dose of 1.3 mGy and 24 mGy was estimated for inductors and resistors, respectively. We will come back to this issue in section 4.2.4. Reproducibility generally is excellent, with no need for test dose normalization. However, this is only true for the proper choice of stimulation time and integration windows, as will be shown with the next sample.

For this, the SAR procedure with test dose normalization was investigated with respect to its performance using the alumina-rich resonator described earlier and a stimulation time of 150 s. The dose response is shown in Figure 4.5, using two different integration windows for signal intensity calculation, together with the evolution of the test dose response in the course of the SAR procedure (Fig. 4.5; cycles 1-8: first measurement; cycles 9-15: second measurement; cycle 8 is the zero-dose point of the first measurement sequence).

In general, the correspondence between the first measurement and second measurement results is excellent. However, there are differences in the corrected OSL dose response according to the integration window that is used. More in particular, the dose response becomes sublinear with doses in excess of 2 Gy if a large integration window for the OSL signal (0-40 s) and late background subtraction is used. According to the Tx/Tn plot, this is due to build-up of test-dose response due to the presence of a residual slow component (SAR cycles 5-6-7 and 13-14-15) even after 150 s stimulation time. The build-up of residual charge is also seen in the presence of a zero-dose OSL signal (see inset below the dose curve in Figure 6a). If a small integration window is used (0-6 s), together with early background subtraction, the residual slow component effectively is canceled out and the Tx/Tn plot now shows a plateau around unity over the 15 SAR cycles, indicating the absence of any build-up of residual charge and/or significant sensitivity changes. Consequently, the dose response using this procedure

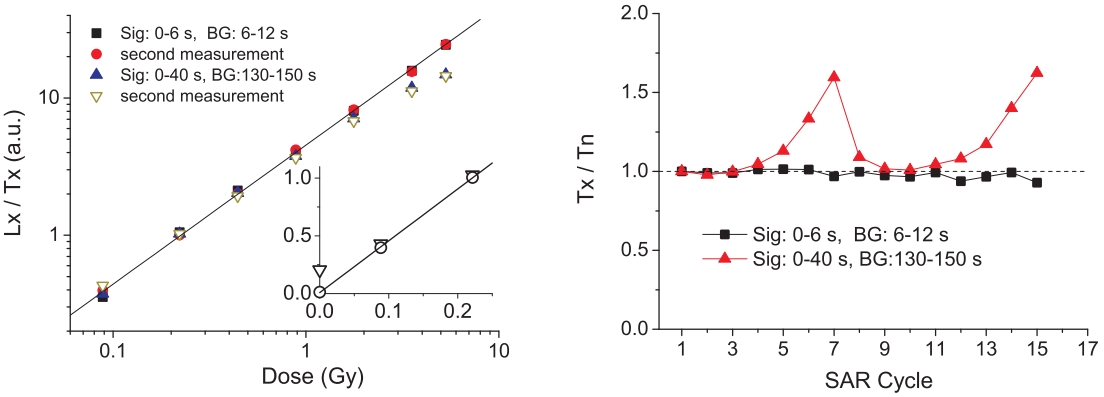

Figure 4.5.: Left panel: OSL dose response curve of a ceramic resonator using the first 6 s of the OSL integral and early background subtraction (6-12 s), and the first 40 s of the OSL integral together with late background subtraction (130-150 s). Total stimulation time was 150 s, and the OSL was corrected using a test dose of 133 mGy. The inset shows the zero-dose response which is significant for the larger OSL integral with late background subtraction (see text for explanation). (b) Monitoring of the OSL test dose response throughout the SAR procedure. The seven first cycles are used to correct the OSL dose points depicted in (a), SAR cycle no. 8 is the zero-dose OSL response while cycles no. 9-15 are used to correct the OSL dose points referred to in (a) as 'second measurement'.

does not show sublinearity in the higher dose region.

4.2.3. A first irradiation trial

In a preliminary irradiation trial, the electronic circuit board of a flash drive with the ceramic resonator (Sony Microvault USM256U2) was irradiated as a whole using ^{60}Co rays (Beerten et al., 2009). The given dose was 977±19 mGy, and this dose was subsequently treated as the unknown accident dose. The resonator was extracted under dark room conditions and measured 35 days after irradiation. An individual fading curve was established using a previously unmeasured resonator from a second flash drive, and the appropriate fading correction factor derived from this curve. Further details are given in Beerten et al. (2009).

The comparison of the OSL decay curves for measurements after gamma- and beta-irradiation and different storage times are given in Fig. 4.6 for the ceramic resonator. OSL curve shapes are nearly identical after gamma- and beta-irradiation for measurements soon after irradiation but a significant slower decay is observed after gamma-irradiation and 35 days storage.

As a consequence, when measuring the simulated accident dose with the built-in beta source, the calculated dose will depend on the integration windows chosen for determination of the OSL signal and background, respectively. Generally, an increase in dose with increasing integration time of the OSL signal is observed until a plateau is reached, in Fig. 4.6 e.g. this is the case for 8-10 s, when choosing the background

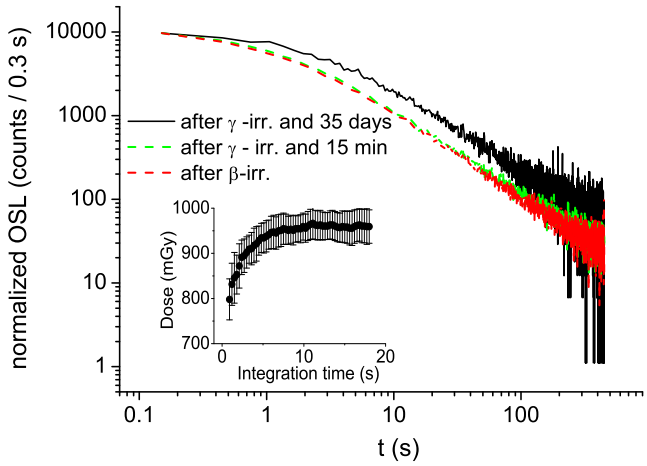

Figure 4.6.: Comparison of OSL decay curves of the ceramic resonator following gamma-irradiation and storage in dark for 35 days (solid line), gamma-irradiation and 15 min storage (dotted line) and beta-irradiation (no storage, dashed-dotted line). OSL decay curves were scaled to coincide for the first channel. The inset shows the (fading corrected) dose versus OSL integration time, when measuring the applied gamma dose 35 days after exposure with the built-in beta source. From Woda et al. (2010).

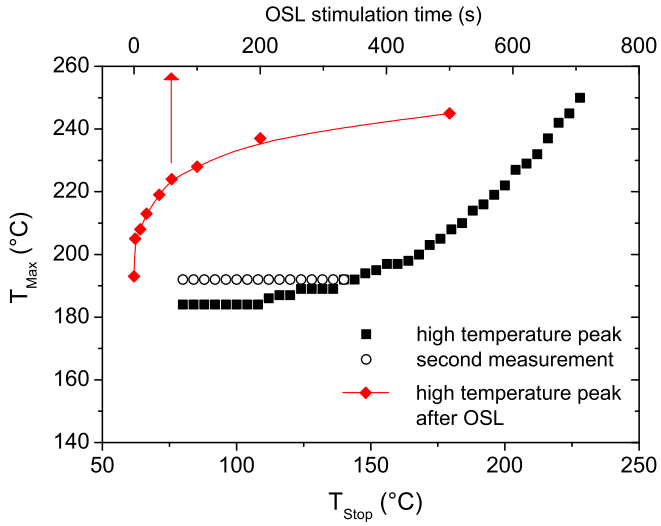

Figure 4.7.: T_{Max}-T_{Stop} curve for the higher temperature TL peak. T_{Stop} was increased in steps of 4°C. Also shown is the dependence of peak temperature of the 190°C TL peak on optical stimulation. The sample was preheated at 100°C for 10 s for these measurements.

window at 18-21 s. For repeated cycles of dosing and OSL measurement, no change in the OSL curve shape was observed. The difference in OSL curve shape in Fig. 4.6 is thus a result of the decay of the fast component of the signal over the storage period.

To further elucidate the observed luminescence properties, the TL peaks associated with the OSL emission were analyzed (see Fig. 4.3).

A T_{Max}-T_{Stop} analysis (McKeever, 1985) for the 184°C TL peak reveals a constant increase in T_{Max} for T_{Stop} larger than 144°C, with no clear flat regions identifiable up to the highest applied stopping temperature of 228°C (Fig. 4.7). This implies that the TL peak is made up of either several closely overlapping or even a quasi-continuous distribution of peaks (McKeever, 1985). For T_{Stop} ranging from 80°C to 144°C, a slight stepwise increase in T_{Max} from 184°C to 192°C is observed, which is accompanied by a slight shift of the overall TL peak structure towards higher temperatures. This effect is no longer seen when re-measuring the lower temperature T_{Stop} range, after completion of the entire T_{Max}-T_{Stop} analysis. It is speculated, that it is due to different sensitization of the different components of the TL peak during the first run. The effect of optical stimulation on the peak temperature was also investigated for stimulation times from 0 s to 500 s. A fast increase of T_{Max} in the first 60 seconds is observed, followed by slower increase for longer stimulation times. Optical stimulation thus leads to a preferential depletion of the lower temperature TL traps first, i.e. there could be a correlation between trap depth and photo-ionization cross-section.

As the 190°C TL peak is shown to be optically sensitive (Fig. 3 a) and the result of a distribution of peaks, it seems reasonable to assume that the OSL decay curve in Fig. 2 is also the result of a distribution of decay functions. This is also supported by

the dependence of the peak temperature on optical stimulation. The fast components in OSL thus are related to the lower temperature peaks in TL. The hyperbolic decay function (eq. 4.1) can then be interpreted as an approximation to the multi-exponential decay resulting from a possible distribution in optical cross-sections. For the isothermal decay in TL, it has been shown that a hyperbolic time dependence (with c=1) can emerge for a Gaussian shaped trap depth distribution under certain circumstances (Hornyak and Franklin, 1988). The situation is however not directly transferable to OSL.

The decay of the fast component of the OSL signal during the storage period implies that the lowest temperature part of the 190°C TL peak fades either thermally or anomalously with a higher rate than the higher temperature part. In an initial investigation of the TL glow curves of several alumina-rich electronic components from a variety of portable electronic devices, a variation in the width of the 190°C TL peak was observed and in some cases also the indication of an additional, optically active peak at 140°C. It would thus seem advisable to apply a higher preheat treatment than 100-120°C. On the other hand, preheating at e.g. 160°C for 10 s will increase the detection limit for the present ceramic resonator by over a factor of three and will not remove the necessity of fading correction. The decisive issue is whether the variability of fading rates between different portable electronic devices can be reduced by applying the higher preheat and whether this outweighs the loss in sensitivity. This will be investigated in the next section.

4.2.4. Detection limit and fading

In Inrig et al. (2008) a minimum detectable dose of less than 10 mGy was reported, when combining several resistors on the measuring cup. However, this was only shown for larger resistors (dimensions of 2×1 mm), taken from a sample kit, while in actual mobile phones these types of resistors are rather rare and the smaller variant (dimensions of 1×0.5 mm) is abundant. As was shown as a first example in Fig. 4.4, the detection limit of 10 of such resistors is more in the order of 20-30 mGy.

In principle, inductors seem to be preferable for dose assessment using OSL, as they are equally suited for dosimetry than resistors but in general are more sensitive to radiation. However, inductors generally can be found only in low numbers (1-12) on the circuit board of mobile phones and are completely absent in other PEDs such as flash drives and cameras, whereas resistors can be found in all PEDs and in large quantities (40-100) in mobile phones. Therefore, the optimum strategy to combine fast dose assessment and high sensitivity, seems to be to first sample all inductors present on the PED, then complement the measuring cup with resistors, sampling the largest ones first, then continuing with the smaller ones, until no more electronic components fit onto the measuring cup (a practical limit seems to be e.g. 25 components of size 1×0.5 mm. When trying to fit more onto the measuring cup, some components will start flipping with their wrong (unmeasurable) side up again). This was done for 22 different PEDs to investigate the optimum achievable detection limit (Fig. 4.8).

As can be seen, with this approach a minimum detectable dose of 0.7 - 10 mGy

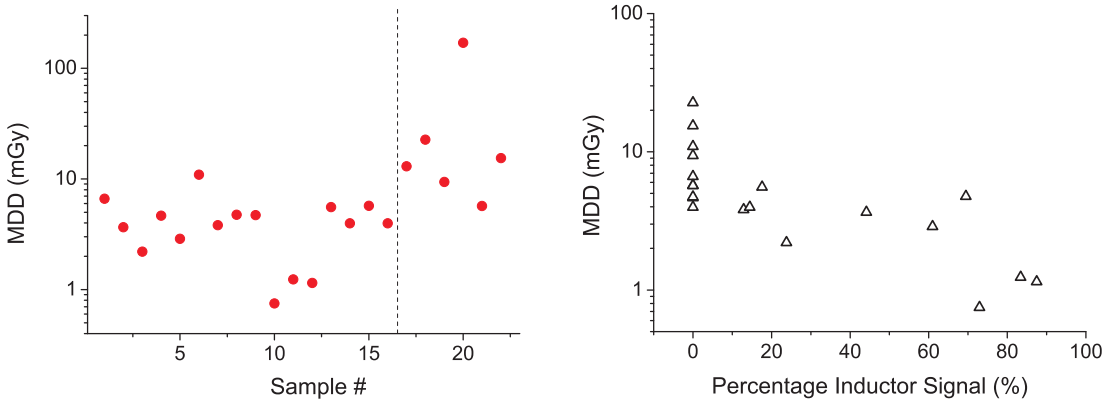

Figure 4.8.: Minimum detectable dose (MDD) immediately after irradiation for 22 different PEDs, when measuring an aliquot with a mixture of resistors and inductors per sample (left). The dashed line separates mobile phones (sample # 1-16) from USB flash drives, music players and digital cameras (sample # 17-22). Dependency of the MDD on the relative contribution of inductors to the OSL signal (right).

is achievable for mobile phones, while it is somewhat higher for USB flash drives, music players and digital cameras. This is not surprising, as the latter PEDs have no inductors and only have one function, in contrast to the multi-functionality of modern mobile phones, in particular smart phones, and therefore are reduced in size (e.g. flash drives) with only a limited number of resistors available. However, with one exception, also for these electronic devices a detection limit at least in the order of a few tens of mGy is achievable. The importance of inductors for the sensitivity is highlighted in the right hand panel of Fig. 4.8, where it is clearly shown that the lowest detection limits are observed for those samples with the highest percentage of inductor signal.

For 21 of these 22 PEDs (excluding the one with the detection limit of > 100 mGy, the variability of the OSL fading rate was analyzed for storage times of a few minutes up to 31 days and applying a low (120°C) and higher (160°C) preheat. To keep the time frame of this experiment within reasonable limits, the components of each measuring cup of one sample was split onto two cups, each of which was then subjected to a different preheat treatment. For each delay time the average and standard deviation of all 21 (normalized) OSL signals was calculated and plotted (Fig. 4.9).

Both fading curves can be described by the well-known equation for anomalous fading (Huntley and Lamothe, 2001), which was also applied by Inrig et al. (2008):

$$I = I_c \left[1 - \frac{g}{100} \log_{10} \left(\frac{t}{t_c} \right) \right] , \tag{4.2}$$

where I_c is the luminescence intensity at some time t_c following irradiation and g is the percent decrease in intensity per decade, meaning a ten-fold increase in time (t_c) since irradiation. For the 120°C preheated data a very similar value of g of 22.4 ± 1.2 compared to 23.7, reported in Inrig et al. (2008), is obtained (with $I_c = 0.70$ for $t_c = 0.346$ days (8.3 h)). The 160°C preheated data only shows a minor reduction in

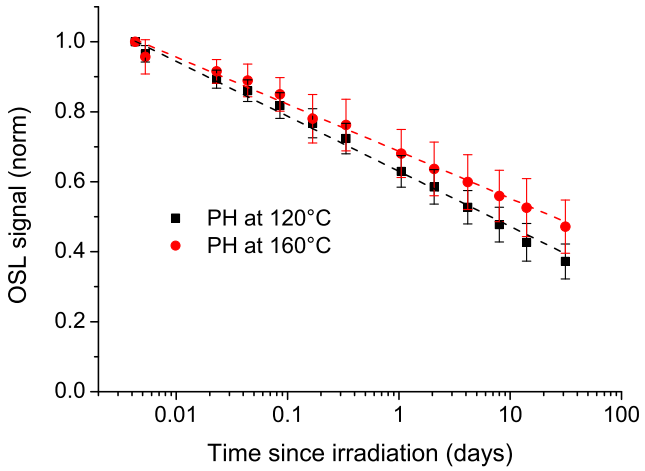

Figure 4.9.: Fading of the OSL signal of a combined resistor and inductor aliquot from 21 of the 22 PEDs shown in Fig. 4.9 for two different preheat temperatures.

the overall fading rate ($g = 18.0 \pm 1.8$ for the same t_c), at the expense of a three to four-fold increase in the detection limit. The degree of variability ranges from 3-13% and 5-16% for the 120°C and 160°C preheated data, respectively. A higher preheat is thus seen not to reduce but actually to increase the degree of variability between different PEDs.

As Fig. 4.10 indicates, this might however be true to a different response of the OSL signal of resistors and inductors to the two different preheat treatments. Whereas for a pure resistor signal, the fading curve for the lower and higher preheat seems to be almost the same, a markedly reduced fading rate is observed for the higher preheat in the case of a predominantly inductor signal. Thus it might be, that the slight reduction

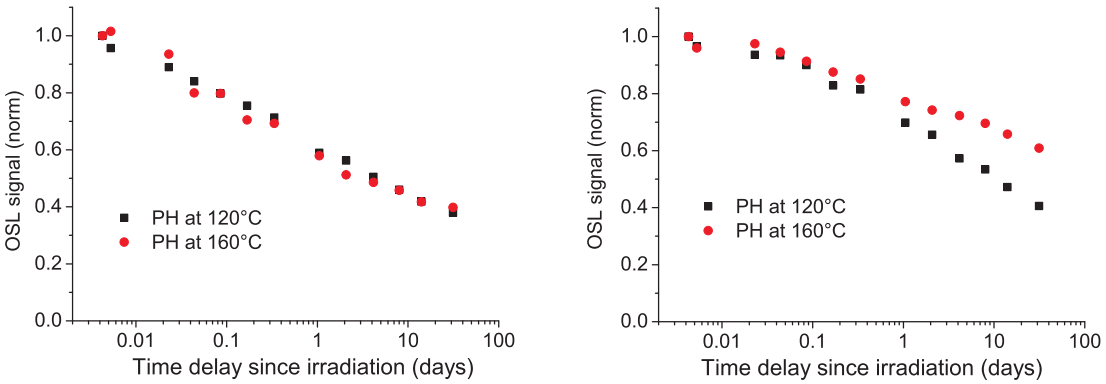

Figure 4.10.: Example of OSL fading curves for aliquots from PEDs with a pure resistor signal (left) and a predominant inductor signal (right).

Sample	Given dose (mGy)	Measured dose (mGy)
Nokia 1661		
20 res	500	537 ± 41
6 ind	500	664 ± 86
1 lres + 5 ind + 10 res	500	459 ± 59
LG GS290		
20 res	200	234 ± 34
4 ind + 16 res	200	228 ± 32

Table 4.1.: Trial irradiations on intact mobile phones with ^{137}Cs. The given dose was the air kerma value at the (presumed) level of the circuit board. The aliquots were measured 8 days after irradiation. The abbreviations are: 'res': resistors of size 1×0.5 mm, 'ind': inductors of size 1×0.5 mm, 'lres': resistor of size 3×1.55 mm.

in fading rate and moderate increase in variability in Fig. 4.9 for the 160°C preheat data is solely due to the inductor signal and would not have been observed, if only pure resistor aliquots had been measured. Although we might thus not expect and increase in scatter for the higher preheat treatment when restricting the sampling to only resistors, we will also not gain any benefits from such an approach and will lose the possibility to optimize the sensitivity. For a mixed aliquot of resistors and inductors, the lower preheat treatment is definitely to be preferred and therefore is generally recommended.

4.2.5. A second irradiation trial

Trial irradiations were carried out on two intact mobile phones, irradiated with 500 and 200 mGy (air kerma) of ^{137}Cs rays, respectively. The samples were disassembled eight days after irradiation and a pure resistor aliquot and a mixed resistor and inductor aliquot measured (for the first sample also a pure inductor aliquot). OSL measurements were done using the 120°C preheat and the dose values corrected for fading using Fig. 4.9. All measured doses are in agreement with the given doses, within the respective uncertainties (Table 4.1).

4.3. Dose assessment using TL

4.3.1. Resistors

In principle, TL could offer two potential advantages over OSL for dose assessment. Firstly, as there is no need for an optical stimulation unit, the PM tube can be brought closer to the sample, leading to an increase in solid angle and light collection and measurements can be made in the blue wavelength range, which, presuming the emission spectra of resistors is identical to Al_2O_3:C, would give a better overlap of emission and detection window. Both effects should lead to an increase in sensitivity and thus to lower detection limits. Secondly, the TL signal will encompass also the slow OSL components and thus potentially offer a reduced fading rate as compared to OSL (using the fast

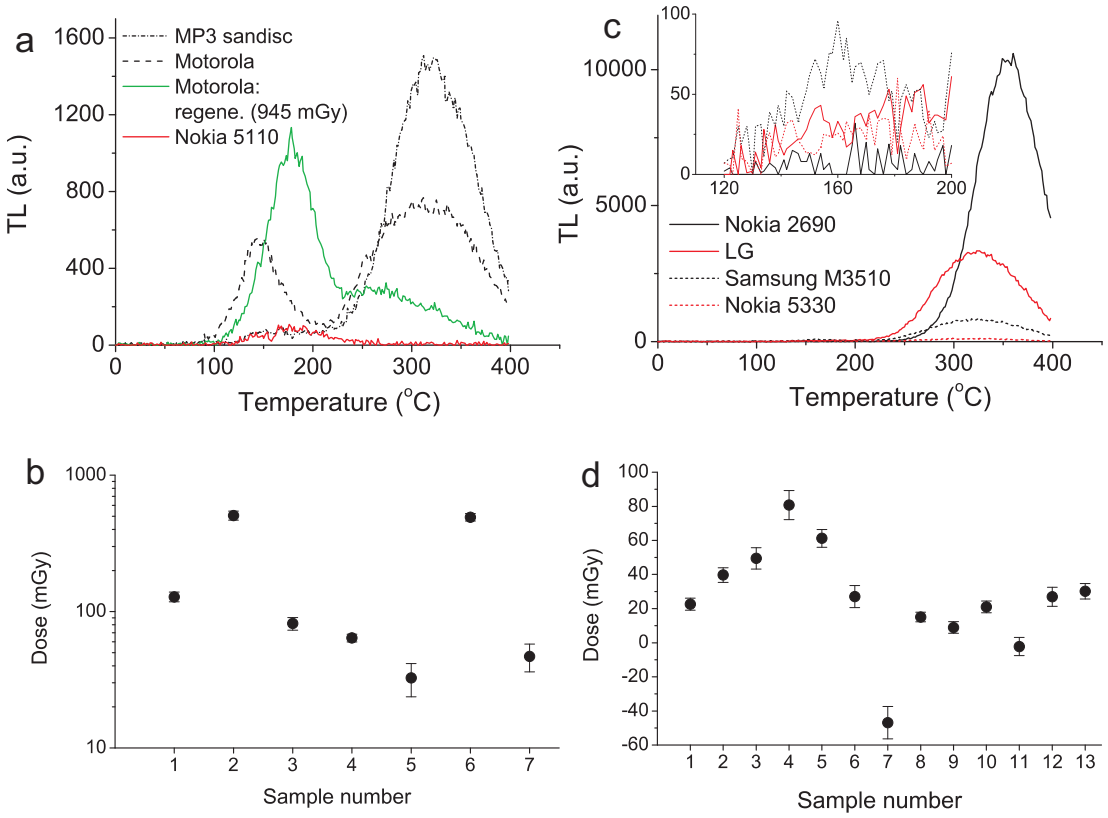

Figure 4.11.: TL glow curves of a set of ten resistors from different unexposed mobile phones extracted under white laboratory lighting (a) and corresponding zero signal dose (b). Panels (c) and (d) display the corresponding data from resistors of unexposed mobile phones extracted under subdued red light conditions. The inset in panel (c) gives an enlarged view of the lower temperature part of the glow curve.

components). A disadvantage would be the somewhat longer measuring times (400 s per per signal including background correction) without the possibility of performing a fast, initial screening of samples. Furthermore, it has been observed by Beerten et al. (2009) that resistors substrates from the investigated Sony flash drive show a zero-dose signal in the higher temperature range (250-400°C), in contrast to the resonator, and it is not clear how far this signal will influence dose assessment using the lower temperature, dosimetric signal (100-200°C). Therefore, the occurrence of a zero-dose signal for a variety of samples is investigated in this section, along with the dosimetric properties and the development and evaluation of a suitable protocol.

4.3.1.1. Zero dose signal in TL

The frequency of the occurrence of a zero dose signal in TL was tested on a number of resistor samples, extracted from a variety of PEDs and prepared first under laboratory

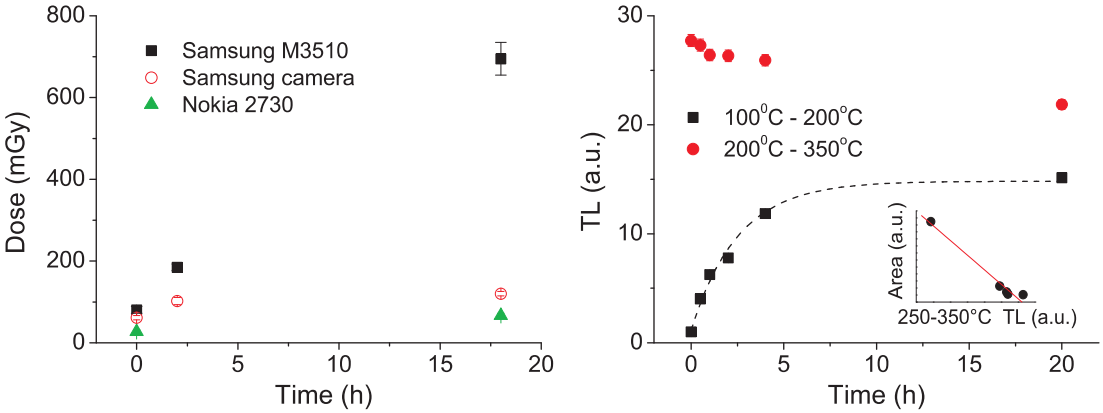

Figure 4.12.: Zero doses in the 100-200°C temperature range of resistors exposed to white light for different times (left) and from kit (right). The 100-200°C TL data in the right hand panel were fitted with an exponential saturation function.

white lighting conditions. For this set of samples, a pronounced zero dose signal was observed not only in the higher temperature range but also in the temperature region of the dosimetric signal (Fig. 4.11 a) and b)). As a result, large zero doses up to several hundreds of mGy's were measured. If resistors were extracted under subdued red light conditions (Fig. 4.11 c) and d)), the pronounced zero dose signal at higher temperatures is still present, however, the corresponding signal in the 100-200°C region is much smaller compared to the samples exposed to white light. Nevertheless, zero doses up to 80 mGy are still observed. The mean and standard deviation of the zero doses for all samples of Fig. 4.11, d, except for No. 7, is 22 ± 11 mGy. Although the radiation-induced TL signal, peaking at approx. 170°C extends well beyond 200°C, the existence of the intense zero dose signal in the higher temperature range limits the possible upper integration limit to 200°C.

Obviously, exposure to white light, even at the moderate level present in the laboratory, leads to an increase in the dosimetric signal. A possible mechanism would be phototransfer from the higher temperature trap into the dosimetric trap. A phototransfer from the 170°C trap into the shallow 80°C trap, for thermally annealed and subsequently irradiated resistor samples, by exposure to green LEDs at room temperature has been observed by Beerten et al. (2009). To test this hypothesis, different resistor samples extracted from three mobile phones under red light were exposed to 0, 4 and 16 hours of white laboratory lighting and the doses corresponding to the generated signals measured (Fig. 4.12, left). It is obvious, that increasing the time of light exposure increases the detected zero dose for all samples, while the percentage of increase varies widely between samples.

One difficulty of the experiment lies in the fact that different resistors from the same mobile phone can be very heterogeneous with regard to their sensitivity and the intensity of the (unexposed) zero dose signal. Therefore, in a second experiment a suite of identical, homogeneous samples were prepared by using identical combinations of

certain chip resistors from the sample kit for different aliquots and giving them all the same pretreatment:

- annealing of pre-existing signals by TL run up to 400°C
- irradiation with a dose of 5 Gy
- thermal cleaning of the lower temperature TL signal by a TL run up to 250°C.

The aliquots were then exposed to white light for different times, similar as before, and the glow curve subsequently measured (Fig. 4.12, right). As can be seen, a well defined increase in the TL signal in the 100-200°C range, which can be described by an exponential saturation function is accompanied by a corresponding decrease in the intensity of the higher temperature TL peak. At first sight, it seems contradictory that the biggest step in decrease for the higher temperature peak is between 4 and 20 hours of light exposure, where the lower temperature TL signal already seems to saturate. However, when comparing the TL signals on a quantitative level, one has to consider that if the phototransfer mechanism is responsible for the observed effects, the filling state of the trap(s) responsible for the lower temperature TL signal will be a result of simultaneous trapping and detrapping of photo-evicted charges from both the lower and higher temperature trap, according to the well-known rate equation (see also section 3.1.7):

$$\frac{dn}{dt} = A_n\,(N-n)\,n_c - \Phi(\lambda)\,\sigma_0(\lambda) n\,, \tag{4.3}$$

where Φ (m^{-2} s^{-1}) is the photon flux and $\sigma_0(m^2)$ the photo-ionization cross-section (Chen and McKeever, 1997). Other symbols have already been explained. The apparent saturation of the TL signal in Fig. 4.12, which corresponds to $dn/dt = 0$, is then the result of a dynamic equilibrium between trapping and detrapping of electrons, which both occur at the same rate (per unit time). This still demands a constant depletion rate of the filling state of the higher temperature trap, otherwise n_c would decrease and the equilibrium be disturbed. For that reason one must not compare intensities, but the area under the growth curve of the lower temperature TL signal with the intensity of the higher temperature TL signal. This is done in the inset of Fig. 4.12, where a correlation between the two is now visible. From these results, the firm conclusion can be drawn, that the origin of the zero dose signal in the 100-200°C temperature range of the TL glow curve is due to phototransfer from the higher temperature trap.

The (experiments) presented so far do not answer the question, why a ceramic substrate of a chip resistors shows a zero dose signal at all, even in the temperature range between 250-400°C, considering that firing temperatures for ceramics are well above that temperature range. Moreover, other electronic components with a similar ceramic substrate as the previously described resonator or inductors (see below) do not show any zero dose signal. A possible explanation lies in the black overcoat of the thin film resistors, which is made up to 75% of an epoxy resin (www.bourns.com). If the epoxy is cured by UV light, similar to the transparent encapsulations of chip cards, then this

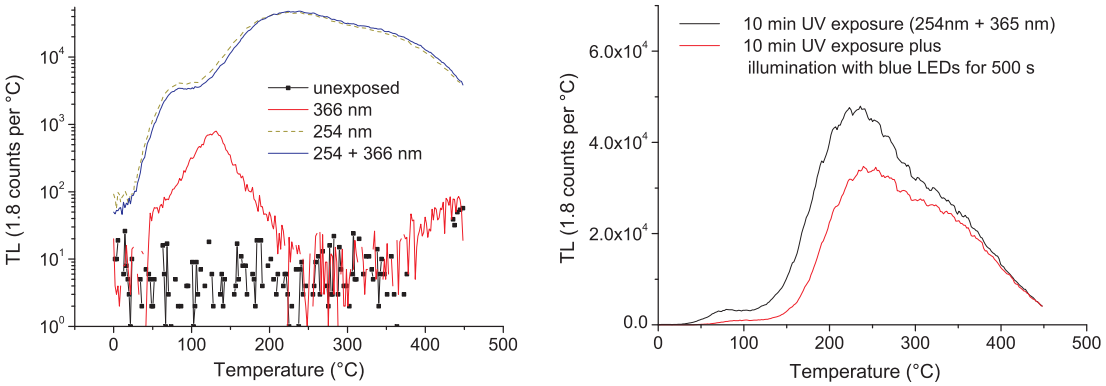

Figure 4.13.: Generating of TL signals in thermally annealed resistors by UV exposure.

exposure might also generate electron-hole pairs in the ceramic itself and thus lead to the formation of latent TL signals.

This is investigated in Fig. 4.13. The left plot shows the effect of UV exposure with two different wavelengths (254 and 366 nm) on thermally annealed resistors (from the kit). The black line demonstrates that there was no signal prior to UV exposure. The red line shows that illumination with 366 nm induces a signal only in the lower temperature range (up to 200°C), whereas illumination with 254 nm (or with both wavelength bands at the same time) induces a signal also in the higher temperature range, similar to what is seen in resistors from mobile phones. The right plot shows that after UV exposure and subsequent exposure to blue LEDs for 500 s (to mimic the prolonged daylight exposure during and after manufacture), the lower temperature part is reduced and we are getting closer to the curve shape of the zero dose signal. If one considers the additional effect of fading during storage, which cannot be mimic in the present experiment, but which will strongly further reduce the lower temperature signal up to 200-250°C and have little effect on the signal in the temperature region >300°C, it is conceivable that one ends up with a TL signal qualitatively similar to the observed zero dose signals.

As the technical details of the production process are, however, not known, this explanation still has to be regarded as a hypothesis and not as a proof.

4.3.1.2. Dose response and dose recovery

The dose response of the TL signal of resistor substrates after erasure of the zero dose signal is linear up to at least 4 Gy (Fig. 4.14, left). For the resistors shown here, which were taken from the sample kit, changes in sensitivity were negligible, therefore uncorrected and sensitivity corrected signals (using a test dose of 187 mGy) are almost identical. For some resistors from mobile phones minor sensitivity changes up to 10% could be observed and in these cases test dose normalization lead to an improvement in accuracy. However, in light of additional uncertainties, introduced by necessary correction procedures to be discussed below and with regard to reducing the time

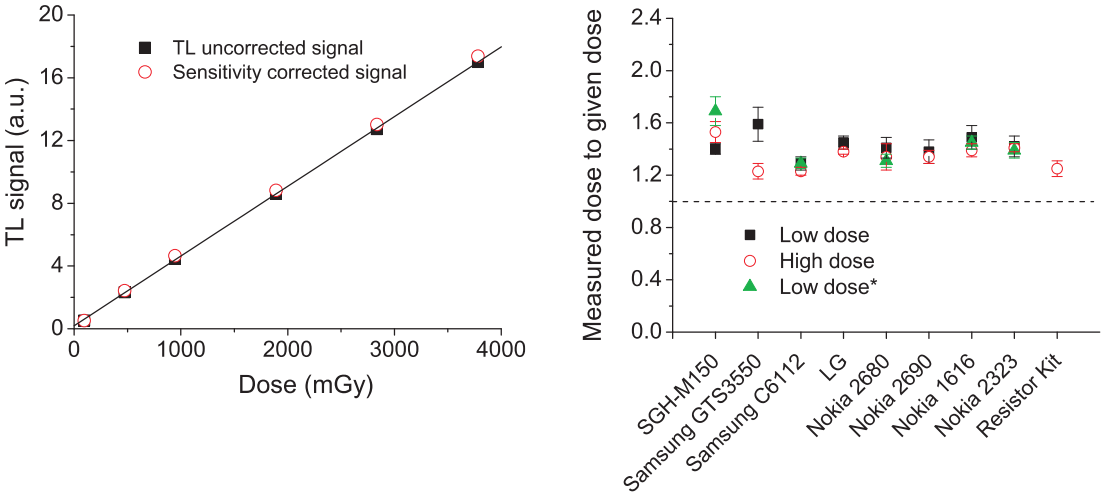

Figure 4.14.: TL dose response curve of a set of 10 resistors (taken from the kit?, left), with and without sensitivity correction. Results of a dose recovery test of resistors extracted from different mobile phones and the kit and with different pretreatments (right). For explanation of the three different pretreatments see text.

needed for dose assessment, it is recommended to accept the minor possible systematic error by sensitivity changes and omit test dose normalization.

Despite the excellent linearity of the growth curve, dose recovery tests reveal an overestimation of the given dose between approx. 20 and 60% (Fig. 4.14, right). To minimize the influence of the zero dose on the test result, three aliquots with 10 resistors each were measured per sample and with each aliquot given a different treatment:

1. Application of a sufficiently high dose, so as to make a possible zero dose negligible (given dose of 6 Gy)

2. Subtraction of the average value of the zero dose determined in the previous section (4.3.1.1), including uncertainty, from the measured dose (given dose of 0.5 Gy, black square symbols in Fig. 4.14)

3. Thermal cleaning of the lower temperature TL signal by a TL run up to 250°C before irradiation (given dose of 0.5 Gy, green triangle symbols in Fig. 4.14).

As can be seen from the figure, except for one sample (Samsung GTS3550), the degree of overestimation is fairly independent of the given dose or treatment. Obviously, there is a sensitivity change in the first TL run (first heating), which is not correctly monitored by the subsequent test dose measurement. A similar effect will be seen for inductors (see below). The average value and standard deviation for the systematic dose overestimation is 1.35 ± 0.11.

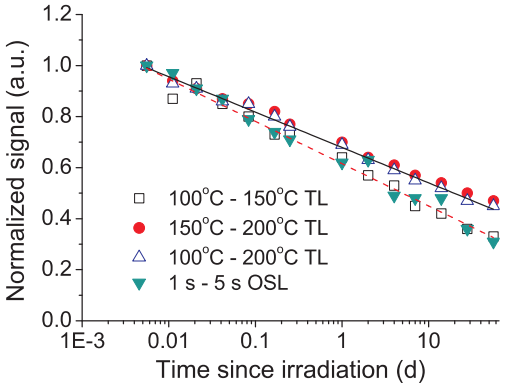

Figure 4.15.: Fading of the TL signal and the corresponding OSL signal of resistors taken from the kit. The different integration intervals of the glow curves are indicated in the legend.

4.3.1.3. Fading

The fading rate of the TL signals was determined by measuring aliquots of 10 resistors, size 1 x 0.5 mm, taken from a sample kit. Aliquots were irradiated with 2 Gy and stored in dark at room temperatures for duration of 8 min to 60 days. For every time range, two unmeasured aliquots with an identical set of resistors were used: one was measured by TL, the other by OSL for comparison. The TL glow curves of the resistor substrates were then analyzed in three different integration intervals: 100-200°C (standard), 100-150°C (lower part of the TL curve) and 150-200°C. OSL was integrated for the first 5 s of stimulation (Fig. 4.15).

The fading rate of the 100-150°C part of the TL curve and of the OSL signal are nearly identical. This corroborates the assertion that the fast components of the OSL signal are correlated with the lower temperature peaks in TL. The fading rate of the 100-200°C and 150-200°C part of the TL curve are also nearly the same, presumably because the peak temperature is located at approx. 170°C and thus only a minor part of the TL signal lies in the 100-150°C range. The fading rate of the whole analyzable area under the TL peak (100-200°C) is indeed lower than the fading rate of the OSL signal but the difference is not very large. To make full use of the reduction in fading rate, a shift of the integration interval of the TL signal towards higher temperatures would be desirable. However, this is impeded by the onset of the zero dose signal for temperatures above 200°C.

4.3.1.4. Evaluation

Trial irradiations on intact mobile phones using gamma sources and applying the described correction procedures will be presented in combination with inductors in Section 4.3.3. Here, we will evaluate the method based on the results obtained so far.

The potential advantages of using TL instead of OSL for dose assessment on resistors could in principle be demonstrated. TL measurements yield stronger signals (higher

sensitivity) than OSL and reduced fading rates are possible, when integrating the TL signal between 100-200°C. However, the impact of these advantages is rather small and they are at least compensated, if not outweighed by the necessity to perform additional corrections (subtraction of zero dose and correction for dose overestimation), introducing additional uncertainties in the dose assessment. Retrospective dosimetry using TL on resistors substrates can be a valuable option for radiation protection agencies equipped with conventional TL readers, without the possibility to perform optical stimulation. It can also be used to independently check the results of the dose assessment using OSL, as will be demonstrated further below. However, for emergency response, where speed of response is an important aspect, TL on resistors will not be the method of choice.

4.3.2. Inductors

In Inrig et al. (2008) indications are given that the TL glow curve of resistors shows little fading in the higher temperature region (250-400°C). The low intensity in this temperature region, as compared to the main dosimetric peak at 190°C and the corresponding OSL signal, however limited potential applications to high dose (>1 Gy) exposures. As has been shown in the previous section, strong zero dose signal in TL for temperatures greater than 250°C are generally observed for resistors, demonstrating that this part of the glow curve is not usable for dose assessment at all. This drawback can potentially be overcome by the use of inductors as sample material. As Fig. 4.3 already indicated, inductors display pronounced signals in the higher temperature region of the TL glow curve. They would thus be highly suited for dosimetry using this part of the TL curve, with the possibility of obtaining both high sensitivity and long term signal stability, thus circumventing the necessity of fading correction, if the absence of a zero dose signal can be shown and a suitable protocol developed. This will be investigated in the sections now to come (Fiedler and Woda, 2011).

4.3.2.1. Glow curve and dose response

A typical glow curve of a set of 10 inductors is shown in Fig. 4.16. The curve has five peaks at approximately 100, 140, 170, 270 and 340°C. In contrast to resistors, the higher temperature peak at 270°C is of an intensity comparable to the 170°C peak. The lower temperature peaks (100-170°C) are photosensitive and are correlated to an OSL signal observed from these components (see section 4.2.1). The peak at 100°C can be removed and the peak at 140°C sufficiently reduced by preheating for 10 s at 120°C. The 170°C peak is generally integrated from 100 to 200°C, the 270°C peak from 220 to 310°C for analysis. All inductors investigated so far have essentially shown no zero dose signal in the TL measurement in contrast to resistors.

The 170°C peak shows a negligible sensitization after 6 cycles of dosing and measurement whereas the sensitivity of the 270°C peak decreases after the first irradiation and increases with further cycles up to 40 % of the initial value. The reason for the sensitivity changes of the two peaks is not clear at present. Inductors extracted from mobile

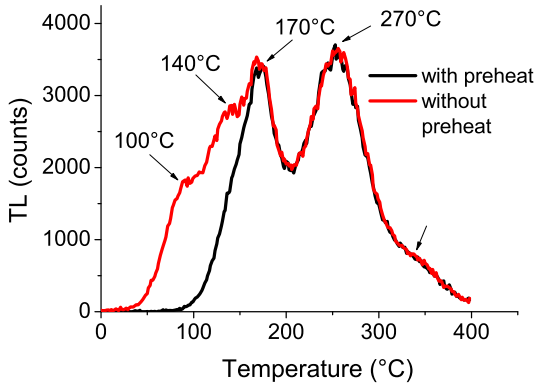

Figure 4.16.: Glow curve of a set of 10 inductors taken from a sample kit (TDK Corporation) and measured with and without preheating. The applied dose was 800 mGy.

phones show a higher decrease after the first irradiation than inductors from sample kits (Fig. 4.17). For the correction of the sensitivity change of both peaks we tested the single aliquot regeneration (SAR) measurement protocol with test dose normalization which is used for OSL measurement of quartz (Murray and Wintle, 2003). With this approach the dose response of the 170 and 270°C peak shows a linear increase in the dose range investigated from 100 mGy to 5 Gy, with excellent recycling ratios as can be seen in Fig. 4.17.

4.3.2.2. Dose recovery

Dose recovery tests were carried out on extracted inductors using the built-in beta source of the luminescence reader. The given doses were in the range from 100 mGy to 3 Gy and a test dose of 200 mGy was used for correcting the sensitivity changes. The tests showed that there is a sensitivity change in the first TL measurement which is not fully corrected by the given test dose. It leads to a systematic dose overestimation of 10 to 40 % (Fig. 4.18, left). This applies for both main peaks. For inductors extracted from mobile phones (sample No. 5-10) the overestimation is higher than for those taken from sample kits (sample No. 1-4). The reason for this behavior is at present not clear. It is possible that glue residues may amplify this effect. The average value and standard deviation for the systematic dose overestimation is 1.33 ± 0.12.

Analysis of the 190°C peak of an alumina rich resonator revealed that the apparent single peak is actually made up of either several closely overlapping or a quasi-continuous distribution of peaks (Woda et al., 2010). The same situation might apply to the 270°C peak of alumina inductors investigated here and in that case the dose overestimation might be dependent on the temperature interval over which the peak is integrated. To investigate this a plateau test was carried out, in which the recovered dose was calculated for small consecutive temperature intervals of 10°C, starting from

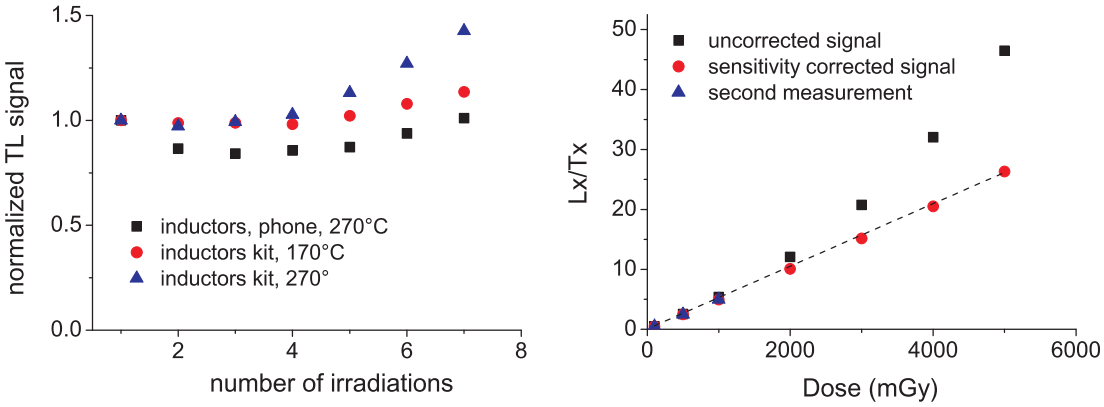

Figure 4.17.: Left panel: Change in sensitivity by repeated cycles of dosing and measurement. The given dose was 200 mGy and each sample consisted of 10 inductors. Right panel: Dose response of the 170°C and 270°C peaks for the uncorrected signals (black squares) and the sensitivity corrected signals (red circles) using a SAR measurement protocol with test dose normalization. The given test dose was 200 mGy. Recycling points are indicated by blue triangles.

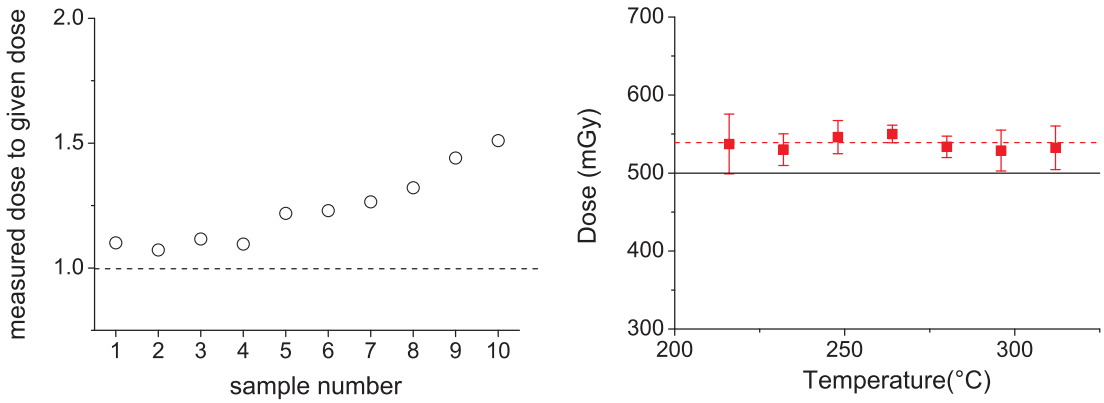

Figure 4.18.: Left panel: Results of the dose recovery tests, the given dose was 500 mGy. Right panel: Plateau test of the 270°C peak. The given dose was 500 mGy (black solid line). The dashed line shows the calculated dose for the integration interval 220-310°C .

220°C and going up to 310°C (Fig. 4.18, right). As can be seen from the figure, there is a homogenous dose information over the entire peak and thus a change of integration limits would not significantly reduce the overestimation of the dose.

4.3.2.3. Fading and detection limit

We studied the fading rate of the TL signal for both main peaks in a time range from some minutes up to two months. The fading rate was determined by measuring aliquots of 10 inductors, size 1 x 0.5 mm, taken from sample kits. For every time range, an unmeasured aliquot with an identical set of inductors was used. As shown in he left hand side of Fig. 4.19, the fading rate of the 270°C peak is considerably lower than that of the 170° peak of inductors and also than that of resistors. Resistors have only one main peak at 170°C in TL. In the first 6 hours the TL signal of the high temperature peak of inductors is relatively stable whereas the intensity of the 170° peak decreases about 10 % and that of the resistors already about 23 %. After one week the 270°C signal fades about 14 %, the 170°C signal of inductors about 31 % and that of resistors about 45 %. Even after two months the TL signal loss of the 270°C peak is only about 20 %, so that even with such a relative long time delay between exposure and measurement, dose assessment should be possible with acceptable accuracy.

First estimations of the signal detection limit (Fig. 4.19, right) for inductors demonstrate some variability dependent on the number of inductors and the type of mobile phone. The numbers of inductors found in different mobile phones can vary widely and also their TL properties such as sensitivity to radiation. In general the inductors from the sample kits used in this study have a lower detection limit than those removed from the mobile phones. A number of 10 inductors per measurement is desirable for a detection limit below 10 mGy.

4.3.2.4. Conclusions

Among the electronic components found in mobile phones alumina rich inductors seem particularly suitable for retrospective and accident dosimetry using TL. In contrast to resistors they show essentially no zero dose signal in TL and similar peak intensities for temperatures above and below 220°C. The 270°C peak of inductors turned out to be relatively stable compared to the OSL signal and the TL signal of resistors. Even weeks after exposure the fading rate is comparably low, the signal decreases by about 20 %. The dose response of the sensitivity corrected signals appears to be linear in the measured dose range from the given calibration doses of 100 mGy to 5 Gy. The dose recovery tests show however that there is a sensitivity change in the first TL measurement which is not fully corrected by the measurement protocol, so that the given dose is systematically overestimated and needs to be corrected. The applicability of a universal correction factor and the impact on the uncertainty of the dose assessment will be investigated in the next section. The detection limit is dependent on the number of inductors. With a number of 10 inductors with a size of 1.0 x 0.5 mm a detection limit of 10 mGy is possible.

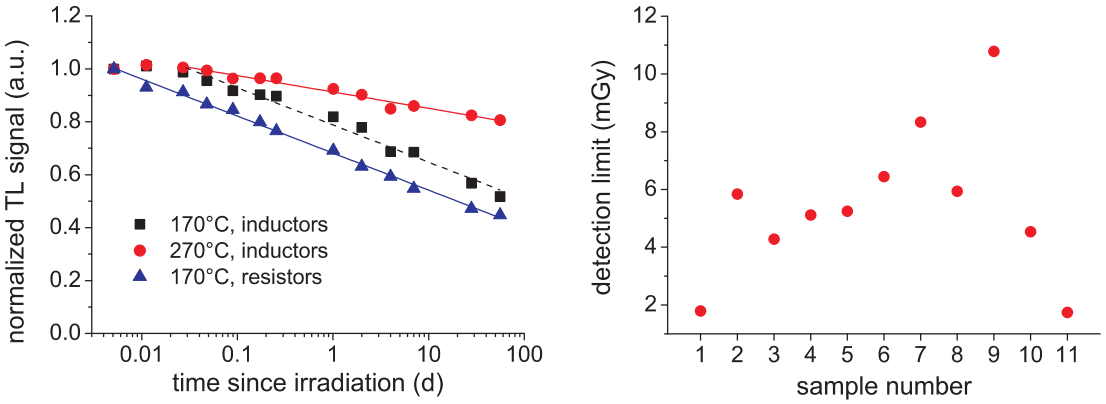

Figure 4.19.: Left panel: Fading of the TL signal for the two main peaks of inductors (taken from an inductor kit) and the 170°C peak (removed from a mobile phone). Right panel: Signal detection limit of inductors taken from the following samples: 1: inductor kit; 2: Nokia 2710; 3: Nokia 2680; 4: Samsung 3510; 5: Nokia 6300; 6: Nokia 2323; 7: Nokia 7230; 8: Nokia 3110; 9: Nokia X3; 10: Samsung 3550; 11: LG GD 330; 12: Nokia 1616 .

4.3.3. Irradiation trials

To evaluate the developed dose assessment techniques using TL on resistors and inductors, trial irradiations were conducted on intact mobile phones using ^{137}Cs gamma rays and affixing the samples to an ISO water slab phantom (ISO, 1999). Administered dose was 500 mGy (air kerma). Distance of the circuit board within the mobile phones to the source was 1 m, with the front side of the phone (display glass) facing the source. After irradiation, mobile phones were disassembled in the laboratory (under dark room conditions), electronic components extracted, cleaned, dried and placed onto the measuring cup. Two cups per phone were prepared with resistors (for TL and OSL) whereas for inductors, the number of available components only allowed the preparation of one cup for TL. Typical delays between mid of irradiation and beginning of measurement were 2 to 3 hours. After data analysis, dose values measured by OSL on resistors were corrected for fading, dose values measured by TL on resistors for fading, zero dose and dose overestimation and dose values measured by TL on inductors only for dose overestimation. Results are presented in Fig. 4.20.

As can be seen dose values measured with both TL and OSL on resistors are in good agreement with the given dose. This demonstrates that the correction procedures developed for TL (zero dose and dose overestimation) work adequately. It should be noted that the air kerma value at the position of the circuit board within the mobile phone, with which the results are compared, is not necessarily the dose that is actually deposited in the electronic components.

For inductors, however, there is a systematic overestimation of the given dose by 30-50%, which is not corrected by the applied correction factor (sample #s 1,2). Comparison with the result obtained for inductors, taken from a sample kit and placed

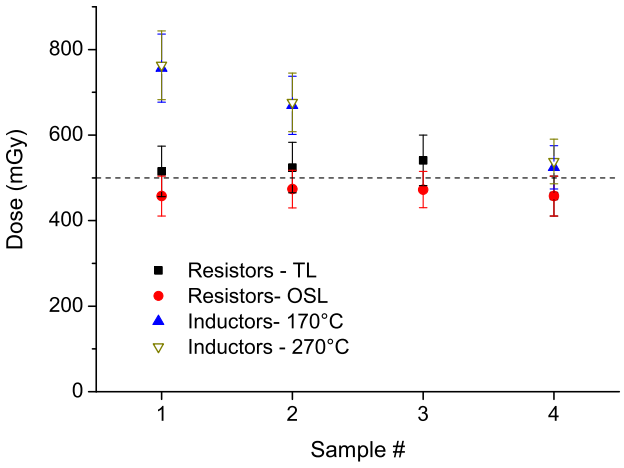

Figure 4.20.: Trial irradiations on intact mobile phones using ^{137}Cs gamma rays. The samples were affixed to the ISO water slab phantom and irradiated with 500 mGy (dashed line). Sample code: 1: Nokia 6600; 2: Nokia 6303ci; 3: Motorola; 4: Resistors and Inductors from sample kits placed in Nokia 6600.

within the mobile phone (sample #4), where good agreement with the given dose is observed, shows that the overestimation cannot be due to a local deposition of a higher dose, as compared to air kerma, in the inductors. The degree of overestimation is the same for the 170°C and 270°C TL peak. Whether this is due to the possibility that the range of overestimation investigated in Fig. 4.18 is not exhaustive (or not yet representative) and much higher overestimation can occur also after beta irradiation or whether there is a systematic difference between beta and gamma irradiation for inductors (for as yet unknown reasons), can at present not be decided. More work is needed to better evaluate the potential of inductors for emergency dosimetry using TL.

4.4. Photon Energy dependence of portable electronic devices

4.4.1. Experimental set-up

The photon energy dependence of resistors in a mobile phone using OSL was investigated within the framework of a bachelor thesis at the Munich University of Applied Sciences (Dürr, 2011). A mobile phone model "Nokia 6300" was used as a representative example (dimensions $107 \times 44 \times 14$ mm), which was introduced into the market in 2011. Around 45 resistors, distributed over the circuit board, were detached, cleaned and dried. At the original locations of the resistors on the board, double-sided adhesive tape was fixed. With this approach, 21 resistors could be easily affixed and removed from the circuit board many times for consecutive cycles of irradiation and measurement. From time to time, resistors were cleaned in acetone to remove gradually

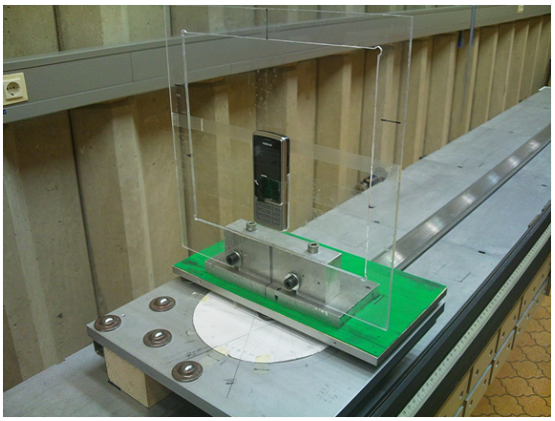

Figure 4.21.: Rotatable board and plastic frame for irradiation of the mobile phone at 80 cm distance from the X-ray source. The circuit board of the mobile phones is at the centre of rotation.

increasing amount of sticking adhesives from the tape.

For the irradiation, a frame out of polystyrol was constructed, with outer dimensions of 30 × 30 cm, inner dimensions of 25 × 25 cm and thickness of 4.6 cm. The mobile phone was fixed in the middle of the frame with the use of adhesive tape (Fig. 4.21).

At 80 distance to the X-ray and gamma sources, the frame was not in the course of rays for angles of incidence up to 60°. The mobile phone was fixed in such a way to the frame that at an angle of incidence of 90°, the frame was not directly between source and circuit board. For comparison, irradiations were also done on extracted resistors, placed in a PMMA holder of 3 mm wall thickness. For the lowest photon energies used (E_{av} of 24 keV and 33 keV), irradiations were additionally done without the PMMA holder, by directly placing the resistors on the adhesive tape. Since a systematic different trend in detector response was not found for irradiations with and without PMMA holder, the mean and standard deviations from the measured OSL signals was calculated for the two energies. Irradiations with a phantom were done using the ISO water slab phantom.

Irradiations were performed at the Secondary Standard Dosimetry Laboratory of the Helmholtz Zentrum München using ^{137}Cs, ^{60}Co and X-ray sources, the latter with ISO narrow spectrum qualities from N30 to N300 (ISO, 1996). To achieve a sufficient signal to noise ratio, the given dose was set to 200 mGy (air kerma free in air). To avoid systematic errors introduced by a fading correction, all irradiations were done using the same dose rate of approx. 50 µGy s^{-1} and always keeping the same time delay between end of irradiation and beginning of measurement. In this way, OSL signals can be compared directly, without the necessity of fading correction. OSL was measured for 150 s, followed by test dose normalization. A final optical readout for 500 s was conducted, prior to the next irradiation and measurement cycle, to sufficiently reduce the slow components.

From repeated cycles of irradiation and measurement at N-150 (118 keV), a mea-

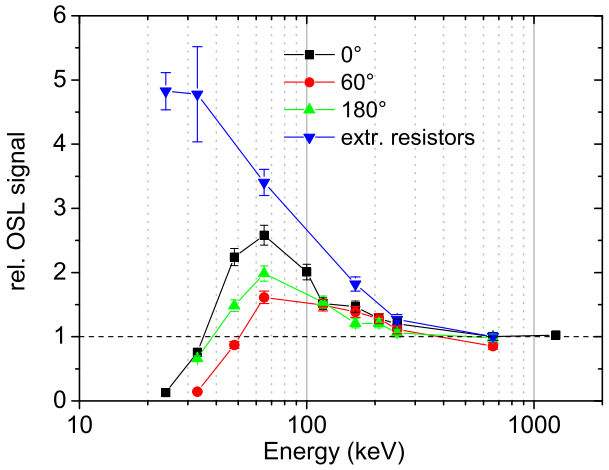

Figure 4.22.: Relative Energy Response (RER) of extracted resistors (blue symbols) and of the same resistors built-in the mobile phone and irradiated at different angles. The response of the extracted and built-in resistors are normalized to their respective value at 662 keV (0°).

surement uncertainty with the experimental set-up of 6% (1 σ) was estimated. Further experimental details can be found in Dürr (2011).

4.4.2. Results

Fig. 4.22 shows that the OSL signal of extracted resistors shows an over-response at low photon energies of a factor of four to five. The shape of the relative energy response (RER) of extracted resistors is qualitatively similar to the one measured by Beerten and Vanhavere (2010) for an extracted ceramic resonator and to the one measured by Akselrod et al. (1990) for α-Al_2O_3:C, although the degree of over-response in the latter was only a factor of three.

However, Fig. 4.22 also clearly demonstrates, that the casing of the mobile phone cannot be ignored and plays and important role in the photon energy response. Above 250 keV, the energy response for extracted and built-in resistors is very similar. In this energy region, Compton scattering is the main mechanism of energy deposition, which, for not too heavy elements, will be independent of the elemental composition and in addition at high enough energies attenuation by either the PMMA holder or the mobile phone casing becomes negligible. For energies below 100 keV, photo effect becomes increasingly important, which has a pronounced dependency on material composition and thus differences in mass thicknesses will make stronger effects. Therefore the maximum over-response for the built-in resistors is reduced to a factor of approx. 2.6 at 65 keV and falls down to 0.16 at 24 keV, due to almost complete shielding of the resistors by the casing at this low energy. As expected, the mobile phones also has a

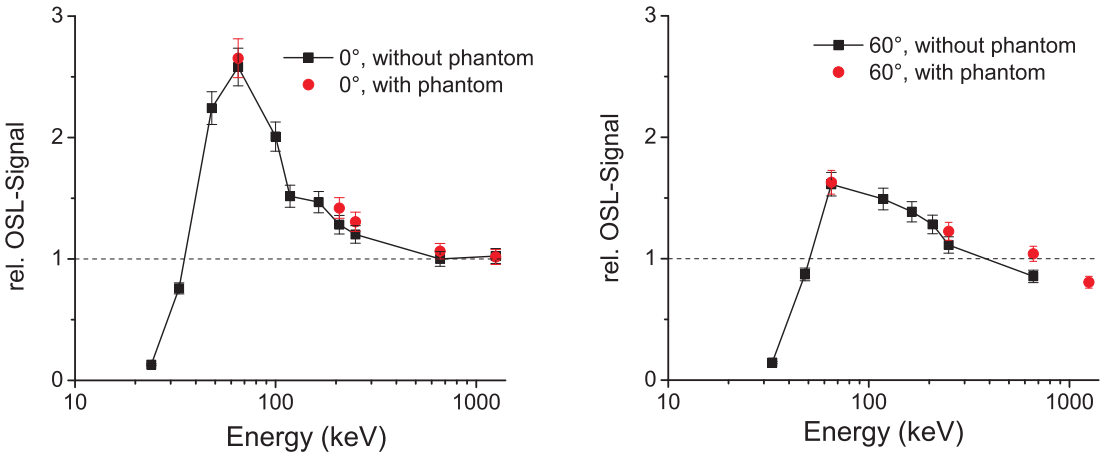

Figure 4.23.: Relative Energy Response of built-in resistors for irradiations with and without water phantom and two different angles of incidence.

clear angular dependence, with the maximum over-response reduced to about 1.6 for an angle of incidence of 60°. The difference in energy response for front (0°) and back (180°) irradiation is due to the stronger shielding effect of the rechargeable battery, as compared to the display window.

Irradiations with the phantom gave very similar results than irradiation free in air (Fig. 4.23). There is some indication for slight enhancement for irradations at 60° and higher photon energies but generally backscattering from the phantom into the circuit board of the mobile phone can be neglected.

In the worst case, an overestimation of the dose in air by a factor between 1.6 and 2.6 could thus occur, in reality it will be less, due to broadening of the photon spectrum as a result of scattering processes in the environment of the exposed person. The strong underestimation of the air kerma value for low energies is not of great concern for emergency dosimetry, as, irrespective of the exposure geometry, the ratio effective dose to air kerma becomes equally small in this energy range, as the layers of skin and muscles will shield the radiation sensitive organs in a very similar way as the casing of the mobile phone does. Fig. 4.22 can thus serve as the basis for calculations of dose conversion coefficients (dose in material to dose in air) for different exposure scenarios.

5. An environmental BeO-OSL dosimeter for emergency response

In the event of a radiological emergency in an urban environment a reliable overview on the radioactive contamination is crucial for decision making. Established post-event measurement approaches for emergency response are car- or airborne measurements of the gamma dose-rate (GDR), initiated in the case of nuclear emergencies when stationary monitoring systems indicate the completion of cloud passage through the respective city. As such these methods miss the contribution to the external exposure from the passing cloud, which could be even more important for a small scale incident such as the deployment of a radiological dispersion device (RDD). As a useful complementary method, an approach using measurements of absorbed dose derived from luminescent detectors pre-fixed at places of high importance (public squares, subway stations) is currently being developed. The data originate from geo-referenced points but do not provide full spatial information. We present a procedure to produce maps of reference gamma dose rate, air kerma, surface contamination and effective dose in urban areas from localized dose measurements. The detector employed should be cheap, environmentally stable up to several years, easy to collect and measure, and give a reasonable estimate of the air kerma at the detector position in the shortest amount of time possible. Environmental monitoring has long been performed using thermoluminescent detectors, such as $CaSO_4$:Dy, CaF_2, LiF:Mg, Ti and LiF:Mg,Cu,P. However, in the past decade optically stimulated luminescence (OSL) has increasingly become an attractive and important alternative dosimetric method, with the potential advantage of faster readouts as compared to TLDs. Carbon doped Aluminum oxide is an example of an ultra-high sensitive and widely used OSL dosimeter, however the higher effective Z as compared to air or soft tissue implies that the combination of several filter elements and detectors is needed for a reasonable flat energy response (Imatoukene et al., 2008). In this study we will focus on the use of BeO as an environmental dosimeter for emergency response. BeO has first been systematically characterized using OSL by Bulur and Göksu (1998) and has received considerable interest in recent years for the use as a personal dosimeter and application in medical dosimetry using OSL (Sommer et al., 2011, 2008, 2007). Purchased in large quantities, it is inexpensive and has highly favourable luminescence properties: high sensitivity, linear dose response up to several Gy, long term signal stability and tissue and near air equivalence (Sommer and Henniger, 2006). We have developed a simple packaging based on black Perspex. The detector is characterized according to light tightness, dose response and angular photon energy dependence. A brief conceptual overview of the approach for map production from the localized dose measurements is also given.

5.1. Experimental design

5.1.1. Pre-considerations

Area dosimeters used to monitor the environmental radiation around nuclear or radiological facilities are usually designed and calibrated to measure the ambient dose equivalent H*(10) (ISO, 1999). From this radiation protection quantity an immediate estimate of the effective dose at the detector position can be estimated if the exposure geometry is not well known. AP irradiation is then usually considered as a conservative estimate (ICRU, 1985). In the present application, however, the aim is somewhat different. Deposition of aerosols from the radioactive cloud occurs either by sweeping over open surfaces under dry conditions (Fig. 5.1, left) or via precipitation with rainfall under wet conditions (Fig. 5.1, right).

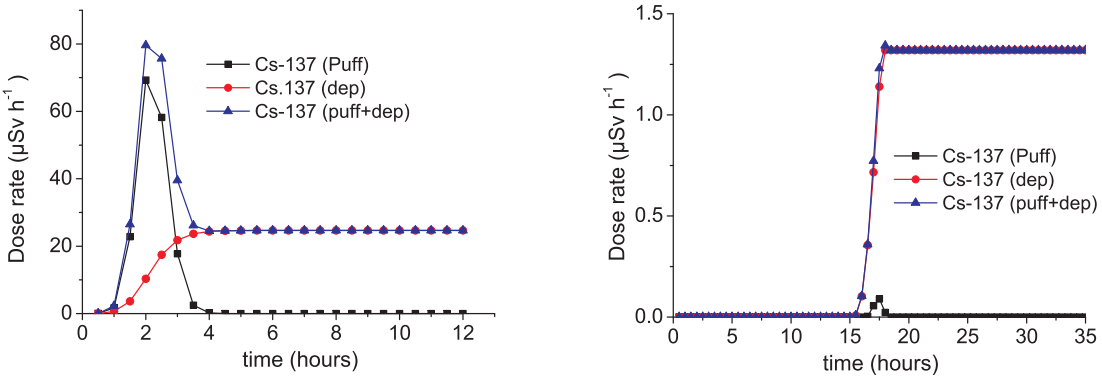

Figure 5.1.: Simulated gamma dose rate (GDR) readings from fixed detectors after nuclear power plant (NPP) accidents for dry deposition (top) and wet deposition (bottom) (thanks to Poul Astrup, Risø, DK). The simulations were carried out for the same amount of released activity (2.16×10^{16} Bq of ^{133}Xe and ^{137}Cs, respectively , released over a period of 6 hours) but for different European countries, weather conditions and sensor distances, explaining the differences in the magnitude of the recorded dose rate. "Puff Cs-137" denotes the dose rate due to ^{137}Cs in the cloud, "dep Cs-137" the dose rate due to ^{137}Cs deposited on the ground.

During dry deposition a substantial dose contribution from cloud shine emerges which cannot be detected by post-event measurements but which would be picked up by the dosimeter. The ratio between effective dose and air kerma for the two simultaneous irradiation geometries (cloud shine and ground shine) can differ up to a factor of two (Fig. 5.2). Therefore the dosimeter should be designed and calibrated to measure the air kerma with reasonable accuracy. The software module for map production can then make separate estimations for effective doses resulting from cloud and ground shine.

5.1.2. Holder design

For the holder black Perspex (PMMA) was chosen as a material with excellent environmental stability. The wall thickness around the dosimeter is 5 mm, which is regarded

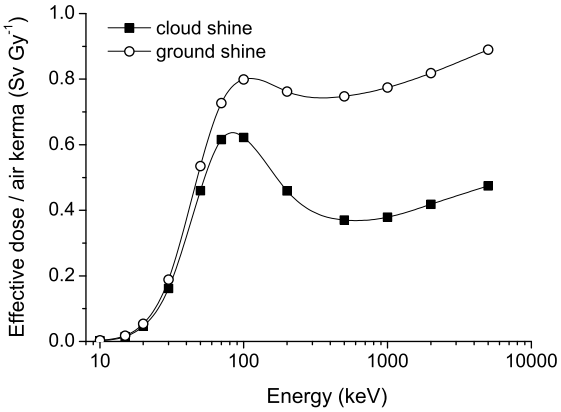

Figure 5.2.: Ratio between effective dose and air kerma for a monoenergetic semi-infinite cloud source (closed squares) and for a monoenergetic plane source at the air-ground interface (open circles). Calculated from data in Eckerman and Ryman (1993).

Figure 5.3.: Example of an OSL detector in a black perspex casing fixed to a building wall at 1 m height.

as a compromise between sufficiently stopping external beta radiation while minimizing the attenuation of low energy photons at the same time. Smaller wall thickness also proved not to provide sufficient light shielding, while for the present holder no depletion of the OSL signal could be detected after two days of storage in direct sun light in July and overnight storage under white fluorescent light. The lid of the holder is fixed with two metallic screws to the bottom; the holder itself can be affixed to a wall at the reference height of 1m using a torque screw. An additional O-Ring ensures water tightness (Fig. 5.3). Disc shaped BeO ceramics (Thermalox TM 995, Brush Wellman Inc., USA) with 4 mm diameter and 0.8 mm thickness were used (production batch from 1989).

5.1.3. Reference radiation and luminescence measurements

Irradiation of the dosimeter with different energies was performed at the Secondary Standard Dosimetry Laboratory of the Helmholtz Zentrum München using ^{137}Cs, ^{60}Co and X-ray sources, the latter with ISO narrow spectrum qualities from N30 to N300 (ISO, 1996). The detector was fixed with adhesive tape to a frame of polystyrol, which in turn was mounted on a rotatable board. The dosimeter was positioned at the center of rotation. All irradiations were done in terms of air kerma free in air, with a dose of 3 mGy, and using the same dose rate of approx. 20 µGy s^{-1}. The incident angles investigated are given in Table 1.

OSL measurements were performed using an automated luminescence reader (model Risø TL/OSL-DA-15), using blue LED's for optical stimulation and a Hoya U-340 filter for detection. The reader houses a beta-irradiator holding a 90Sr/90Y source (1.48 GBq). Following Bulur and Yeltik (2010), the BeO discs were annealed at 650°C for 1 h prior to irradiation and OSL was measured at 50°C following a preheat of 10 s at 160°C (5°C s^{-1}).

5.2. Results and discussion

5.2.1. Dose response

The luminescence reader employed operates in photon counting mode and uses no count divider (pers. comm. H. Christiansen, Risø), therefore loss of counts will occur above 5 MHz. For the BeO ceramics this implies that only doses up to approx. 300 mGy can be measured with full stimulation power. For measurement of higher doses, neutral density filter or aluminum diaphragm could be applied, however this requires an a-priori knowledge of the dose, which is not given in an emergency situation. Alternatively, the dosimeters can be first stimulated with only 1% power for 5 s (Fig. 5.4).

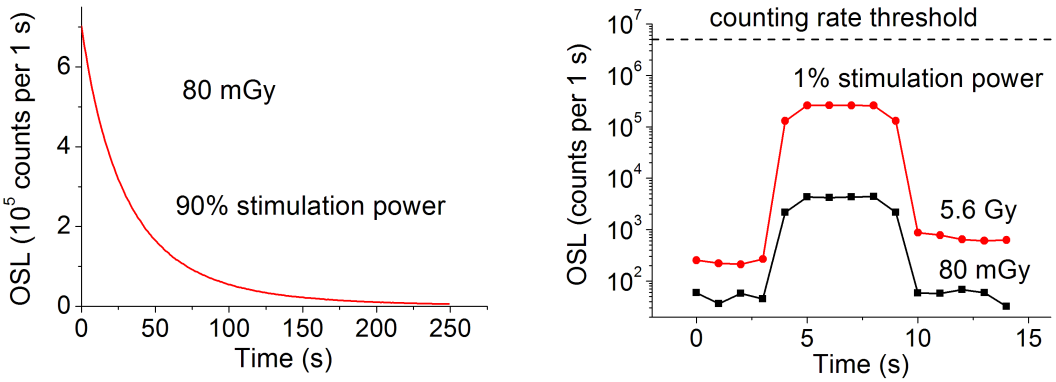

Figure 5.4.: OSL readout of the BeO dosimeters at two different stimulation powers using an automated Risø luminescence reader.

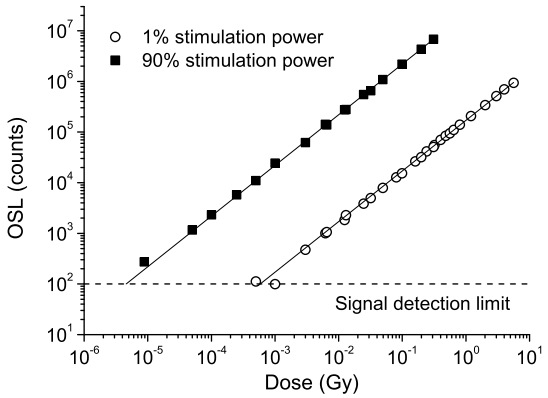

Figure 5.5.: OSL dose response of the BeO dosimeters. Irradiations above and below 80 mGy were performed using the beta source of the luminescence reader and the ^{137}Cs source of the SSDL with casing, respectively. A line through origin is fitted to both dose response curves.

This will enable a measurable dose range from tens of Gy's down to approx. 1 mGy without loss of information. Subsequently those dosimeters showing no signal can be stimulated at 90% power to open the measurable dose range between a few mGy and the minimum detectable dose of around 5 µGy for the present system (Fig. 5.5). The detection limit is close to the value found by Bulur and Yeltik (2010) using similar equipment and BeO ceramics. This value is only valid for freshly thermally annealed samples. Within the present concept, with BeO detectors affixed to building walls or structures and possibly stored for several years before a radiation incident, the detection limit will be mainly determined by the uncertainty in the background dose estimate.

Results from fading experiments indicate that the relative contribution of shallow traps of the OSL signal might be less than 5% (Sommer and Henniger, 2006; Sommer pers. comm.). Thus for the degree of accuracy needed here it might be possible to do without preheating. If the dosimeters have been calibrated in advance and the values stored in a database or if a subset from a large production batch with acceptable homogeneity can be chosen, then pure optical readouts of 5-10 s are sufficient for dose estimation. Even when taking into account the two-step readout process (screening with 1% power and subsequent full readout of selected dosimeters with 90% power) it should thus be easily possible to process up to 60 dosimeters per hour.

5.2.2. Energy response

The relative response of the dosimeter as a function of photon energy, expressed in air kerma for incident angles of 0° and 60° is given in Fig 5.6, left. As expected, the response decreases moderately for lower energies as a result of the slightly lower effective Z of BeO as compared to air and the additional shielding by the Perspex. If the detector is

calibrated to the response at N-150, then the variation lies in between ±25% for 0° and only increases to –35% on the lower energy side for 60°. This qualifies as an essentially flat energy response.

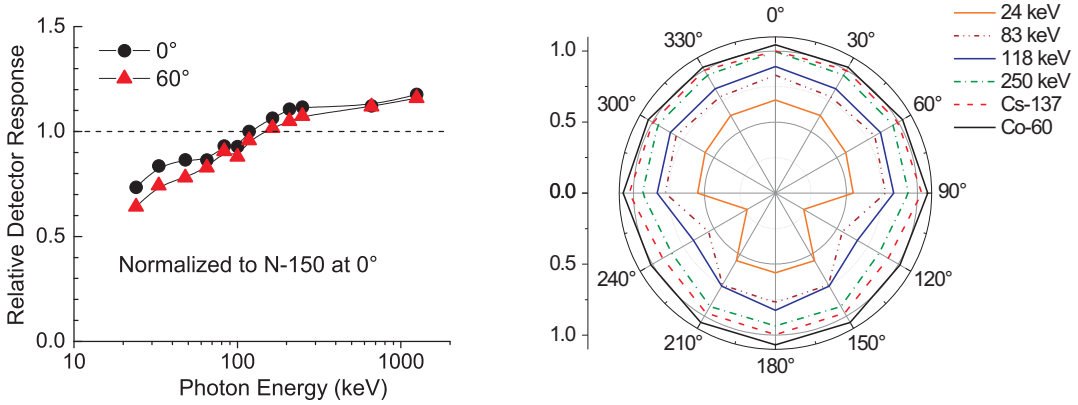

Figure 5.6.: Left: Relative detector response, measured in terms of air kerma, for incident angles of 0° (closed circles) and 60° (open triangles). The data are normalized to the response at N-150 (E_{av} = 118 keV) at 0°. Measurement uncertainty was estimated at around 3% and is smaller than the size of symbols. Right: Angular response of the detector at different photon energies. Values between 180° and 360° are duplicated from the respective values between 0° and 180°, which is justified by the symmetric design of the casing. At angles of 120° and 240°, the metallic screws are in the beam.

This is also true for most angles of incidence, except for 120°C and 240°C, where in the present set-up the metallic screws are directly in between source and detector (5.6, right). This however will only decrease the backscatter by the building material and therefore is a desirable property. Excluding these two angles the variation in angular response ranges from 2% for ^{137}Cs to around 8% for 24 keV. The difference between measured dose and true air kerma with the detector affixed to various building materials remains to be investigated.

5.2.3. Map production and double detector technology

In urban areas, the dose measured by the dosimeter strongly depends on the detector environment. To account for this dependence, each dose is multiplied by a location factor, which quantifies the deviation of the recorded dose from the hypothetical dose obtained over a reference surface of an infinitely extended lawn (Meckbach et al., 1988). For a fixed BeO detector the environment is known in advance. Hence, the location factor can be determined with good precision.

After correction with location factors high resolution maps are produced from the localized dose measurement using two approaches, depending on the number of measurements and/or the scenario:

- For very few measurements, as can be expected after an RDD event, the doses are fitted to a Gaussian plume model, with known meteorological input parameters (see next chapter). The model can then make separate estimation of effective doses from ground and cloud shine over the area of interest.
- If enough measurements (> 10) are available, which is the typical situation after a NPP accident with large-scale emissions, the Inhabited Areas Monitoring Module (IAMM, Kaiser and Pröhl 2007) is applied. IAMM is an operational module of the European decision support systems RODOS and ARGOS (Raskob and Hugon, 2010) and uses geo-statistical interpolation or data assimilation for map production. The module will however only make estimation of contributions from ground shine. By placing two detectors at the same location and by collecting the first promptly after cloud passage and the second some hours later, dose contributions from ground shine and cloud shine can be separated experimentally.

5.3. Conclusions

The conceptual design to produce maps of radioactive contamination in urban areas from OSL detector measurements consists of

- Use of BeO as an inexpensive, environmentally stable dosimeter with highly favourable properties
- Installation of two BeO detectors at pre-defined urban locations
- Collection of detectors promptly after deposition and some hours later
- Rapid processing of up to 60 dosimeters per hour with a detectable dose range of 6 orders of magnitude
- Signal correction with location factors
- Map production with plume model fitting or geo-statistical interpolation

BeO detectors provide information of the actual exposure during the event, which cannot be detected by post-event measurements. Their dose response curve allows a reconstruction at low doses which are not accessible with either biodosimetry methods or fortuitous dosimeters such as chip cards or mobile phones.

6. Map production from localized dose measurements

6.1. The Inhabited Area Monitoring Module (IAMM)

The Inhabited Area Monitoring Module (IAMM) is an operational module of the European decision support systems RODOS and already installed at the BfS. In its present form, it can produce maps of contamination in urban environments from localized dose rate measurements (after correction for the detector environment), e.g. from car-borne measurements with a dose-rate meter. In order to be able to process the dose readings from the BeO detectors, the dose measurements must be pre-processed and converted into synchronized dose rate measurements. The synchronization is important because interpolation only works for comparable measurements at the same time t_m (time of map production), whereas the dosimeters around the city might have been collected and measured at different times t_γ. The formal approach for processing of the dose data is developed in this section.

Let D be the total dose, as sum of the nuclide doses: $D\left(t-t_0\right) = \sum_i d_i(t-t_0)$. From the OSL detector measurements and from air- or car-borne gamma spectrometric measurements following the radiological incident, the dose $D\left(t_\gamma - t_0\right)$ at the time t_γ and the nuclide weights $w_i\left(t_\nu\right)$ at a certain time t_ν are known (t_ν is the time of nuclide vector measurement) . The gamma dose rate g_i at time t due to the i_{th} nuclide then is:

$$g_i\left(t\right) = \exp\left[-\lambda_i\left(t-t_o\right)\right]\, g_i\left(t_0\right)\ , \tag{6.1}$$

and the corresponding dose from time of deposition t_0 to a certain time t_1:

$$d_i\left(t_1-t_0\right) = \int_{t_0}^{t1} g_i\left(t\right) dt = \underbrace{\frac{g_{i(t_0)}}{\lambda_i}}_{d_i(t\to\infty)} \left[1-\exp\left[-\lambda_i\left(t_1-t_o\right)\right]\right]\ . \tag{6.2}$$

With the nuclide weights w_i, the nuclide dose rate at the time of deposition$g_i(t_0)$can be related to the total gamma dose rate at time of deposition $G(t_0)$ via $g\left(t_0\right) = w_i\left(t_0\right) G\left(t_0\right)$ and $G\left(t_0\right) = \sum_i g_i\left(t_0\right)$. For the ratio of the total dose at two different times t_1 and t_2 we then get:

$$\frac{D\left(t_2-t_0\right)}{D\left(t_1-t_0\right)} = \frac{\sum_i \left(1-\exp\left[-\lambda_i\left(t_2-t_0\right)\right]\right)\frac{w_i(t_0)}{\lambda_i}}{\sum_i \left(1-\exp\left[-\lambda_i\left(t_1-t_0\right)\right]\right)\frac{w_i(t_0)}{\lambda_i}} \tag{6.3}$$

$$= \frac{P\left(t_2-t_0\right)}{P\left(t_1-t_0\right)}, \tag{6.4}$$

with $P\left(t-t'\right) = \sum_i \frac{w_i(t')}{\lambda_i}\left(1-\exp\left[-\lambda_i\left(t-t'\right)\right]\right)$ denoting a "propagator". Note that $G(t_0)$ cancels out in equation 6.3. The weights $w_i(t')$ are defined as:

$$w_i\left(t'\right) = w_i\left(t_\nu\right)\exp\left[-\lambda_i\left(t'-t_\nu\right)\right]/N\left(t'-t_\nu\right) \ ,$$

with $N(t'-t_\nu)$ denoting a "normalization factor":

$$N\left(t'-t_\nu\right) = \sum_i w_i\left(t_\nu\right)\exp\left[-\lambda_i\left(t'-t_\nu\right)\right] \ .$$

With the definitions for the "Normalisator" for the gamma dose rate and the "Propagator" for dose (note that these definitions depend only on the nuclide vector and decay, not on measurements):

$$N\left(t-t'\right) = \sum_i w_i\left(t'\right)\exp\left[-\lambda_i\left(t-t'\right)\right]$$

$$P\left(t-t'\right) = \sum_i \frac{w_i\left(t'\right)}{\lambda_i}\left(1-\exp\left[-\lambda_i\left(t-t'\right)\right]\right) \ ,$$

the following useful relations apply for the derivative:

$$\frac{\partial P\left(t-t'\right)}{\partial t} = N\left(t-t'\right) \ ,$$

for the time propagation:

$$N\left(t-t''\right) = N\left(t-t'\right)\cdot N\left(t'-t''\right) \ ,$$

and for the inverse:

$$N\left(t-t'\right) = \frac{1}{N\left(t'-t\right)} \ .$$

$N(t-t')$ can also be interpreted as the propagator for the gamma dose rate, as:

$$G\left(t\right) = N\left(t-t'\right)G\left(t'\right) \ ,$$

whereas the reason for calling $P(t-t')$ the propagator for dose becomes evident from the following:

$$D\left(t-t_0\right)=\int_{t_0}^{t}G(t')\,dt'=\int_{t_0}^{t}N(t'-t_0)G(t_0)\,dt'=P(t-t_0)G(t_0)\,.$$

Finally, the developed formalism also displays the additive dose relationship, as it should be:

$$D\left(t-t_0\right)=D\left(t-t'\right)+D\left(t'-t_0\right)$$

and

$$P\left(t-t_0\right)=P\left(t-t'\right)N\left(t'-t_0\right)+P\left(t'-t_0\right)\ .$$

Having established the necessary formalism, we are now in a position to sketch the procedure, how to process dose measurements in IAMM:

Input data are $D\left(t_\gamma-t_0\right)$, the OSLD measurements at t_γ (after multiplication with the appropriate location factor) and $w_i(t_\gamma)$, the nuclide weights at t_ν. The synchronization of the gamma dose rate measurements:

$$G\left(t_m\right)=\frac{N\left(t_m-t_\nu\right)}{N\left(t_\gamma-t_\nu\right)}G\left(t_\gamma\right)$$

is now replaced by the synchronization of dose measurements:

$$G\left(t_m\right)=\frac{N\left(t_m-t_\nu\right)D\left(t_\gamma-t_0\right)}{N\left(t_0-t_\nu\right)P\left(t_\gamma-t_0\right)}\,.$$

In this way, the dose measurements $D\left(t_\gamma-t_0\right)$ at different times t_γ are converted into synchronized gamma dose rates $G(t_m)$ at the desired time of map production, t_m. These gamma dose rates $G\left(t_m\right)$can then be interpolated with IAMM to produce a map of surface contamination (for details see Kaiser and Pröhl (2007)). From the interpolated gamma dose rates the doses at specific points of interest can then be back calculated via:

$$D\left(t_m-t_0\right)=\frac{P\left(t_m-t_0\right)}{N\left(t_m-t_0\right)}G\left(t_m\right)\ ,$$

and, if desired, also the nuclide-specific dose:

$$d_i\left(t_m-t_0\right)=\frac{p_i\left(t_m-t_0\right)}{N\left(t_m-t_0\right)}G\left(t_m\right)\ ,$$

with

$$p_i=\frac{w_i\left(t_0\right)}{\lambda_i}\left(1-\exp\left[-\lambda_i\left(t_m-t_0\right)\right]\right)\ .$$

6.2. The Gaussian Dispersion Model

The interpolation approach of IAMM requires a certain minimum amount of dose measurements to produce reasonable results. Certainly interpolation is meaningless when only a few OSLD readings, say two to three, are available. This, however, is exactly the probable scenario after a small scale distribution of radionuclides in the environment, such as the deployment of a RDD device in a public square. In order to be able to make at least a rough estimate of the degree of urban contamination and human exposure in this case, a complementary approach is developed here, based on the application of a simple Gaussian dispersion model in order to estimate the spread of the material both in the air and on the ground. By combining information from OSLD measurements and known meteorological parameters, the source term can be inversely determined from the Gaussian dispersion model by using the Levenberg-Marquardt Algorithm. A simple routine **OPTLMDOSE.f90** has been written which calculates the source term by making use of this approach. In the following sections the implementation of Gaussian plume model in the routine and the calculation of total γ-dose is described in section 6.2 and 6.3. The routine that calculates optimization using the Levenberg-Marquardt Algorithm is presented in section 6.4. The application of the routine to synthetic and real experimental data is described in 6.5 and 6.6 respectively. The routine is provided as text in the Appendix.

The Gaussian dispersion model Pasquill (1974) describes the dispersal of material over distances up to 10 km from a source Q_r. It is an approximated solution of the classical diffusion equation $\frac{dC}{dt} = Q(x, y, z, t)$ where Q is the source term and C is the concentration of contaminant in case of a continuous release of pollutant. The basic assumptions for deriving the model are:

- Windspeed and direction are constant from source point to receptor (for a windspeed of 2 m/s and a distance of 10 km, 80 minutes of constant conditions would be needed).
- Atmospheric turbulence is also constant throughout the plume travel distance.
- All of the the plume is conserved, meaning: no deposition or washout of the plume components; components reaching the ground are reflected back into the plume; no components are absorbed by bodies of water or by vegetation; and components are not chemically transformed.
- Only vertical and crosswind dispersion occurs (i.e., no downwind dispersion).
- The dispersion pattern is probabilistic and can be described exactly by Gaussian distribution.
- The plume expands in a conical fashion as it travels downward, whereas the ideal "coning plume" is only one of many observed plume behaviors.
- Terrain conditions can be accommodated by using one set of dispersion coefficients for rural terrain and another set for urban terrain. The basic Gaussian dispersion

equation is not intended to handle terrain regimes such as valleys, mountains or shorelines.

The Gaussian models assume an ideal steady-state of constant meteorological conditions over long distances, idealized plume geometry, uniform flat terrain, complete conservation of mass, and exact Gaussian distribution. The dispersion factor

$$\chi(x,y,z;H) = \underbrace{\frac{1}{2\pi\sigma_y(x)\sigma_z(x)u(x)}}_{1} \underbrace{\exp^{-\frac{y^2}{2\sigma_y(x)^2}}}_{2} \underbrace{\left(e^{-\frac{(z-H)^2}{2\sigma_z(x)^2}} + e^{-\frac{(z+H)^2}{2\sigma_z(x)^2}}\right)}_{3} \tag{6.5}$$

can be interpreted as the time integrated concentration of spread material by a unity source in $[s/m^3]$. The coordinate system is Cartesian and depends on the location of the source and on its wind direction. The source is located in the origin of the system at a given release height z above the surface. The positive x-axis lies in the direction of the mean wind. The z-coordinate is the height above the surface. The y-axis lies in the crosswind direction. The wind speed u (m/s) is accounted in term 1; term 2 and 3 account the effective height H of the plume and its width of the plume. In particular term 2 describes the crosswind shape of the plume as a Gaussian curve with dispersion coefficient σ_y peaked on the x-axis; Term 3 describes the reflecting effect of ground surface which adds a ($z-H$ component to the $z+H$). In this work, complete reflection is assumed.

6.2.1. Meteorological parameters

The χ factor strongly depends on the height H of the release, the wind velocity and the dispersion coefficients σ_y (m) and σ_z (m). Important quantities that need to be considered are listed below:

- - STACK HEIGHT : the actual plume height of the release may not be the physical stack height. Plume rise can occur because of the velocity of stack emission, temperature differential between the stack area and the surrounding air. Therefore, the rise of the plume results in an increase in the release height. Effective release height leads to lower integrated concentrations at ground level and it also 'shifts' the maximum concentration point of the plume towards higher x values. In this work, however, plume rise calculation is for sake of simplicity neglected and the value for the effective height is left as input parameter H.
- - WIND VELOCITY: The wind velocity is measured at a given reference height h_{ref} from the ground. The wind velocity profile is then given by

$$v(z) = v\left(h_{ref}\right)\left(\frac{z}{h_{ref}}\right)^p \tag{6.6}$$

  where p depends on the stability class **?**

- - WIND DIRECTION: In the Gaussian dispersion model the wind direction is assumed to be in the x-axis direction.

- - DISPERSION COEFFICIENTS: The dispersion coefficients are a function of atmospheric stability and depend on the downwind distance x Their general form is:

$$\sigma_{y,z}(x) = \frac{ax}{(1+bx)^c} \tag{6.7}$$

  where x is the downwind distance in meters and a, b and c depend on the cloud cover and wind speed. They are taken from Briggs Briggs (1973) combined with observations out to downwind distance of 10 km. The set of equations used for $\sigma_{y,z}$ are associated with dispersion experiments and are widely used (e.g they are also implemented in HOTSPOT Health physics code Homann). These formulas are applicable from a distance 0.1 km from the source to approximately 10 km.

Stability classes range from A to B where class A is the stability class that describes the most stable weather condition and F is the most unstable one. In an unstable atmosphere there is more mixing and plumes are wider and higher than in a stable atmosphere.

6.2.2. Dry deposition

The process of dry deposition accounts for aerosols depositing on surfaces as a result of turbulent diffusion and Brownian motion. Chemical reactions, impaction etc., combine to keep them at ground level. The effective deposition velocity v_d (m/s) is empirically defined as the ratio of the observed deposition flux F_r $([Bq/m\ s])$ and the observed air concentration Bq/m^3 near the ground. The deposition velocity varies several orders of magnitude depending on the chemical properties of the source. As this material is deposited on the ground, the plume is depleted and the source term decreases with downwind distance. This is accomplished by multiplying the original source term by the so-called depletion factor $DF(x)$. The depletion factor $DF(x)$ is given by Van der Hoven (1968)

$$DF(x) = \left[\exp\left(\int_0^x \frac{1}{\exp\left(\frac{H^2}{2\sigma_z^2(x')}\right)\sigma_z(x')}dx'\right)\right]^{-\frac{v_d}{u}\sqrt{\frac{2}{\pi}}} \tag{6.8}$$

Figure 6.1 shows the behaviour of the depletion factor calculated with **OPTLM-DOSE.f90** for test described in section 6.5.

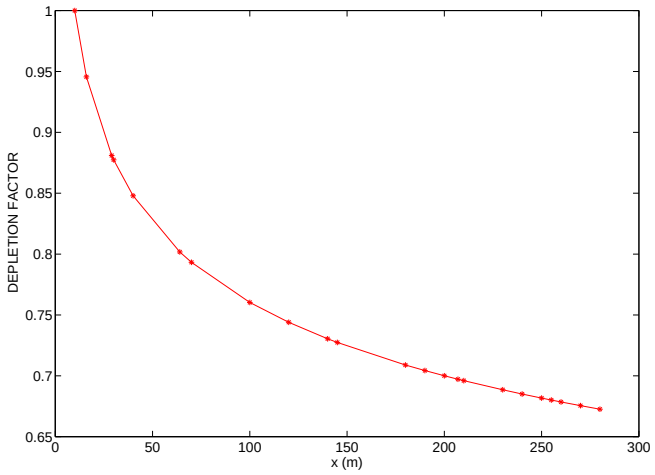

Figure 6.1.: Depletion factor: chemical reactions, impaction and other processes combine to keep the released substance at ground level

6.2.3. Wet Deposition

In case of rain, deposition on the ground is also a function of rain intensity. It is characterized by the scavenging effect of water droplets to the aerosols. The so-called wash-out coefficient W is given by

$$W(x) = \frac{\Lambda}{\sqrt{2\pi}\sigma_y(x)u(x)} e^{-\frac{y^2}{2\sigma_y^2(x)}} \tag{6.9}$$

with $\Lambda = \Lambda_0 \left(\frac{I}{I_0}\right)^{0.8}$ where I is the measured rain intensity and I_0 is the unit rain intensity [mm / h]. $\Lambda_0 = 7 \cdot 10^{-5}$ s^{-1} is the wash-out coefficient related to I_0.

6.2.4. Limits of the Gaussian Dispersion model

The Gaussian dispersion model is a steady-state model which does not account for time and space variation of wind and turbulence. It also does not differentiate among orografic differences in the calculation area and does not cope simultaneously with different sources. In addition, the model does not consider the physical mechanisms underlying the explosion itself, which would has consequences in the source term distribution and in the effective height H estimate. The main limitations of the model, therefore, can be summarized in the following:

- The accuracy in the estimate of the emission height H used in the Gaussian dispersion equation.
- The accuracy of the dispersion coefficients used in the Gaussian dispersion equation.

- The assumption of the averaging time period represented by the calculated ground-level pollutant concentrations as determined by the dispersion coefficients used in the Gaussian equation.
- The model itself does not describe the explosion of a radioactive bomb

Besides the assumptions and constraints in deriving the Gaussian equation, the methods for obtaining certain parameters used in the Gaussian models are also subject to many assumptions and constraints. Those methods include: obtaining the atmospheric stability classifications (which characterize the degree of turbulence available to enhance dispersion), determining the profiles of windspeed versus emission height, and converting ground-level short-term concentrations from one averaging time to another. This discussion of shortcomings in the Gaussian dispersion models is not unique. Deriving the Gaussian dispersion equation requires the assumption of constant conditions for the entire plume travel distance from the emission source point to the downwind ground-level receptor. Yet we cannot say with any reasonable certainty that the windspeed at the plume centerline height and the atmospheric stability class are known exactly or that they are constant for the entire plume travel distance. Whether such homogeneity actually occurs is a matter of pure chance, particularly for large distances.

6.3. Calculation of total dose

In order to calculate the total dose to which a person can be exposed the contributions from submersion (radioactivity in the air), deposition (radioactivity deposited on the ground) and inhalation (radioactivity which is inhaled) have to be considered.

6.3.1. Ground deposition B_r

Ground deposition $[Bq/m^2]$ is calculated from equation 6.5 and by considering both dry deposition and wet deposition.

$$B_r(x,y) = Q_r(v_d\ DF(x)\ \chi(x,y,0) + W(x))e^{-\lambda_r\ t} \tag{6.10}$$

where λ_r is the decay constant of the radionuclide r and $t = x/u(x)$.

6.3.2. External gamma dose

The thermoluminescence dosimeters measure the total γ dose H_{tot}. This consists of a submersion dose H_{wr} which is due to spread of radionuclides in the air and a deposition dose H_{br} due to the emitted γ radiation of radionuclides deposited on the ground:

$$H_{tot}(x,y,z) = H_{wr}(x,y,z) + H_{br}(x,y,0) \tag{6.11}$$

To calculate a dose to which a human being is being exposed, the so-called dose conversion factors (DCF) are used. They link the γ-dose rate $[Gy/s]$ recorded by a detector

to the surface contamination Bq m^{-2} or concentration in air Bq m^{-3}. The absorbed dose rate Gy/s is converted into dose equivalent rate Sv/s by using a weighting factor 1 (average on whole body). Therefore, the units of DCF are $\frac{Gy\ m^3}{Bq\ s}$ or $\frac{Sv\ m^3}{Bq\ s}$ and $\frac{Gy\ m^2}{Bq\ s}$ or $\frac{Sv\ m^2}{Bq\ s}$ for submersion dose g_{wr} and deposited dose g_{br}, respectively. Since OSLD dosimeters measure air kerma, the dose is given in Gy. For five radionuclides (^{133}Xe, ^{99m}Tc, ^{132}Te, ^{131}I, ^{137}Cs) the values tabulated in Zäringer and Sempau (1997) are shown in figure 6.2. For deposited dose the distribution of radionuclides is assumed to be exponentially distributed in the soil. For wet deposition relaxation mass is $\beta = 1\ g/cm^3$ whereas for dry deposition $\beta = 0.1\ g/cm^3$. For submersion dose, instead, radionuclides are homogeneously distributed in the air.

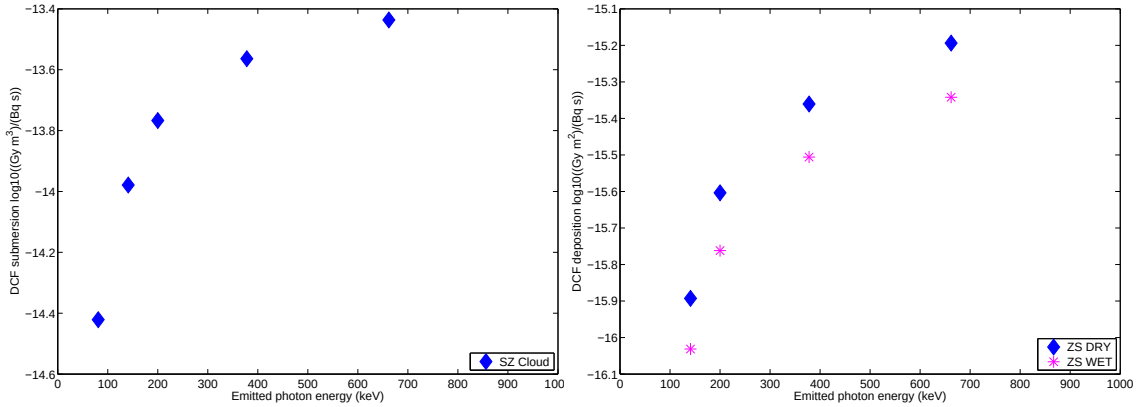

Figure 6.2.: Dose conversion factors for 5 radionuclides (^{133}Xe, ^{99m}Tc, ^{132}Te, ^{131}I, ^{137}Cs) for submersion (left) and deposited dose (right).

The submersion dose is then calculated as

$$H_{wr}(x, y, z) = Q_r \chi(x, y, z) g_{wr} \tag{6.12}$$

whereas the deposition dose is calculated as

$$H_{br}(x, y, 0) = Q_r(\chi(x, y, 0) v_d DF(x) + W(x)) b\ g_{br} K_{br} \tag{6.13}$$

where $K_{br} = \frac{1-e^{-\lambda_r \Delta t}}{\lambda_r}$ is integration term, Δt is the duration of exposure $[s]$ and b is 1 short after the rain. In this work, the OSLD dosimeters are assume to be placed at $z = 1$.

6.3.3. Internal gamma dose

Although OSLDs measure only external exposure, for sake of completeness, also exposure due to inhalation is described here. Dose to which human beings are exposed via inhalation is calculated as:

$$H_{hr}(x, y, 0) = Q_r \chi(x, y, z) g_{hr} 3.34 \cdot 10^{-4} \tag{6.14}$$

where g_{hr} is the DCF for inhalation and $3.34 \cdot 10^{-4}$ $[m^3/s]$ is the normal breathe rate of an adult.

6.4. OPTLMDOSE.f90 routine

Optimization with Levenberg-Marquardt Algorithm is obtained using the MINPACK package More et al. (1984). Details of the algorithm are not described here and can be looked up in the MINPACK manual. Input data which needs to be inserted manually is included in a namelist file called: *namelist*. The data included is in order:

- radionuclide (rnuclide)
- wind velocity ($wind_{ref}$) in m/s
- stability class
- release height (H) in m
- deposition velocity (v_d) in m/s
- reference height for wind measurement (h_{ref}) in m
- type of deposition "DRY" or "WET"
- rain intensity (I_{rain}) mm/h
- type of model "EXPONENTIALX" or "DIFFUSIVEX"
- position of the center of the peak $xdata_0$
- width of Gaussian profile in x-direction σ_x
- time at which contour plot needs to be produced Dt_{plot}
- initial guess for activity Q_r in Bq

The experimental data for the *Dose* is given as input file *doseinput.dat* in the format: x (km), y (km), *Dose* (Gy), Dt (s) where Dt is the difference between the time of explosion and the time of removal of the OSLD. Sometimes experimental data suggests that in the x-direction diffusion processes dominate e.g. a Gaussian behaviour of the plume is visible. This can happen, for example, in case of very slow winds (less than 1 m/s). In this case, by choosing as type of model "DIFFUSIVEX" equation 6.5 is considered with an added term

$$DIFFX(x) = e^{\frac{(x-x_0)^2}{2\sigma_x^2}} \tag{6.15}$$

which accounts for diffusion also in x-direction. In this case also x_0 and σ_x have to be set to some known value. In general with very few points it is not possible to identify

whether in the x-direction diffusion is dominant. It is therefore suggested to apply the exponential model by selecting "EXPONENTIALX" for the x-direction unless there is clear evidence of different profile.

6.4.1. The objective function and the optimization algorithm

In the main program the subroutine FCN.f90 (see appendix) is called which calculates the objective function and the Jacobian matrix, which is internally calculated with finite difference method. The objective function is the difference between the experimental measurement and the calculated one. Therefore, the objective function is defined as:

$$F(\mathbf{x}) = log_{10}(Dose_{data}(\mathbf{x})) - log_{10}(Dose(\mathbf{x})) \; . \tag{6.16}$$

Calculation with the logarithm is preferred due to the large ranging scale of values typically involved in distribution of doses.

In general a non-linear square least problem is specified by a function F such that:

$$||F(x_{sol})|| \leq ||F(x)|| \; , \tag{6.17}$$

where if the domain of definition of x_{sol} is the entire domain of function F then x_{sol} is a global solution. If x_{sol} is a solution of the nonlinear least square problem, then x_{sol} solves the system of nonlinear equations

$$\sum_{i=1}^{m} f_i(x) \nabla f_i(x) = 0 \; , \tag{6.18}$$

which in terms of Jacobian matrix implies the orthogonality condition:

$$F'(x_{sol})^T F(x_{sol}) = 0 \; . \tag{6.19}$$

Technically the algorithm from MINPACK determines a correction p to x that produces a sufficient decrease in the residuals of F at the new point $x+p$; it then replaces x with $x+p$ and begins an other iteration. The correction p depends upon a diagonal scaling matrix D, a step bound Δ and an approximation J to the Jacobian matrix of F The optimization routine LMDIF from MINPACK delivers the optimized results together with information whether optimization has been successfully completed or not. In general, to understand whether the results of the optimization are good it is convenient first of all to compare visually the optimized function versus the experimental one. In a second step it is useful to calculate the standard deviation for the optimized value and to look at whether the squared-sum of the residuals has decreased towards zero during the optimization steps. A plot of the residuals gives information about quality of optimization. In addition, by using the covariance matrix, an estimate of the standard deviation of the obtained value can be given. It is important to mention that in this work a routine which calculates non-linear square fits has been applied although at present only one unknown parameter (the source term) which is linearly dependent on

the dose is considered. However, the use of this routine makes it possible in the future to consider other unknowns, e.g. deposition velocity which is non-linearly dependent, and therefore to broaden the analysis.

6.4.2. Convergence to a solution

The LMDIF routine More et al. (1984) does various convergence tests between the approximation x and the solution x_{sol}. Details related to these convergence tests are to be found in the MINPACK manual. Here they are only briefly outlined:

- if the tolerance TOL is 10^{-K} (usually set to machine precision) the final residual norm has K significant decimal digits then INFO is set to 1.
- D is a diagonal matrix whose entries contain scale factors for the variables. The larger component of $D \cdot x$ have K significant digits and INFO is set to 2.
- If both 1 and 2 are satisfied the INFO is set to 3
- if the norm of the residuals is orthogonal to the columns of the Jacobian to machine precision then INFO is set to 4

INFO 1, 2 and 3 indicate that convergence has been successfully achieved whereas INFO 4 should be checked carefully e.g. by changing initial guesses, as it does not guarantee that a global minimum has been found. However, once an optimized value has been obtained, it is always good to check whether the result stays the same by slightly changing the initial guess. In this way, it is possible to understand whether the result is robust.

6.4.3. Estimate of the standard deviation of optimized value

The COVAR routine included in the program computes the covariance matrix as inverse(J'*J) where J is the Jacobian of the least squares function. Some additional scaling is required to obtain standard deviation as the error on the measurement is not known as the objective function is not weighted with the experimental uncertainty. The scaling needed is an unbiased estimate of the noise variance. The Mean Squared Error (MSE) is a biased estimate, but for problems with large degrees of freedom it is a good estimate. MSE can be calculated as SSE/N where SSE is the sum-of-squared error, N is the number of data points. A better estimate of noise variance is SSE/DOF where DOF is degrees-of-freedom and is equal to the number of data-points minus the number of model-parameters (M-N). In the present case N=1, therefore, the unbiased uncertainty has to be considered with caution. Nevertheless, it gives an estimate of the uncertainty of the fit.

6.5. Application of the inverse fit to Gaussian dispersion model by using synthetic data from HOTSPOT

To test the implemented optimization routine, synthetic data for a Gaussian plume model is created with HOTSPOT 2.07 Homann. The synthetic data is then considered as "experimental" data and the source term Q_r is inversely estimated by applying the Levenberg-Marquardt Algorithm. A run with the code HOTSPOT was carried out for calculating a general plume deposition and dose pattern. The chosen source material is Tc-99m with a half-life of 6.02 hours. The material at risk contained an initial activity of 5.8×10^8 Bq. The effective release height was taken to be $H = 2.5$ m and the wind speed, measured at 2 meters height, was 3.3 m/s. Therefore, the wind speed at the effective height was 3.35 m/s. Stability class was chosen to be $'A'$, that is sunny weather conditions were assumed. Deposition velocity was taken to be 10 cm/s. Receptor height was fixed to 1 meter (implying that $z = 1$ in equation 6.5) and sampling time was 10 minutes. The total exposure time was taken to be 1 minute which is the time it takes the plume to reach the last measured point.

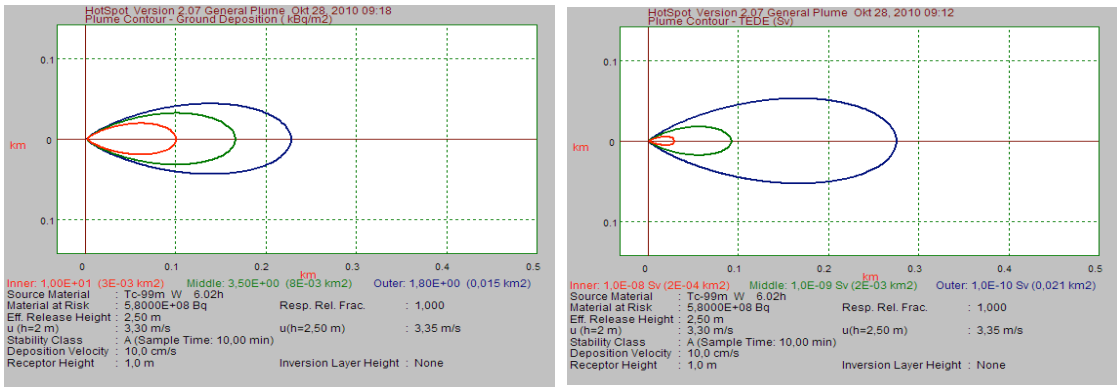

Figure 6.3.: Output plots from HOTSPOT for the test run for Ground deposition (left) and Total Effective Dose Equivalent (right).

The data obtained consists of 23 points measured along the centerline of the plume up to a distance of 280 m from the source for which both Ground deposition and Total Effective Dose Equivalent including also inhalation are calculated. HOTSPOT considers DCF from ICRP (2005) in units $\frac{Sv\ m^3}{Bq\ s}$ therefore the dose obtained are in Sv. As a consequence the routine has been tested with DCF from Eckerman and Ryman (1993) instead of Zäringer and Sempau (1997). An other difference between HOTSPOT model and **OPTLMDOSE.f90** model is that the integration for the Depletion factor (see equation 6.8) in the first case is done with trapezoidal rule whereas in the second case Gauss integration is applied. Calculations with **OPTLMDOSE.f90**, in fact, are carried out with very few points and therefore trapezoidal rule is not suited. However, since HOTSPOT delivers output results via interface it has not been possible to quantify the difference due to different integration procedure. As a consequence calculations of the Gaussian plume with HOTSPOT and **OPTLMDOSE.f90** are expected to be

very similar but not identical. The contour plot of the ground deposition and dose from HOTSPOT is shown in figure 6.3. The ground deposition is plotted with 3 main isolines at 10, 3.5 and 1.8 kBq m^{-2}. The dose is plotted with 3 main isolines 10^{-8}, 10^{-9}, and 10^{-10} Sv.

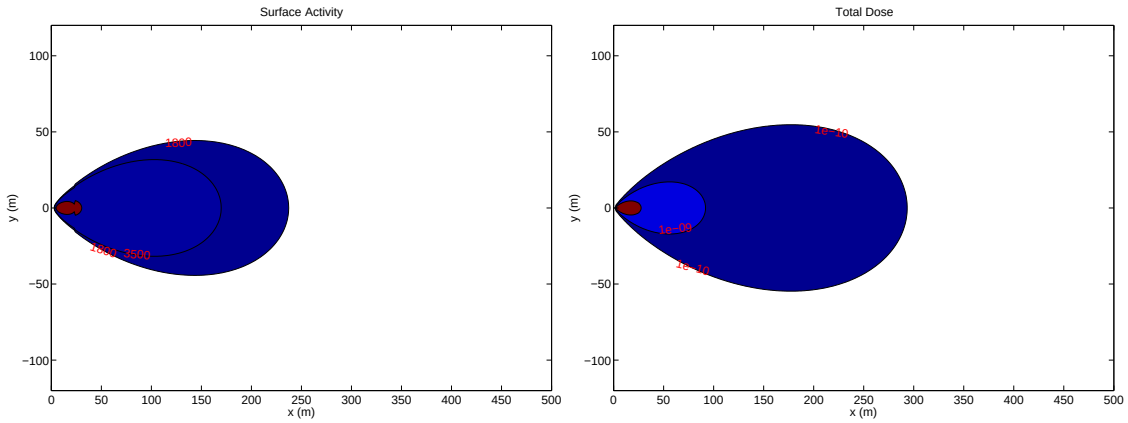

Figure 6.4.: Output results from the optimization routine **OPTLMDOSE.f90** for Ground deposition (left) and Total Effective Dose Equivalent (right).

The results from the inverse fit are shown in figure 6.4. The initial guess is set to $Q_r = 5.80 \cdot 10^8$ Bq. After 9 iterations the routine delivers an optimized value $Q_r = 4.36 \cdot 10^8$ with an unbiased uncertainty $\sigma_{Q_r} = 2.08 \cdot 10^7$. The initial norm of the residuals (which is assumed to be the difference due to depletion factor) is 0.62 whereas with final one goes down to 0.21. The final mean value of the residual is very close to zero (10^{-11}) whereas the initial mean value for the residual is 0.12. The routine has been also tested to check its robustness in case very few number of points (e.g experimental measurements) are available, which is often the case. Figure 6.5 shows that by reducing the number of points used the optimized value for the source term remains very much close to the one obtained with 23 points. Also the dependency on the position of the points on the area considered has been checked and no different trend was found. The error bars become very large for fewer number of points due to the small difference (M-N) in the unbiasing factor for calculating the standard deviation. Also with 1 point only, it is possible to apply the inverse fit.

6.6. Application of the inverse fit to Gaussian dispersion model by using real experimental data

Experiments in which small amounts of ^{99m}Tc were dispersed over a testing area have been carried out in 2008 by Prouza et al. (2010). In this work, such measurements (in particular data from test 2) for surface activity (Bq/m^2) have been used to inversely determine the source term by means of Levenberg-Marquardt algorithm and **OPTLMDOSE.f90**.

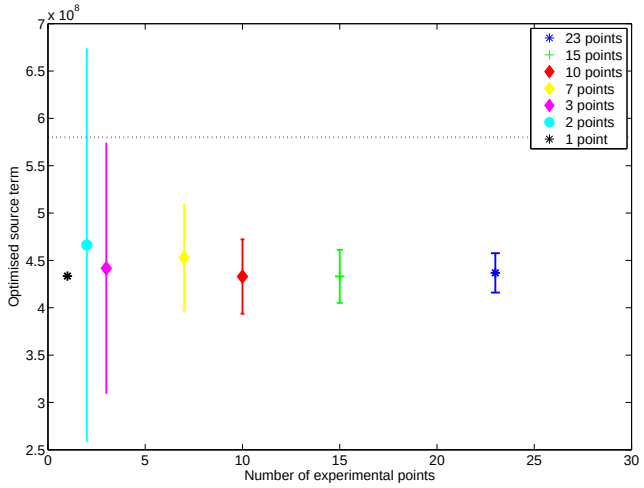

Figure 6.5.: Optimized source term in dependence of the number of points

The known activity at time of explosion is 910 MBq, wind velocity at 2 meters height is 1.1 m/s. Weather conditions are such that stability class is assumed to be class 'B'. From experimental observations the release height H during the explosion is estimated to be 5 meters. The deposition velocity delivers by far the greatest uncertainty in the experiment since no measurements are available which indicate how much the source term is bound to the 4 different aerosols' sizes identified in the exercise.

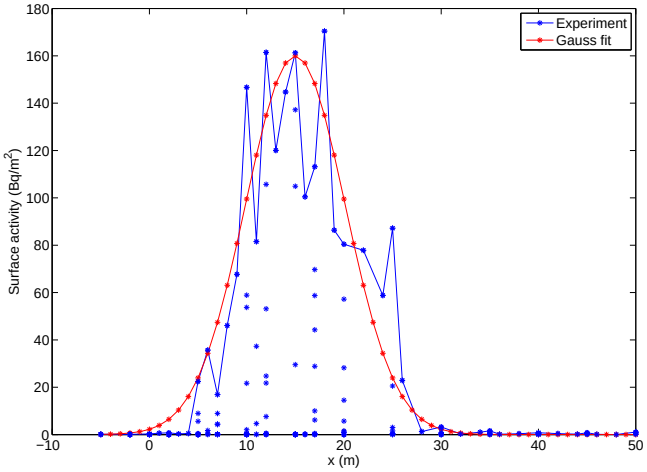

Figure 6.6.: Fit to a Gaussian profile of surface activity measurements for test 2 along x-axis

221 detectors are placed over a 50m x 40 m area which measure surface activity (Bq / m^2). The behaviour of the data in the x-direction does not follow an exponential decay as instead predicted by a typical Gaussian plume model. In addition, very slow wind velocity suggests that also in the x-direction a diffusive process may take place. Indeed,

figure 6.6 shows how well a Gaussian profile centered at $x_0 = 15$ m and with $\sigma_x = 5.13$ m fits the experimental curve. Therefore in order to fit well experimental data the diffusive term 6.15 is switched on in **OPTLMDOSE.f90** by selecting "DIFFUSIVEX". In this case, the objective function considered is $F(x) = log_{10}(B_r + 1) - log_{10}(B_r + 1)$ to guarantee stability of the optimization when B_r values are very close to zero. The initial guess is set to a very low value compared to real one 9.1×10^4 Bq. The result of the fit for an effective deposition velocity $v_{d_{eff}} = 0.01$ m/s is shown in figure 6.7 where experimental contour plot of surface activity is shown together with the calculated one. The initial norm of the residual is 40.5 and at the optimization goes down to 23.6 and after 33 iterations the optimal source term found is $9.4 \cdot 10^8$ Bq.

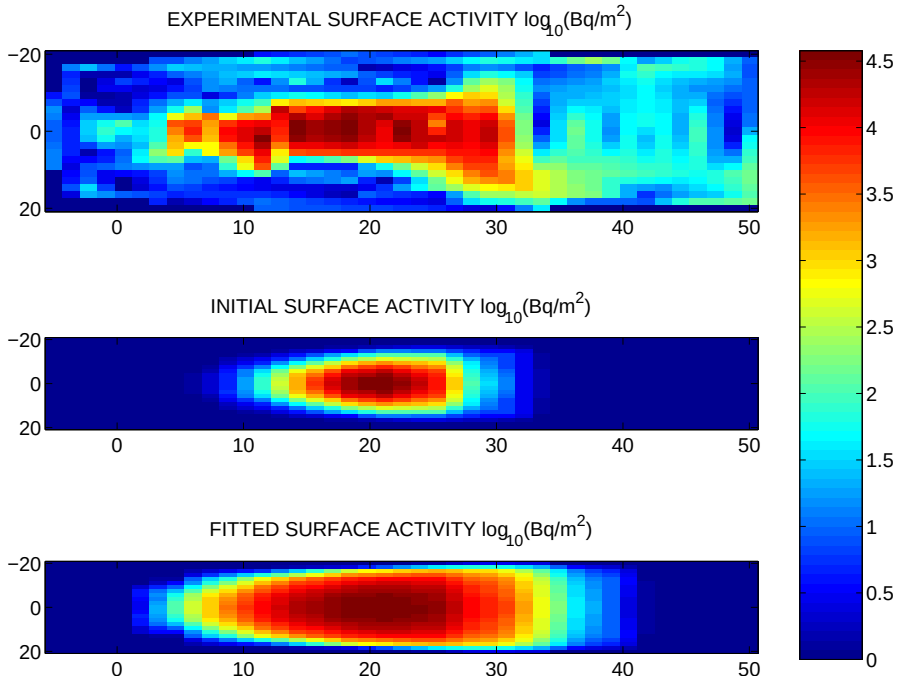

Figure 6.7.: Test 2: experimental contour plot versus contour plot obtained with optimized value $Q_r = 9.41 \cdot 10^8$ and $v_{d_{eff}} = 0.01$ m/s

The experimental, initial and optimized profiles in the x-axis and y-axis direction are shown in figure 6.8 showing the initial guess profiles of the plume in these two directions which are very low compared the experimental ones. Nevertheless, their shape is similar to the experimental one. The optimized profiles, instead, differ by one order of magnitude from the experimental ones (logarithmic scale).

In order to account for the uncertainty in the deposition velocities, the optimal source term is calculated for other different plausible *effective* deposition velocities. The strong linear dependence of the value of the source term Q_r versus v_d is shown in figure 6.9.

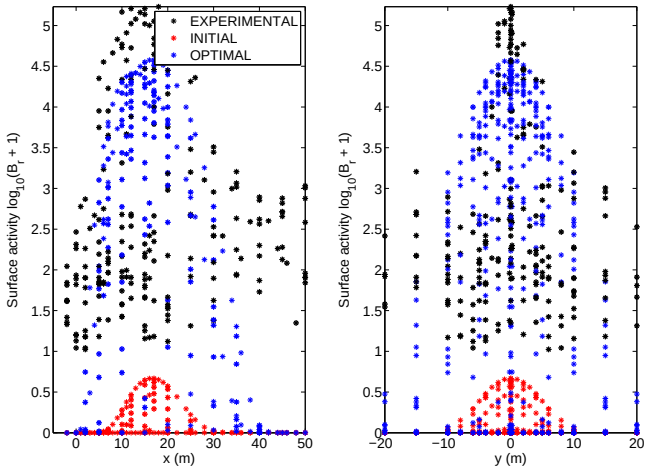

Figure 6.8.: Test 2: experimental, initial and optimized profile in the x-axis and y-axis direction.

6.7. Conclusion

An optimization routine based on Levenberg-Marquardt Algorithm and Gaussian plume model has been applied in order to inversely determine the source term after an accidental nuclear release e.g. dirty bomb explosion. Experimental data considered comes from optically stimulated luminescence dosimeters which measure external dose. For testing the routine, synthetic data and real experimental data have been considered. Such a type of analysis is meant to give an order of magnitude result for the source term and a 'feeling' for the level of danger to which population groups have been exposed. Such a simple method is meant to provide a rapid and robust estimate of the source term involved. This work focused on indications obtained in SSK (2004).

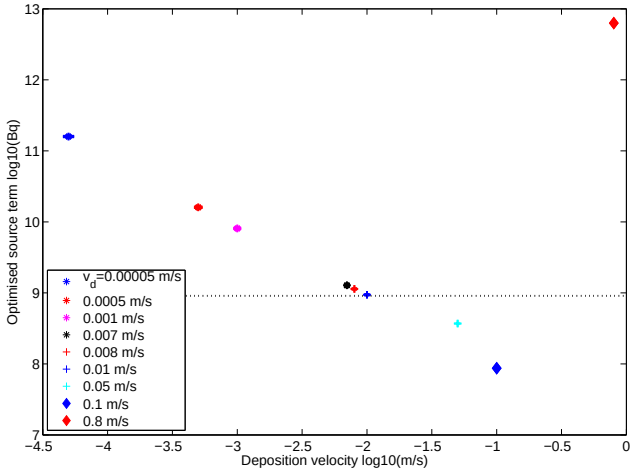

Figure 6.9.: Dependency of optimized source term Q_r on the assumed effective deposition velocity v_d

7. Overall Conclusions and recommendations

In this project, it could be shown that chip card modules with a UV-cured, translucent encapsulation, that are frequently found in debit, credit, health insurance and SIM-cards have high potential for reconstruction of individual radiation exposure in radiological emergencies. The dynamic range covered by the chip cards goes from less than 10 mGy well up to 10 Gy and possibly beyond, with the lower limit increasing to 20 mGy for dose assessments 10 days after the incident. It could thus be shown that using blue OSL as the method of measurement, the existing chip card technology already fulfills the requirement set up by the BfS, without the need for adding phosphorescent powder to the encapsulant, which was the state-of-the art before the project.

At the moment, the preferred measurement protocol doesn't include any preheating or other pretreatment, which maximizes the sensitivity and the overall performance of the dose measurement but also leads to considerable signal fading. From the detailed kinetic analysis, performed in this project, the possibility arises that the observed fading of the OSL signal is a pure thermal effect, caused by the direct recombination pathways. This would open the way to isolate thermally more stable signals for OSL dosimetry by appropriate preheat treatment, while simultaneously keeping the zero-dose signal, caused by the thermo-optical release of charge carriers from the epoxy, at a minimum, by e.g. an extended low temperature preheat. More research is therefore recommended, to better understand the luminescence mechanism and in this way to open new possibilities for dose assessment.

The luminescence properties of wire-bond chip card modules with molding also clearly demonstrated a high potential for emergency dosimetry in a similar dynamic range as the chip cards with a translucent encapsulation. However, more research is necessary and recommended into the fading characteristics and the influence of the sample preparation procedure (chemical extraction of the filler material) on the fading correction as dose recovery experiments so far had not been satisfactory. The greatest impact of the chemical preparation procedure has been found for contactless modules with molding, where more than an order of magnitude in sensitivity could be achieved. Thus it might be possible to also use electronic ID cards and passports as emergency dosimeters in the future. In Germany, the electronic ID card was introduced in Fall 2010 and research into this area is highly recommended as this would significantly enlarge the range of suitable personal objects for reconstructing individual radiation exposures.

In the future, it is expected that more and more chip cards will be produced using the flip chip technology, where no more encapsulant with filler material is necessary and therefore radiation sensitivities are very low (Göksu et al., 2007). However, it should

be emphasized that from the arbitrary chip cards collected from the employees of the Helmholtz Zentrum, which were all produced and issued in the last three to four years not a single one had a flip-chip but more than 60% were wire-bond with a UV-cured encapsulation and high radiation sensitivity. It thus might still take many years, before flip-chips will have a significant share in the chip card market.

For portable electronic devices, the results from the literature on the suitability of electronic components (resistor substrates) could be confirmed and additional electronic components (inductors) with higher sensitivity identified. The dynamic range found is similar to that of inductors, with detection limits at or below 10 mGy (when measuring a combination of inductors and resistors) and dose linearity beyond 10 Gy. However, the PEDs are also similar to chip cards in that way that they also show pronounced signal fading with time (50% in 10 days), that so far seems to follow the law of anomalous fading. The variability of fading rates was seen to be around 3-13%, depending on the storage time and when applying a preheat of 120°C, thus the fading curve determined in this project seems to be universally applicable within tolerable uncertainties.

While OSL on electronic components in PEDs has thus been shown to work quite well, the situation is more complex for dose assessment using TL. For resistors the possible higher sensitivity and lower fading rates of the TL method could only be shown to a moderate degree and were outweighed by the occurrence of a zero-dose signal and a systematic dose overestimation, which made additional corrections with higher uncertainties necessary. For the irradiation trials conducted here, TL and OSL on resistor substrates seemed to work equally well (for given doses of 500 mGy) but in real emergency scenarios, OSL will probably be the method of choice. For inductors, investigations using TL could demonstrate the potential of the 170°C TL peak for dose assessment, which showed the highest stability by far for all measurement modes and materials. However, the systematic dose overestimation observed in irradiation trials using a gamma source indicates that more research is also necessary here, to fully establish inductors as fortuitous dosimeters using TL.

The measurement of the photon energy dependence of the OSL signal of resistor substrates in a representative mobile phone emphasized the importance of considering the whole mobile phone, including the casing, as the shielding effects of the latter reduced the overresponse from a factor of almost five for extracted resistors to a factor of 1.6 to 2.6, depending on the angle of incidence. The thorough characterization of the energy response, which was achieved within this project, can thus serve as the basis for future calculations of dose conversion coefficients (dose in material to dose in air) for different exposure scenarios. In this context, it is recommended to assess the influence of the casing for a number of mobile phones in future projects by e.g. replacing the resistors by highly sensitive Al_2O_3:C.

All materials from personal objects investigated so far have the common feature of showing a long-term signal instability for storage at room temperature, implying that the time of exposure has to be known for fading correction. This situation is given for scenarios such as an attack with a radiological dispersion device or a major accident in a nuclear power plant. For an attack with a hidden source (Radiological Exposure

Device), the time of exposure is generally unknown and fading correction becomes difficult or impossible. However, by combining several emergency dosimeters with different fading rates, it should be in principle possible to reconstruct the time of exposure and in this way correct the signal fading without having any additional information. Alternatively, new measurement protocols could open the possibility of performing the dose assessment only on stable or sufficiently stable signals (see above). This might also be possible for alumina rich electronic components in PEDs, as new insights into the mechanism of anomalous fading in feldspar minerals has very recently lead to the development of a fading-free protocol for this material (Jain and Ankjærgaard, 2011). Further research into this area is highly recommended.

For the second workpackage, a maintenance-free BeO based luminescence detector was developed, which can be placed at locations of high importance (e.g. public squares) and which allows a comparatively quick local dose assessment from µGy's to several tens of Gy's (for freshly thermally annealed aliquots). With the developed holder an essential flat photon energy response could be realized, while simultaneously guaranteeing light- and water-tightness. As the system is maintenance-free and BeO chips inexpensive when bought in large quantities, an emergency dosimetry network in Germany could be established at relatively low costs, when compared to existing radiation monitoring networks (e.g. IMIS). Two computational procedures were developed to produce maps of contamination or effective dose from the localized dose measurements, depending on the number of available measurements and using either geo-statistical interpolation or Gaussian plume fitting. The latter is strictly speaking not applicable in urban environments, where free propagation in cross-wind directions is not necessarily met but can still serve as a useful method to get at least a rough, order of magnitude feeling for the level of exposure over a contaminated area when only one or two dose readings are available.

Acknowledgments

This project was supported by the German Federal Office of Radiation Protection and the German Federal Ministry for the Environment, Nature Conservation and Nuclear Safety under the contract 3607S04560. We thank P. Jacob for helpful discussions and his continuous support of this work. We thank C. Dürr and J. Ademola for contributing to the project within the framework of her bachelor thesis and Humboldt Fellowship, respectively. We are grateful to the mechanical workshop of the Helmholtz Zentrum München (J. Promoli) for the great help in the designing and the construction of the BeO holder. Finally all members of the research groups "Radioecological Modeling and Retrospective Dosimetry" and "Radiation Risk" are thanked for their discussions and input.

A. Protocols

Regardless of the material, all sample preparation steps have to be done under subdued red light conditions.

A.1. Chip cards

A.1.1. UV-cured chip cards

Punch out chips using a punch with 10 mm diameter. Place chips with contact side (gold foil) facing down in measuring cup. With a Risø luminescence reader, use blue LEDs for OSL with 90% optical stimulation power. Measure OSL at room temperature without preheat.

Fast protocol:

- set sequence option "Run 1 at a time"
- Run #1: Measure OSL for 30 s (150 channels) = L_{nat}
- Run #2: Irradiate with 1 Gy
- Run #3: Measure OSL for 30 s (150 channels) = L_1
- Evaluate Signals as $L_i = (0 - 10\,\mathrm{s}) - (10 - 20\,\mathrm{s})$
- Calculate uncorrected Dose as $D_{app} = {}^{L_{nat}}/_{L_1}\mathrm{Gy}$
- Determine degree of fading F from equation of Fig. 3.5
- Calculate corrected dose as $D = \frac{D_{app}}{F}$

Full protocol:

If the fast protocol hasn't been applied before, start with Run #1, otherwise start with Run #3.

- set sequence option "Run 1 at a time"
- Run #1: Measure OSL for 300 s (1500 channels) = L_{nat}
- Run #2: Irradiate with Test Dose (approx. 200 mGy)

- Run #3: Measure OSL for 300 s (1500 channels) = T_{nat}
- Run #4: Irradiate with Regenerative Dose D_1
- Run #5: Measure OSL for 300 s (15000 channels) = L_1
- Run #6: Irradiate with Test Dose
- Run #7: Measure OSL for 300 s (1500 channels) = T_1
- Repeat Run #'s 4-7 with increasing regenerative doses (3-4 doses sufficient). Omit Run #4 in the last repetition (no irradiation).
- Evaluate Signals as $L_i\,, T_i = (0 - 10\,\mathrm{s}) - (10 - 20\,\mathrm{s})$.
- Plot L_i/T_i against D_i . Evaluate errors of each L_i/T_i datapoint using the approach described in Galbraith, 2002. Fit a straight line $y = a + b \cdot x$ through datapoints (weighted fit)
- Calculated (uncorrected) dose as $D_{app} = 1/b\,(L_{nat}/T_{nat} - a)$
- Determine degree of fading F from equation of Fig. 3.5
- Calculate corrected dose as $D = \frac{D_{app}}{F}$

A.1.2. Chip cards with molded encapsulations

Sample preparation (for contact-based modules)

Fuming HNO_3 is a very aggressive acid and documented necessary precautions for safe handling should be followed (appropriate fume cupboard, protective gloves and clothing, eye protection).

- Punch out chip from card or cut out chip with utility knife.
- Use heatable ultrasonic bath (with insert basket and spring clamps) in fume cupboard. Set temperature of bath to 80°C. Check with digital thermometer that temperature has been reached.
- Fill 15-20 ml fuming HNO_3in 50 or 100 ml Erlenmeyer flask and put chip in. Fix flask in spring clamp in insert basket of the ultrasonic both. Wait for 15 min or until chip is completely dissolved. Use gripping tongs to handle flask.
- Take flask out of bath and let cool to room temperature. Carefully and slowly decant excess HNO_3in waste beaker, taking care that silica grains remain in beaker.
- Dilute with distilled water, shake and let stand and slowly decant again. Repeat two to three times. Check pH.
- Fill acetone in beaker, shake and let stand.

- Use 20 µl pipette. Pipette grains in several cycles onto measuring cup. Wait in between cycles until excess acetone has evaporated from cup.
- Place measuring cup in luminescence reader.

Protocol

Use blue LEDs for OSL with 90% optical stimulation power. Set temperature of OSL measurement to 140° (heating rate of 2°C s^{-1}). Wait 5 s before OSL measurement. Use preheat of 150°C for 20 s (heating rate of 2°C s^{-1}).

- set sequence option "Run 1 at a time"
- Run #1: Preheat. Measure OSL at 140°C for 300 s (1500 channels) = L_{nat}
- Run #2: Irradiate with Test Dose (approx. 200 mGy)
- Run #3: Preheat. Measure OSL at 140°C for 300 s (1500 channels) = T_{nat}
- Run #4: Irradiate with Regenerative Dose D_1
- Run #5: Preheat. Measure OSL at 140°C for 300 s (1500 channels) = L_1
- Run #6: Irradiate with Test Dose
- Run #7: Preheat. Measure OSL at 140°C for 300 s (1500 channels) = T_1
- Repeat Run #'s 4-7 with increasing regenerative doses (3-4 doses sufficient). Omit Run #4 in the last repetition (no irradiation).
- Evaluate Signals as $L_i\,, T_i = (0 - 10\,\mathrm{s}) - (10 - 20\,\mathrm{s})$.
- Plot L_i/T_i against D_i . Evaluate errors of each L_i/T_i datapoint using the approach described in Galbraith, 2002. Fit a straight line $y = a + b \cdot x$ through datapoints (weighted fit)
- Calculated uncorrected dose as $D_{app} = 1/b\,(L_{nat}/T_{nat} - a)$.
- Determine degree of fading F from Fig. 3.22
- Calculate corrected dose as $D = \frac{D_{app}}{F}$

A.2. Portable electronic devices

Sample preparation

- Disassemble PED using special screw drivers.
- Remove resistors and inductors from circuit board under pair of binoculars (red light!) with utility knife

- Clean electronic components in acetone in ultrasonic bath for 15 min (fume cupboard). Decant excess acetone, wash with new acetone and decant again
- Dry in cabinet dryer at 50°C
- Spray thin layer of silicone onto measuring cup
- Place 20 components onto one cup. Only mix resistors with inductors with white and grey colour. Do not mix inductors with green and black colour
- Place resistors with dark side down, inductors with grey and white side on the side

Protocol (OSL)

Use blue LEDs for OSL with 90% optical stimulation power. Set temperature of OSL measurement to 100° (heating rate of 2°C s^{-1}). Wait 5 s before OSL measurement. Use preheat of 120°C for 10 s (heating rate of 2°C s^{-1}).

- set sequence option "Run 1 at a time"
- Run #1: Preheat. Measure OSL at 100°C for 150 s (500 channels) = L_{nat}
- Run #2: Irradiate with Regenerative Dose D_1
- Run #3: Preheat. Measure OSL at 100°C for 150 s (500 channels) = L_1
- Repeat Run #'s 2 -3 with increasing regenerative doses (3-4 doses sufficient). Omit Run #2 in the last repetition (no irradiation).
- Evaluate Signals as $L_i = (0 - 10\,\mathrm{s}) - (10 - 20\,\mathrm{s})$.
- Plot L_i against D_i . Evaluate errors of each L_i datapoint from counting statistics and dark noise variation. Fit a straight line $y = a + b \cdot x$ through datapoints (weighted fit)
- Calculated uncorrected dose as $D_{app} = 1/b\,(L_{nat} - a)$.
- Determine degree of fading F from Fig. 4.9
- Calculate corrected dose as $D = \frac{D_{app}}{F}$

Protocol (TL)

Only use cups with either resistors or inductors for TL. Do not mix. Set maximum temperature of TL to 400°C. Use a heating rate of 2°C s and background correction. Use preheat of 120°C for 10 s (heating rate of 2°C s^{-1}).

- set sequence option "Run 1 at a time"

- Run #1: Preheat. Measure TL (I_{nat})
- Run #2: Irradiate with Regenerative Dose D_1
- Run #3: Preheat. Measure TL (I_1)
- Repeat Run #'s 2 -3 with increasing regenerative doses (3-4 doses sufficient). Omit Run #2 in the last repetition (no irradiation).
- Integrate Signals for resistors between 100°C and 200°C
- Integrate Signals for inductors between 220°C and 310°C
- Plot I_i against D_i . Evaluate errors of each L_i datapoint from counting statistics and dark noise variation. Fit a straight line $y = a + b \cdot x$ through datapoints (weighted fit)
- Calculated uncorrected dose as $D_{app} = 1/b\,(L_{nat} - a)$
- Determine degree of fading F from Fig. 4.15 for resistors and Fig. 4.19 for inductors
- For resistors, calculate corrected dose as $D = \frac{(D_{app} - D_{Zero})}{F \cdot C}$
- Use $D_{zero} = 22 \pm 11$ mGy and $C = 1.35 \pm 0.11$ for resistors and $D_{zero} = 0$ and $C = 1.33 \pm 0.12$ for inductors

B. Construction sketches

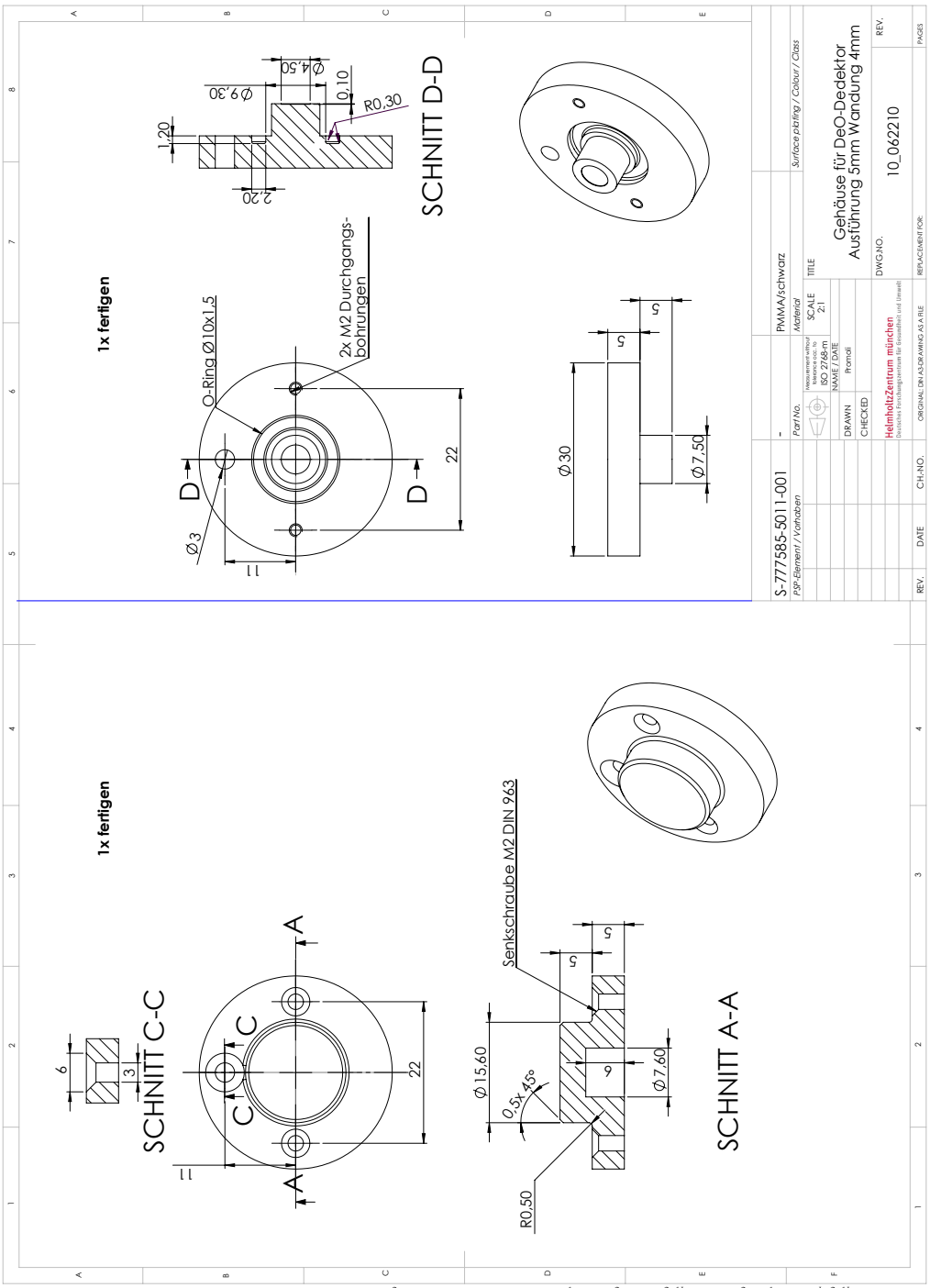

C. Source code

OPTLMDOSE.f90

```
PROGRAM OPTLMDOSE
USE exp_values
IMPLICIT NONE
DOUBLE PRECISION ENORM, dpmpar
DOUBLE PRECISION FJNORM
! CALL MANUALLY INPUT PARAMETERS
NAMELIST / global_para / rnuclide, wind_ref,&
     & stability_class, H, vd, h_ref, &
     & dep_model, I_rain, eq_model, xdata0, sigmax, Dt_plot,  Qr
N             = 1
pi            = 3.14159265d0
Mplot         = 1000
Open (UNIT=15,FILE="namelist",STATUS="OLD",POSITION="REWIND")
READ (UNIT=15,NML=global_para) ! read global parameters
CLOSE (UNIT=15)
print*, 'number of unknowns', N
write (N_string, '(I1)') N
write (Dtplot_string, '(I5)') Dt_plot
filename_read =  "doseinput.dat"
filename_save =  "doseoutput.dat"
M             = nlines(filename_read)
print*, 'number of experimental points', M
CALL allocate_exp_values
CALL initialise_exp_values
hz=1.00d0
X(1)=Qr
!-----------------------------------------
! READ IN EXPERIMENTAL DATA
open(12,file=TRIM(filename_read))
do i =1, M

    read(12,*) D1, D2, D3, D4
    xdata(i)=D1*1D3       ! meters
    ydata(i)=D2*1D3       ! meters
    Dosedata(i) =D3       ! Sv
    Dt(i)       =D4        ! seconds

enddo
close(12)
!-----------SORT INCREASING ORDER X----------
CALL sort2(xdata(:),ind_incr(:),W(:),M)
xdata = xdata(ind_incr)
ydata = ydata(ind_incr)
Dosedata  = Dosedata(ind_incr)
```

```
!-----------------------------------------
print*, 'radionuclide:  ', rnuclide
! DCF values from Zaeringer-Sempau BfS-IAR-2/97
! GROUNDSHINE (Gy m2)/(Bq s)
! CLOUDSHINE  (Gy m3)/(Bq s)
!                            Xe-133    Tc-99m     Te-132   I-131     Cs_137
!AIRK_rnuclides_cloud_ZS  = [3.79D-15  1.05D-14  1.71D-14  2.73D-14  3.66D-14];
!AIRK_rnuclides_DRY_ZS    = [0.0d0     1.28D-16  2.49D-16  4.36D-16  6.40D-16];
!AIRK_rnuclides_WET_ZS    = [0.0d0     9.30D-17  1.73D-16  3.12D-16  4.55D-16];
! PICK UP RADIONUCLIDE
if (rnuclide .eq. 'Cs-137') then
    lambda_r = log(2.0d0)/(30.0d0 * 3.1536D7)
    gwr=3.66D-14
    if (dep_model .eq. 'DRY') then
       gbr=6.40D-16
    elseif (dep_model .eq. 'WET') then
       gbr=4.55D-16
    endif
elseif (rnuclide .eq. 'I-131') then
    lambda_r =log(2.0d0)/(8.0207d0 * (6.93D5))
    gwr=2.73D-14
    if (dep_model .eq. 'DRY') then
       gbr=4.36D-16
    elseif (dep_model .eq. 'WET') then
       gbr=3.12D-16
    endif
elseif (rnuclide .eq. 'Xe-133') then
    lambda_r=log(2.0d0)/(5.245d0* (6.93D5))
    gwr=3.79D-15
    if (dep_model .eq. 'DRY') then
       gbr=0.0d0
    elseif (dep_model .eq. 'WET') then
       gbr=0.0d0
    endif
elseif (rnuclide .eq. 'Te-132') then
    lambda_r =log(2.0d0)/(2.49d0 * (9780.d0))
      gwr=1.71D-14
    if (dep_model .eq. 'DRY') then
```

```
        gbr=2.49D-16
    elseif (dep_model .eq. 'WET') then
       gbr=1.73D-16
    endif

elseif (rnuclide .eq. 'Tc-99m') then

    lambda_r =log(2.0d0)/(21660)
    gwr=1.05D-14
    if (dep_model .eq. 'DRY') then
        gbr= 1.28D-16
    elseif (dep_model .eq. 'WET') then
        gbr= 9.30D-17
    endif

endif
!-----------------------------------------
print*, 'pick up stability class: ', stability_class
! sigmay and sigmaz formulas: BRIGGS (1973)
! formulas are applicable from a distance of 0.1 km
! to approximately 10 km and are thought to be extendible to 20-30 km
! it is not recommended to extrapolate sigmay and sigmaz below a distance
of 10 meters
! PICK UP STABILITY CLASS - STANDARD TERRAIN
if (stability_class .eq. 'A') then

    do i =1, M
       sigmay(i) = (0.22d0 * xdata(i))/(sqrt(1.0d0+ 0.0001d0 * xdata(i)))
    enddo
    p_coeff   = 0.07d0

elseif (stability_class .eq. 'B') then

    do i =1, M
       sigmay(i) = (0.16d0 * xdata(i))/(sqrt(1.0d0+ 0.0001d0 * xdata(i)))
    enddo
    p_coeff   = 0.07d0

elseif (stability_class .eq. 'C') then

    do i =1, M
       sigmay(i) = (0.11d0 * xdata(i))/(sqrt(1.0d0+ 0.0001d0 * xdata(i)))
    enddo
    p_coeff   = 0.1d0

elseif (stability_class .eq. 'D') then
```

```
    do i =1, M
       sigmay(i) = (0.08d0 * xdata(i))/(sqrt(1.0d0+ 0.0001d0 * xdata(i)))
    enddo
    p_coeff   = 0.15d0

elseif (stability_class .eq. 'E') then

    do i =1, M
       sigmay(i) = (0.06d0 * xdata(i))/(sqrt(1.0d0+ 0.0001d0 * xdata(i)))
    enddo
    p_coeff   = 0.35d0

elseif (stability_class .eq. 'F') then

    do i =1, M
       sigmay(i) = (0.04d0 * xdata(i))/(sqrt(1.0d0+ 0.0001d0 * xdata(i)))
    enddo
    p_coeff   = 0.55d0

endif
! exponential factor p_coeff IRWIN (1979)
!-----------------------------------------
!print*, SUM(sigmay(:))/M
do i=1, M

    if (sigmaz(xdata(i),stability_class) .lt. 0.0d0) then
        print*, i, xdata(i), 'sigma_z negative?'
    endif
    wind_velocity(i) = wind_ref * (H/h_ref)**p_coeff

enddo
! DEPLETION FACTOR
! VAN DER HOVEN ("Deposition of particles and Gases",
! Metereology and Atomic Energy 1968 D.H Slade, Ed.)
INT_DEPLETION(1) =0.0d0
! GAUSS INTEGRATION
if (stability_class .eq. 'A') then

    do i=2, M
       INT_DEPLETION(i) = GAUSS(FA,xdata(1),xdata(i), 1D-8)
    enddo

elseif (stability_class .eq. 'B') then

    do i=2, M
       INT_DEPLETION(i) = GAUSS(FB,xdata(1),xdata(i), 1D-8)
    enddo
```

```
elseif (stability_class .eq. 'C') then

    do i=2, M
       INT_DEPLETION(i) = GAUSS(FC,xdata(1),xdata(i), 1D-8)
    enddo

elseif (stability_class .eq. 'D') then

    do i=2, M
       INT_DEPLETION(i) = GAUSS(FD,xdata(1),xdata(i), 1D-8)
    enddo

elseif (stability_class .eq. 'E') then

    do i=2, M
       INT_DEPLETION(i) = GAUSS(FE,xdata(1),xdata(i), 1D-8)
    enddo

elseif (stability_class .eq. 'F') then

    do i=2, M
       INT_DEPLETION(i) = GAUSS(FF,xdata(1),xdata(i), 1D-8)
    enddo

endif
do i=1, M
   DF(i)= (exp(INT_DEPLETION(i)))**((-(vd)/wind_velocity(i))*
   (sqrt(2.0d0/pi)))
enddo
open(112,file=TRIM('DEPLETION_dose_GAUSS.dat'))
do i=1,M
   write(112,*)  xdata(i), DF(i), INT_DEPLETION(i)
enddo
close(112)
!-----------------------------------------
! CREATE INITIAL PLUME
if (eq_model .eq. 'EXPONENTIALX') then
   do i=1, M
      Chi(i)  = (1.0d0/(2.0d0*pi * (sigmay(i)) *
(sigmaz(xdata(i),stability_class)) * wind_velocity(i)))*   &
           &        exp(-(ydata(i)**2)/(2*(sigmay(i)**2)))*
&
           &        (exp(-((hz-H)**2)/(2*(sigmaz(xdata(i),
stability_class)**2)))+&
           &        exp(-((hz+H)**2)/(2*(sigmaz(xdata(i),
stability_class)**2))))
           Chi_0(i)  =  (1.0d0/(1.0d0*pi * sigmay(i) * sigmaz(xdata(i),stability_c
```

```
           &        exp(-(ydata(i)**2)/(2*(sigmay(i)**2)))*                    &
           &        exp(-(H**2)/(2*(sigmaz(xdata(i),stability_class)**2)))
   enddo
elseif (eq_model .eq. 'DIFFUSIVEX') then
 do i=1, M
    Chi(i)  = (1.0d0/(2.0d0*pi * (sigmay(i)) *
(sigmaz(xdata(i),stability_class)) * wind_velocity(i)))*   &
          &        exp(-(ydata(i)**2)/(2*(sigmay(i)**2)))*                    &
          &        (exp(-((hz-H)**2)/(2*(sigmaz(xdata(i),
stability_class)**2)))+&
           &       exp(-((hz+H)**2)/(2*(sigmaz(xdata(i),
stability_class)**2))))*&
           &       exp(-((xdata(i)-xdata0)**2)/(2*sigmax**2))
           Chi_0(i)  =  (1.0d0/(1.0d0*pi * sigmay(i) *
sigmaz(xdata(i),stability_class) * wind_velocity(i)))*    &
           &       exp(-(ydata(i)**2)/(2*(sigmay(i)**2)))*
&
           &        exp(-(H**2)/(2*(sigmaz(xdata(i),stability_class)**2)))*
&
           &        exp(-((xdata(i)-xdata0)**2)/(2*sigmax**2))
     enddo
endif
! CALCULATE DOSE
Wash_coeff0 = 7.0D-05
I_rain0     = 1.0d0
Wash_coeff  = Wash_coeff0 * (I_rain/I_rain0)**0.08d0
do i=1, M
   kbr(i)     = (1.0d0-exp(-lambda_r*Dt(i)))/lambda_r
   Washout(i) = (Wash_coeff/(sqrt(2.0d0*pi) * sigmay(i) * wind_velocity(i))) &
        &* exp(-(ydata(i)**2.0d0)/(2*(sigmay(i))**2.0d0))
   Br(i) = X(1) * (DF(i)*vd* Chi_0(i) +  &
        &Washout(i)) * exp(-lambda_r * xdata(i)/ wind_velocity(i))
   Dose_cloud(i)= X(1) * Chi(i) * gwr
   Dose_dep(i)  = Br(i)* kbr(i)* gbr
   ext_Dose(i)  = Dose_dep(i)+Dose_cloud(i)
   Tot_Dose(i) = ext_Dose(i)
enddo
open(112,file=TRIM('INI_dose.dat'))
do i=1,M
      write(112,*) ydata(i), xdata(i), Br(i), Dose_cloud(i),&
           &Dose_dep(i), ext_Dose(i), Tot_Dose(i)
enddo
close(112)
```

```
open(112,file=TRIM('residual_INI.dat'))
do i=1,M
      write(112,*) xdata(i), log10(Tot_Dose(i))-log10(Dosedata(i))
enddo
close(112)
print*,'Initial Guess: ' , X(1)
CALL Plume_to_plot
open(112,file=TRIM("INI_dose_plot.dat"))
do j=1,Mplot
      write(112, *) 'INITIAL GUESS FOR SPATIAL DISTRIBUTION FOR DOSE AT
t='//TRIM(Dtplot_string)//' seconds'
      write(112, *) ( Tot_Dose_plot(i,j),  i=1,Mplot)
enddo
close(112)
! standard settings for optimization
TOL = sqrt(DPMPAR(1))
FTOL = TOL
XTOL = TOL
GTOL = TOL
maxfev = 200*(N+1)
epsfcn = sqrt(DPMPAR(1))
mode = 1
FACTOR=100.0d0
nprint=1
ldfjac=M
lipvt = N
print*, 'start OPTIMIZATION'
CALL FCN(M,N,X,FVEC,IFLAG)
FNORM=ENORM(M,FVEC)
print*, 'norm of the residual first iteration ', FNORM
print*, 'standard deviation for the NORM at  first iteration: (norm of the
residual divided &
         & by degrees of freedom (# points-# of parames-1))', FNORM/(M-N-1)
CALL LMDIF(FCN,M,N,X,FVEC,FTOL,XTOL, GTOL, maxfev, epsfcn,&
& diag, mode, factor, nprint, INFO, nfev, fjac, ldfjac, ipvt,&
& qtf, wa1, wa2, wa3, wa4)
print*, 'number of iterations: ', nfev
open(112,file=TRIM('/home/laura/fortran/OPT_LM/OPT_LM_BfS/residual.dat'))
do i=1,M
      write(112,*) xdata(i), FVEC(i)
enddo
close(112)
print*, 'mean value of the residual ', sum(FVEC)/(max(1,size(FVEC)))
```

```
FNORM=ENORM(M,FVEC)
print*, 'norm of the residual last iteration ', FNORM
print*, "standard deviation of the residual at last iteration: (norm of the
residual divided &
         & by degrees of freedom (# points-# of parames-1))", FNORM/(M-N-1)
R     = fjac(1:N,1:N)
LDR=N
CALL COVAR(N,R,LDR,IPVT,TOL,WA)
print*,"info: ", INFO,"opt values X: ", (X(J),J=1,N)
!print*, "correlation between X(1) and X(1): ",
R(1,1)/(sqrt(R(1,1))*sqrt(R(1,1)))
print*,"standard deviation sigma_X:sqrt(R(1,1))",sqrt(R(1,1))
print*,"standard deviation sigma_X:UNBIASED sqrt(R(1,1)*(MSE/(m-n)))
 ",sqrt(R(1,1)* (FNORM/(M-N-1)))
corr = (M * SUM(Dosedata(:)*(ext_Dose(:))) -
SUM(Dosedata(:))*SUM(ext_Dose(:)))/&
     & (sqrt((M*SUM(Dosedata(:)**2.0d0)-(SUM(Dosedata(:)))**2.0d0))*&
     sqrt((M*SUM((ext_Dose(:))**2.0d0)-(SUM(ext_Dose(:)))**2.0d0)))
print*, 'save optimized plume'
! save optimized PLUME
do i=1, M
   Br(i) = X(1) * (DF(i)*vd* Chi(i) +  &
        &Washout(i)) * exp(-lambda_r * xdata(i)/ wind_velocity(i))
   Dose_cloud(i)= X(1) * Chi(i) * gwr
   Dose_dep(i)  = Br(i)* kbr(i) * gbr
   ext_Dose(i)  = Dose_dep(i)+Dose_cloud(i)
   Tot_Dose(i)  = ext_Dose(i)
enddo
!-------------------------------
open(112,file=TRIM(filename_save))
write(112,*) 'info ', INFO, 'M',   M, 'N',  N, 'opt_value ',  X, &
     & 'NORM ', FNORM, 'unbiased sigmaX ', sqrt(R(1,1))/(M-N)
close(112)
open(112,file=TRIM('OPT_dose.dat'))
do i=1,M
      write(112,*) ydata(i), xdata(i), Br(i), Dose_cloud(i), Dose_dep(i),
Tot_Dose(i)
enddo
close(112)
CALL Plume_to_plot
open(112,file=TRIM('xdata_plot.dat'))
do i=1,Mplot
   write(112,*) xdata_plot(i)
```

```
enddo
close(112)
open(112,file=TRIM('ydata_plot.dat'))
do i=1,Mplot
   write(112,*) ydata_plot(i)
enddo
close(112)
open(112,file=TRIM("OPT_dose_plot.dat"))
do j=1,Mplot
      write(112, *) 'OPTIMAL SPATIAL DISTRIBUTION FOR DOSE AT
t='//TRIM(Dtplot_string)//' seconds'
      write(112, *) (Tot_Dose_plot(i,j), i=1,Mplot)
enddo
close(112)
call deallocate_exp_values
end PROGRAM OPTLMDOSE
*-----------------------------------------------------------------------*
SUBROUTINE FCN(M,N,X,FVEC,IFLAG)
USE exp_values, ONLY : i, vd, lambda_r, xdata, &
     & Dosedata,  wind_velocity, DF,&
     & Washout, kbr, Chi,  gbr, gwr, Chi_0
implicit none
integer m,n,iflag
double precision X(n),FVEC(M), Br(M), Dose_cloud(M), Dose_dep(M),
ext_Dose(M)
double precision Dose_inh(M), int_Dose(M), Tot_Dose(M)
print*, 'OPIMIZING THE VARIABLE X: ', X
!evaluate the function at the starting point
!     and calculate its norm.
do i=1,M

    Br(i) = X(1) * (DF(i)*vd* Chi_0(i) +  &
            &Washout(i)) * exp(-lambda_r * xdata(i)/ wind_velocity(i))
    !print*, Br(i)
    Dose_cloud(i)= X(1) * Chi(i) * gwr
    Dose_dep(i)  = Br(i)* kbr(i) * gbr
    ext_Dose(i)  = Dose_dep(i)+Dose_cloud(i)
    Tot_Dose(i)  = ext_Dose(i)
    FVEC(i) = log10(Tot_Dose(i)) - log10(Dosedata(i))

enddo
return end subroutine FCN
```

Bibliography

Berichte der Strahlenschutzkommission (SSK) des Bundesministerium für Umwelt, Naturschutz und Reaktorsichereit, 2004.

Akselrod, M.S., Kortov, V.S., Kravetsky, D.J., and Gotlib, V.I. Highly Sensitive Thermoluminescent Anion-Defect Alpha-$Al_2O_3$3:C Single Crystal Detectors. *Radiat. Prot. Dosim.*, 33(1-4):119–122, 1990. URL http://rpd.oxfordjournals.org/content/33/1-4/119.abstract.

Barkyoumb, J.H. and Mathur, V.K. Epoxy encapsulant as serendipitous dosimeters during radiological/nuclear events. *Radiat. Meas.*, 43(2-6):841 – 844, 2008. ISSN 1350-4487. doi: DOI:10.1016/j.radmeas.2007.11.081.

Beerten, K. and Vanhavere, F. Photon energy dependence of three fortuitous dosemeters from personal electronic devices, measured by optically stimulated luminescence. *Radiat. Prot. Dosim.*, 140(3):294–299, 2010. URL http://rpd.oxfordjournals.org/content/140/3/294.abstract.

Beerten, K., Woda, C., and Vanhavere, F. Thermoluminescence dosimetry of electronic components from personal objects. *Radiat. Meas.*, 44(5-6):620 – 625, 2009. URL http://www.sciencedirect.com/science/article/pii/S1350448709000262.

Breen, B.N., Goldberger, C., and Talalaevsky, L. The accu-l-multilayer inductor for high frequency applications. Technical report, Technical Informations, AVX Israel Ltd P.O.B.23383, Jerusalem 91233 Israel.

Briggs, G.A. Diffusion estimation for small emissions. Atdl contribution file no. (draft) 79, Air Resources Atmospheric Turbulence and Diffusion Laboratory, NOAA, Oak Ridge, Tennessee, 1973.

Bulur, E. and Göksu, H. Y. OSL from BeO ceramics: new observations from an old material. *Radiat. Meas.*, 29(6):639 – 650, 1998. URL http://www.sciencedirect.com/science/article/pii/S1350448798000845.

Bulur, E. and Yeltik, A. Optically stimulated luminescence from BeO ceramics: An LM-OSL study. *Radiat. Meas.*, 45(1):29 – 34, 2010. URL http://www.sciencedirect.com/science/article/pii/S1350448709001528.

Chen, R. and McKeever, S.W.S. *Theory of Thermoluminescence and related phenomena*. Worl Scientific Publishing Co., 1997.

Dürr, Claudia. *Charakterisierung der Photonenenergieabhängigkeit elektronischer Bauteile in Mobiltelefonen hinsichtlich deren Nutzung als Notfalldosimeter*. Bachelor thesis, Hochschule für Angewandte Wissenschaften München, 2011.

Eckerman, K. F. and Ryman, J. C. *External Exposure to radionuclides in air, water, and soil*. Federal Guidance Report No. 12, 1993.

Fiedler, I. and Woda, C. Thermoluminescence of chip inductors from mobile phones for retrospective and accident dosimetry. *Radiat. Meas.*, In Press, Corrected Proof:–, 2011. doi: DOI:10.1016/j.radmeas.2011.05.077. URL http://www.sciencedirect.com/science/article/pii/S1350448711002903.

Göksu, H.Y. Telephone chip-cards as individual dosemeters. *Radiat. Meas.*, 37(6): 617 – 620, 2003. URL http://www.sciencedirect.com/science/article/pii/S1350448703000829.

Göksu, H.Y., Meckbach, R., Wieser, A., and Niedermayer, M. *Dosisrekonstruktion im Ereignisfall mit Hilfe von Lumineszenz- und EPR-Methoden an Umgebungsmaterialien*. ISSN 1612-6386. Bundesministerium für Umwelt, Naturschutz und Reaktorsicherheit, 2003.

Göksu, H..Y, Wieser, A., and Ulanovsky, A. *Retrospective individual dosimetry using luminescence and EPR after radiation accidents*. ISSN: 1612-6386. Bundesministerium für Umwelt, Naturschutz und Reaktorsicherheit, 2007.

Goedicke, Christian. Calibration of a ^{90}Sr/^{90}Y-source for luminescence dating using OSL. *Radiat. Meas.*, 42(9):1427 – 1431, 2007. doi: DOI:10.1016/j.radmeas.2007.09.014. URL http://www.sciencedirect.com/science/article/pii/S1350448707003812.

Homann, S. G. *Health Physics Code Version 2.07 User's Guide*. Lawrence Livermore National Laboratory.

Hornyak, William F. and Franklin, Alan D. Single level isothermal TL-decay (with energy level distribution and retrapping). *Nucl. Tracks. Radiat. Meas.*, 14(1-2):81 – 89, 1988. URL http://www.sciencedirect.com/science/article/pii/1359018988900453.

Huntley, D J and Lamothe, M. Ubiquity of anomalous fading in k-feldspars and the measurement and correction for it in optical dating. *Canadian Journal of Earth Sciences*, 38(7):1093–1106, 2001. doi: 10.1139/e01-013. URL http://www.nrcresearchpress.com/doi/abs/10.1139/e01-013.

ICRP, editor. *Publication 96: Protecting People Against Radiation Exposure in the Event of a Radiological Attack*. 2005.

ICRU. *(International Commission on Radiation Units and Measurements). Determination of dose equivalents resulting from external radiation sources.* Report 39, Bethesda, Maryland, USA, 1985.

Imatoukene, D., Abdelaziz, F., Mezaguer, M., and Lounis-Mokrani, Z. Development of new system for environmental monitoring based on Al2O3:C detectors. *Radiat. Meas.*, 43(2-6):668 – 671, 2008. URL http://www.sciencedirect.com/science/article/pii/S1350448708000255.

Inrig, E.L., Godfrey-Smith, D.I., and Khanna, S. Optically stimulated luminescence of electronic components for forensic, retrospective, and accident dosimetry. *Radiat. Meas.*, 43(2-6):726 – 730, 2008. ISSN 1350-4487. URL http://www.sciencedirect.com/science/article/pii/S1350448707005410.

ISO. International Organization for Standardization. X and gamma reference radiation for calibrating dosemeters and doserate meters and for determining their response as a function of photon energy - part 1: radiation characteristics and production methods. Technical report, ISO 4037-1, Geneva, 1996.

ISO. (International Organization for Standardization). X and gamma reference radiation for calibrating dosemeters and doserate meters and for determining their response as a function of photon energy - part 3: calibration of area and personal dosemeters and the measurement of their response as a function of energy and angle of incidence. Technical report, ISO 4037-3, Geneva., 1999.

Jain, M. and Ankjærgaard, C. Towards a non-fading signal in feldspar: Insight into charge transport and tunnelling from time-resolved optically stimulated luminescence. *Radiation Measurements*, 46(3):292 – 309, 2011. URL http://www.sciencedirect.com/science/article/pii/S1350448710004038.

Kaiser, J.C. and Pröhl, G. Harnessing monitoring measurements in urban environments for decision making after nuclear accidents. *Kerntechnik*, 72:218–222., 2007.

Mathur, V.K., Barkyoumb, J.H., Yukihara, E.G., and Göksu, H.Y. Radiation sensitivity of memory chip module of an ID card. *Radiat. Meas.*, 42(1):43 – 48, 2007. URL http://www.sciencedirect.com/science/article/pii/S1350448706001016.

McKeever, S., Moscovitch, M., and Townsend, P. *Thermoluminescence dosimetry materials: properties and uses.* Nuclear Technology Publishing, 1995.

McKeever, S.W.S. *Thermoluminescence of solids.* Cambridge University Press., 1985.

Meckbach, R., Jacob, P., and Paretzke, H.G. Gamma Exposures due to Radionuclides Deposited in Urban Environments. Part I: Kerma Rates from Contaminated Urban Surfaces. *Radiat. Prot. Dosim.*, 25(3):167–179, 1988. URL http://rpd.oxfordjournals.org/content/25/3/167.abstract.

More, J. J., Sorensen, D.C., Hillstrom, K. E., and Garbow, B. S. *Sources and Development of Mathematical Sofware*, chapter The MINPACK Project, pages 88–111. Prentice-Hall, 1984.

Murray, A. S. and Wintle, A. G. The single aliquot regenerative dose protocol: potential for improvements in reliability. *Radiat. Meas.*, 37(4-5):377 – 381, 2003. URL http://www.sciencedirect.com/science/article/pii/S1350448703000532.

Pasquill, F. *Atmospheric Diffusion: The dispersion of Windborne Material from Industrial and Other Sources*. New York: John Wiley and Sons., 2nd edition edition, 1974.

Prouza, Z., Beckova, V., Cespirova, I., Helebrant, J., Hulka, J., Kuca, P., Michalek, V., Rulik, P., Skrkal, J., and Hovorka, J. Field tests using radioactive matter. *Radiat. Prot. Dosim.*, 139(4):519–531, 2010. URL http://rpd.oxfordjournals.org/content/139/4/519.abstract.

Raskob, W. and Hugon, M, editors. *Enhancing nuclear and emergency management and rehabilitation - Key results of the EURANOS European Project*, volume 45. Radioprotection, 2010.

Sommer, M. and Henniger, J. Investigation of a BeO-based optically stimulated luminescence dosemeter. *Radiat. Prot. Dosim.*, 119(1-4):394–397, 2006. URL http://rpd.oxfordjournals.org/content/119/1-4/394.abstract.

Sommer, M., Jahn, A., and Henniger, J. Beryllium oxide as optically stimulated luminescence dosimeter. *Radiat. Meas.*, 43(2-6):353 – 356, 2008. URL http://www.sciencedirect.com/science/article/pii/S1350448707004763.

Sommer, M., Jahn, A., and Henniger, J. A new personal dosimetry system for HP(10) and HP(0.07) photon dose based on OSL-dosimetry of beryllium oxide. *Radiat. Meas.*, In Press, Corrected Proof:–, 2011. doi: DOI:10.1016/j.radmeas.2011.07.002. URL http://www.sciencedirect.com/science/article/pii/S1350448711003325.

Sommer, Marian, Freudenberg, Robert, and Henniger, Jürgen. New aspects of a BeO-based optically stimulated luminescence dosimeter. *Radiat. Meas.*, 42(4-5): 617 – 620, 2007. URL http://www.sciencedirect.com/science/article/pii/S1350448707000650.

Spooner, N.A. and Questiaux, D.G. Kinetics of red, blue and uv thermoluminescence and optically-stimulated luminescence from quartz. *Radiat. Meas.*, 32(5-6):659 – 666, 2000. doi: DOI:10.1016/S1350-4487(00)00067-6.

Van der Hoven. *Metereology and Atomic Energy*, chapter Deposition of Particles and Gases. 1968.

Veronese, I., Giussani, A., Göksu, H. Y., and Martini, M. The trap parameters of electrons in intermediate energy levels in quartz. *Radiat. Meas.*, 38(4-6):743 – 746, 2004. doi: DOI:10.1016/j.radmeas.2004.01.012.

Woda, C. and Spöttl, T. On the use of OSL of wire-bond chip card modules for retrospective and accident dosimetry. *Radiat. Meas.*, 44(5-6):548 – 553, 2009. URL http://www.sciencedirect.com/science/article/pii/S1350448709000420.

Woda, C., Greilich, S., and Beerten, K. On the OSL curve shape and preheat treatment of electronic components from portable electronic devices. *Radiat. Meas.*, 45(3-6): 746 – 748, 2010. URL http://www.sciencedirect.com/science/article/pii/S1350448710000429.

Woda, C., Ulanovsky, A., Bougrov, N.G., Fiedler, I., Degteva, M.O., and Jacob, P. Potential and limitations of the 210 °c tl peak in quartz for retrospective dosimetry. *Radiat. Meas.*, 46(5):485 – 493, 2011. doi: DOI:10.1016/j.radmeas.2011.03.019.

Zäringer, M. and Sempau, J. *Calibration Factors for Dose Rate Probes in Environmental Monitoring Networks Obtained from Monte-Carlo-Simulations*. BfS-IAR, 1997.

| Verantwortung für Mensch und Umwelt |

Kontakt:
Bundesamt für Strahlenschutz
Postfach 10 01 49
38201 Salzgitter
Telefon: + 49 30 18333 - 0
Telefax: + 49 30 18333 - 1885
Internet: www.bfs.de
E-Mail: ePost@bfs.de
Gedruckt auf Recyclingpapier aus 100 % Altpapier.

Bundesamt für Strahlenschutz